Computation of Losses in HTS Under the Action of Varying Magnetic Fields and Currents

Francesco Grilli, Enric Pardo, *Member, IEEE*, Antti Stenvall, Doan N. Nguyen, Weijia Yuan, and Fedor Gömöry, *Member, IEEE*

(Invited Paper)

***Abstract*—Numerical modeling of superconductors is widely recognized as a powerful tool for interpreting experimental results, understanding physical mechanisms, and predicting the performance of high-temperature-superconductor (HTS) tapes, wires, and devices. This is particularly true for ac loss calculation since a sufficiently low ac loss value is imperative to make these materials attractive for commercialization. In recent years, a large variety of numerical models, which are based on different techniques and implementations, has been proposed by researchers around the world, with the purpose of being able to estimate ac losses in HTSs quickly and accurately. This paper presents a literature review of the methods for computing ac losses in HTS tapes, wires, and devices. Technical superconductors have a relatively complex geometry (filaments, which might be twisted or transposed, or layers) and consist of different materials. As a result, different loss contributions exist. In this paper, we describe the ways of computing such loss contributions, which include hysteresis losses, eddy-current losses, coupling losses, and losses in ferromagnetic materials. We also provide an estimation of the losses occurring in a variety of power applications.**

***Index Terms*—Alternate current (ac) losses, coupling losses, eddy-current losses, hysteresis losses, magnetic materials, numerical modeling.**

I. Introduction

THE capability of computing ac losses in high-temperature superconductors (HTSs) is very important for designing and manufacturing marketable devices such as cables, fault current limiters, transformers, and motors. As a matter of fact, in many cases, the prospected ac loss value is too high to make the application attractive on the market, and numerical calculations can help to find solutions for reducing the losses.

In the past decades, several analytical models for computing the losses in superconductor materials have been developed. In general, these models can provide the loss value for a given geometry in given working conditions by means of relatively simple formulas. While these models are undoubtedly fast and very useful for basic understanding of the loss mechanisms and for predicting the loss value for a certain number of geometries and tape arrangements, they have several important limitations, which restrict their usefulness for an accurate estimation of the ac losses in real HTS devices. Numerical models, on the other hand, can overcome these limitations and can simulate geometries and situations of increasing complexity. This increased computing capability comes at the price of more complex software implementation and longer computation times. This paper focuses on methods for computing ac losses by means of analytical and numerical techniques.

Technical superconductors consist of different materials in addition to the superconductor itself (metal, buffers and substrates, magnetic materials, etc.), some of which, depending on the operating conditions, can give a significant contribution to the total losses. These loss contributions can be divided into four categories, which are summarized in the following list and schematically illustrated in Fig. 1:

1) Hysteresis losses, which are caused by the penetration and movement of the magnetic flux in the superconducting material;
2) Eddy-current losses, which are caused by the currents induced by a magnetic field and circulating in the normal metal parts of a superconducting tape;
3) Coupling losses, which are caused by the currents coupling two or more superconducting filaments via the normal metal regions separating them;
4) Ferromagnetic losses, which are caused by the hysteresis cycles in magnetic materials.

This paper is structured as follows. Sections II–V focus each on a different loss contribution, as in the list above. Section VI gives the loss estimation for various power applications. The two appendices contain the details of calculations used in Section II-B.

Manuscript received September 24, 2012; accepted April 16, 2013. Date of current version October 23, 2013. The work of F. Grilli was supported by the Helmholtz University Young Investigators Program under Grant VH-NG-617. The work of E. Pardo was supported by the Agency for the Structural Funds of the European Union from the Ministry of Education, Science, Research and Sports of the Slovak Republic under Contract 26240220028. The work of A. Stenvall was supported in part by the Academy of Finland under Project 131577, by the Foundation for Technology Promotion in Finland, and by the Emil Aaltonen Foundation. The work of D. Nguyen was supported by the Los Alamos National Laboratory through the Laboratory Directed Research and Development Program under Grant 20120603ER. This paper was recommended by Associate Editor P. J. Masson.

F. Grilli is with the Institute for Technical Physics, Karlsruhe Institute of Technology, 76131 Karlsruhe, Germany (e-mail: francesco.grilli@kit.edu).

E. Pardo and F. Gömöry are with the Institute of Electrical Engineering, Slovak Academy of Sciences, 814 38 Bratislava, Slovak Republic.

A. Stenvall is with the Tampere University of Technology, 33101 Tampere, Finland.

D. N. Nguyen is with the Los Alamos National Laboratory, Los Alamos, NM 87545 USA.

W. Yuan is with the University of Bath, Bath BA2 7AY, U.K.

Color versions of one or more of the figures in this paper are available online at http://ieeexplore.ieee.org.

Digital Object Identifier 10.1109/TASC.2013.2259827

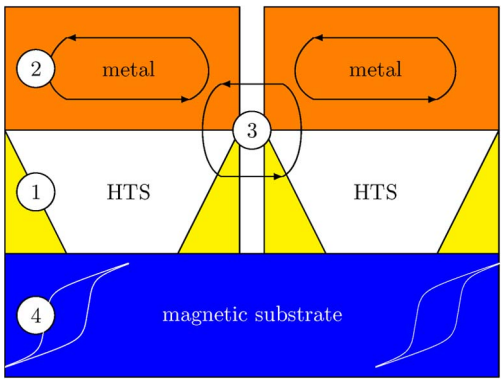

Fig. 1. Schematic of the different loss contributions in technical HTSs, e.g., ReBCO-coated conductor (tape's cross section displayed): 1) Hysteresis losses in the superconductor; 2) eddy current losses in the normal metal stabilizer; 3) coupling losses between filaments (e.g., through conducting paths due to imperfections of the striation process); and 4) ferromagnetic losses in the substrate.

II. Hysteresis Losses

This section is divided into different parts as follows. First, we describe the two most commonly used models for describing a superconductor with the purpose of ac loss computation. Then, we explain how to solve the electromagnetic quantities. Afterward, we illustrate how to compute the ac losses once the electromagnetic quantities are known. Finally, we show the solutions for several particular cases relevant for applications.

A. Models for the Superconductor

The reason why hard superconductors are able to carry large electrical currents is that the magnetic field (penetrating type-II superconductors in the form of supercurrent vortices, each carrying the same amount of magnetic flux) is pinned in the volume of the superconducting material. Due to this mechanism, the vortices do not move under the action of the Lorentz force that is pushing them in the direction perpendicular to both the flow of the electrical current and the magnetic field. In addition, a gradient in the density of vortices is reluctant to any rearrangement. Thus, once a dc is established in a hard superconductor, it will also persist after switching the driving voltage off (circulation of an electrical current with less resistance). However, in the ac regime, the vortices must move to follow the change of the magnetic field: The pinning force represents an obstacle, and superseding it is an irreversible process. The accompanied dissipation is called the hysteresis loss in hard superconductors.

It is not easy to link the interaction between a current vortex (and the involved pinning centers) and the material's properties that can be used in electromagnetic calculations. However, in the investigation of low-temperature superconductors (LTSs), such as NbTi or Nb_3Sn, it was found that, for practical purposes, one can obtain very useful predictions utilizing the phenomenological description introduced in [1] and [2], commonly known as the critical-state model (CSM). The model is valid on a macroscopic scale that neglects the details of electrical current distribution in individual vortices and replaces it with an average taken over a large number of vortices. The CSM

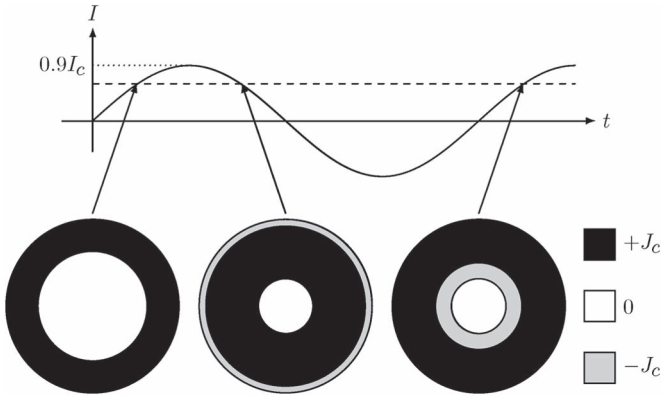

Fig. 2. Current density distribution in the cross section of a round superconducting wire carrying a current of $0.6I_c$, taken at different instants of a sinusoidal signal with an amplitude of $0.9I_c$.

states that, in any (macroscopic) part of a hard superconductor, one can find either no electrical current or a current with density J equal to the so-called critical current density J_c.

In the original formulation, J_c is constant, and it fully characterizes the properties of the material in the processes of magnetic field variation. In addition, it was formulated for bodies of high symmetry such as infinitely long cylinders and slabs. Its value is controlled by the magnetic history, according to these two general principles.

- No current flows in the regions that are not previously penetrated by the flux vortices.
- In the rest of the superconductor, the flux vortices arrange with a gradient of density that could be of a different direction but always the same magnitude.

Since the penetration of vortices is accompanied by a change of local magnetic flux density B that is directly proportional to the density of vortices, the mathematical formulation of the principle of the critical state with constant J_c is as follows:

$$|J| = \begin{cases} 0, & \text{in regions where } B = 0 \\ J_c, & \text{elsewhere.} \end{cases} \tag{1}$$

One should note that the direction of the current density is not defined by this formula. Fortunately, many problems of practical importance can be simplified to a 2-D formulation, e.g., in devices made of straight superconducting tapes or wires, which can be considered infinitely long. The advantage of a 2-D formulation of the critical state is that the current density is always parallel to the longitudinal direction. Therefore, here, we assume that the task is to find a 2-D distribution.

We now illustrate the use of (1) for the problem of a round wire carrying a sinusoidal transport current with amplitude of $0.9I_c$. The wire's critical current I_c is simply obtained by multiplying the critical current density J_c by the wire's cross section. Fig. 2 shows the current density distributions when the transport current equals $0.6I_c$, which are taken at three different instants of the sinusoidal signal.

The significant difference of the current density distribution is due to the "history" of the arrangement of the flux vortices in the superconductor during the sinusoidal signal.

The solutions shown in Fig. 2 are derived by utilizing (1) and by considering that, due to the circular symmetry and according

to Maxwell equations, in the region with $B = 0$ also $J = 0$, (no current can flow without generating a magnetic field). In his subsequent work [3], Bean transformed his formulation using the fact that any change in the magnetic field is linked to the appearance of electric field E. Then, he stated that, in a hard superconductor, there exists a limit in the macroscopic current density that it can carry, and any electromotive force, however small, will induce this current to flow. This formulation of critical state can be written as

$$|J| = \begin{cases} 0, & \text{in regions where } E = 0 \text{ in all past history} \\ J_c, & \text{elsewhere.} \end{cases} \tag{2}$$

Interestingly, the most general $J(E)$ relation of the CSM for infinitely long conductors is [4]

$$\begin{cases} |J| \le J_c, & \text{if } E = 0 \\ |J| = J_c, & \text{otherwise.} \end{cases} \tag{3}$$

For conductors of finite thickness, this equation is equivalent to (2) [39]. The generalization given is essential for thin strips, which present regions where $0 < |J| < J_c$. In addition, it is also useful for numerical purposes.

Establishing the correspondence between the current density and the electric field is a standard technique in electromagnetic calculations. On the other hand, (2) is multivalued because, for $|J| = J_c$, any value of E is possible. The value of E is determined by the electromagnetic history of the whole sample. This hinders the direct use of this $E(J)$ relation in calculations. Nevertheless, with this approach, the principal analytical formulas for the estimation of ac losses in LTS devices have been derived [5]–[9], and early numerical techniques have been proposed [10]. The CSM still represents the first approximation that allows predicting important features of HTS materials and devices, such as current density and magnetic field profiles.

Due to the rapid development of computer technology in both computing power and price affordability, we can now include various refinements of the $E(J)$ relation, which in certain cases are quite important. These include the following:

1) thermal activation leading to substantial flux creep [11];
2) dependence of J_c on the amplitude and orientation of the magnetic field;
3) spatial variation of J_c (e.g., due to nonuniformities related to the manufacturing processes).

The first item of this list is of fundamental importance because it provides a new formulation of the model for the electromagnetic properties of hard superconductors. The superconductor's behavior described by 1 or 2 is independent of the time derivative of the electromagnetic quantities; this, for example, means that any part of the time axis shown in the upper part of Fig. 2 could be stretched or compressed without influencing the resulting distributions. Only the *existence* of an electric field E and not its magnitude matters. On the other hand, thermal activation is a process happening on a characteristic time scale. Thus, if thermal activation is taken into account, the current density distribution depends on the rate of change—in the case that is illustrated in Fig. 2 on the frequency—and on the shape of the waveform of the transport current.

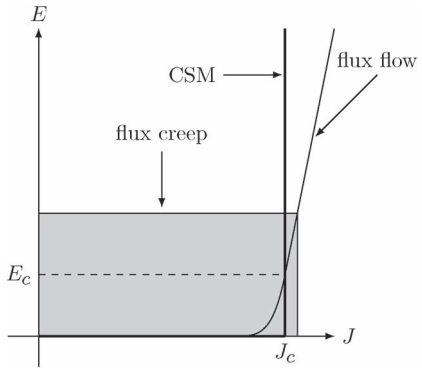

Fig. 3. Typical $E(J)$ characteristics for HTS (thin line). Differently from the CSM [thick line, (3)] there is always $dE/dJ > 0$ (not visible at low currents because of the used linear scale) caused by the significant flux creep. The CSM is a good approximation in the shaded area. It does not consider the flux-flow regime that would prevail at electric fields much higher than E_c.

Experimental observations of strongly nonlinear current–voltage characteristics of hard superconductors (e.g., [12]) led to a formulation where the link between the current density and the electric field is expressed as

$$J = J_c \left(\frac{E}{E_c} \right)^{1/n} \tag{4}$$

where E_c is the characteristic electric field (which is usually set equal to 10^{-4} V/m) that defines the current density J_c, and the power exponent n characterizes the steepness of the current–voltage curve. The asymptotic behavior for $n \to \infty$ in practice leads to the same dependence between the current density and the electric field as in (2). Nevertheless, there is one substantial difference: In (4), J depends on the *actual* value of E at the same given instant. This feature enables the incorporation of hard superconductors in electromagnetic calculations by considering it an electrically conductive and nonmagnetic material with conductivity that depends on the electric field, i.e.,

$$\sigma_{\mathrm{SC}} = \frac{J}{E} = \frac{J_c}{E_c^{1/n}} E^{\frac{1-n}{n}}. \tag{5}$$

This description is valid until the current density reaches the level causing a microscopic driving force on the vortices, which overcomes the pinning force. Then, the movement of vortices enters the so-called flux-flow regime, which can be defined by differential resistivity as [12]

$$\rho_{\mathrm{FF}} = \frac{\Delta E}{\Delta J} \approx \rho_n \frac{B}{B_{c2}} \tag{6}$$

where ρ_n is the normal state resistivity, and B_{c2} is the upper critical magnetic field. The different regimes and the interval where the CSM is applicable are schematically illustrated in Fig. 3.

In the calculation of critical current or ac losses in HTS materials, it is desirable to take also into account the dependence of the critical current density on the magnetic field and its orientation. In the case of Bi-2223 multifilamentary tapes, the use of a modified Kim's formula [12] was quite successful in reproducing experimental data [13]. In the so-called elliptical

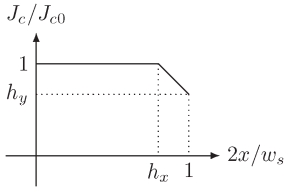

Fig. 4. Simplified model describing the nonuniformity of the current density across the tape's width (in the direction of the coordinate x) by the piecewise linear profile of $J_c(x)$ defined by (8). The tape width is w_s, and the profile is symmetric with respect to the tape center $x = 0$.

approximation, J_c depends on the components of the magnetic field parallel and perpendicular to the flat face of the tape by means of the anisotropy parameter γ (with $\gamma > 1$), i.e.,

$$J_c(B_\perp, B_\parallel) = \frac{J_{c0}}{\left(1 + \frac{\sqrt{B_\perp^2 + B_\parallel^2/\gamma^2}}{B_0}\right)^\beta}. \tag{7}$$

The cutoff value at low fields and the rapidity of the J_c reduction are given by B_0 and β, respectively.

An alternative way to express the asymmetric scaling of J_c with respect to the perpendicular and parallel magnetic field components is by introducing the angular dependence of the characteristic field B_0 [14]. With the introduction of artificial pinning centers in the superconductor, the simple description given by the four-parameter expression (7) is no longer adequate; more elaborated expressions are necessary to describe the experimentally observed behavior of the samples [15].

The issue of possible variations of the superconductor's critical current density with respect to spatial coordinates is quite important in the case of HTSs. The longitudinal uniformity is assessed by the determination of critical current variations along the conductor length. Since the loss at full penetration is proportional to the critical current, the change of ac losses due to longitudinal nonuniformity is only marginal for commercial tapes, which typically present a fluctuation of the critical current below 10%. On the contrary, the nonuniformity across the tape's width, which is investigated in detail for Bi-2223 multifilamentary tapes in [16] and [17], has been proposed as explanation for anomalous loss behavior of coated conductor tapes [18]–[20]. This effect is of particular importance for low-loss configurations, such as bifilar coils used in resistive fault current limiters. Due to the manufacturing process, the critical current density is lower at the tape's edges than in the center, where it is usually quite uniform. As the first approximation is to take this nonuniformity into account, a symmetric piecewise linear profile, as shown in Fig. 4, can be used. Its mathematical form is

$$J_c(x) = J_{c0} \times \begin{cases} 1, & \text{if } x \le h_x \frac{ws}{2} \\ 1 - (1 - h_y)\frac{2|\frac{x}{ws}| - h_x}{1 - h_x}, & \text{if } x > h_x \frac{ws}{2}. \end{cases} \tag{8}$$

B. How to Solve the Electromagnetic Quantities

The main step to calculate the ac losses in superconductors is to solve the electromagnetic state variable. Depending on the simulation method, the state variable can be current density $\mathbf{J}(t, \mathbf{r})$, magnetic field $\mathbf{H}(t, \mathbf{r})$, the pair composed of the current vector potential and the magnetic scalar potential $\mathbf{T}(t, \mathbf{r}) - \Omega(t, \mathbf{r})$ [21], [22], or vector potential $\mathbf{A}(t, \mathbf{r})$, where t and $\mathbf{r}$ are the time and the position vector, respectively. Additionally, scalar potential $\phi(t, \mathbf{r})$ may be an extra variable. For formulations using the vector potential, the gauge is usually the Coulomb gauge (see Appendix B). All the methods reviewed in this paper assume that the displacement current is negligible, i.e., $|\mathbf{J}| \gg |\partial \mathbf{D}/\partial t|$, where $\mathbf{D}$ is the displacement vector.

Once the state variable is solved for the time-varying excitation, the power loss can be calculated by using the methods in Section II-C. The time-varying excitation can be cyclic or not, such as a ramp increase in dc magnets. It can be transport current $I(t)$, applied field $\mathbf{H}_a(t, \mathbf{r})$ (which can be nonuniform and with an orientation varying in time; see Section II-D for particular solutions), or a combination of both.

1) Cross-Sectional Methods: In the following, we outline the methods that solve the state variable for an arbitrary combination of the current and the applied field. Other methods optimized for particular situations and their results are summarized in Section II-D. These methods solve the cross section of infinitely long conductors and bodies with cylindrical symmetry; hence, they are mathematically 2-D problems. Simulations for bidimensional surfaces and 3-D bodies are treated in Sections II-B.3 and II-B.4, respectively.

A superconductor with a smooth $E(J)$ relation can be solved by calculating different electromagnetic quantities. Brandt's method [23], [24], which is generalized for simultaneous currents and fields by Rhyner and Yazawa *et al.* [25], [26], solves $\mathbf{J}$ and ϕ in the superconductor volume. Alternatively, finite-element method (FEM) models solve $\mathbf{H}$ [20], [27]–[29], $\mathbf{T}$, and Ω [30]–[33], or $\mathbf{A}$ and ϕ [34]–[36] in a finite volume containing the superconductor and the surrounding air, forming the simulation volume. All FEM models require setting the boundary conditions of the state variable on the boundary of the simulation volume. For most of the methods, the boundary conditions are for asymptotic values; hence, the simulation volume is much larger than the superconducting one. However, for the implementation of Kajikawa *et al.*, the boundary conditions only require to contain the superconductor volume [28], thus reducing the simulation volume and computation time. In this sense, Brandt's method is also advantageous because it only simulates the superconductor volume. On the other hand, FEM simulations are suitable for commercial software, which simplifies the implementation and analysis. The computing time for all the methods aforementioned dramatically increases for a power-law $E(J)$ relation with a high exponent. Variational methods may also be applied to solve problems with a smooth $E(J)$ relation [4], [37]–[39], although they are mostly used for the CSM.

Critical-state calculation models are ideal to simulate superconductors with a large exponent in the power-law $E(J)$ relation. Moreover, they are also usually faster than the simulations with a smooth $E(J)$ relation for relatively low n. This improvement in speed may justify the sacrifice in accuracy caused by using the critical-state approximation. However, the CSM cannot describe relaxation effects or overcurrent situations.

Most of the existing methods for the general current and applied field imply variational methods. They were first proposed by Bossavit [4], although their most important contribution is from Prigozhin, who developed the J formulation [38], [40]. Later, Badia and Lopez proposed the $\mathbf{H}$ formulation [41]. An alternative numerical implementation to minimize the functional in the $\mathbf{J}$ formulation and to set the current constraints is the minimum magnetic energy variation (MMEV) (this method sets the current constraints directly, not through the electrostatic potential). The general formulation is described in [42] and [43], although it was first introduced in [44] for magnetization cases. The early works on MMEV implicitly assume that the current fronts penetrate monotonically in a half-cycle. This occurs in some practical cases but not in general cases [42].

In addition, FEM models with the A formulation can solve the critical state situation, as shown by Gömöry *et al.* [45], [46], by means of the A variation method. This technique is inspired by Campbell's A formulation for superconductors with both reversible and irreversible contributions to pinning [47], [48]. Another method based on the A formulation was developed by Barnes *et al.* [49], who merged the FEM technique with the critical-state constraint on J, $|J| \leq J_c$. Methods assuming a smooth $E(J)$ relation can also approximate the CSM by considering an $E(J)$ relation with piecewise linear segments or a power law with a high exponent [28], [37], [50].

All the given methods, both for a smooth $E(J)$ relation and the CSM, can take the magnetic field dependence of the critical current density into account and, in principle, position dependence.

2) On the $\mathbf{A}-\phi$ and $\mathbf{T}-\Omega$ Formulations: For completeness, we next discuss the meaning of the scalar and vector potentials for the $\mathbf{A}-\phi$ and $\mathbf{T}-\Omega$ formulations. Further details can be found in a dedicated paper in this issue [51]. First, we consider the $\mathbf{A}-\phi$ formulation and, later, the $\mathbf{T}-\Omega$ formulation.

In the Coulomb gauge, scalar potential ϕ is the electrostatic potential created by the electrical charges (see Appendix B). In practice, the scalar potential needs to be taken into account in the $\mathbf{A}-\phi$ formulation in the following cases.

The first case is when there is a net transport current. In the Coulomb gauge, the current distribution creates a nonzero $\partial\mathbf{A}/\partial t$ at the current-free core (see Fig. 2 for a typical current distribution), whereas the electric field $\mathbf{E}=-\partial\mathbf{A}/\partial t-\nabla\phi$ vanishes. Therefore, it is necessary to have a certain $\nabla\phi$ in order to compensate for $\partial\mathbf{A}/\partial t$. One may include $\nabla\phi$ in $\mathbf{A}$ as a gauge, i.e., $\mathbf{A}'=\mathbf{A}+\nabla\phi$, where $\mathbf{A}$ is in the Coulomb gauge. As a result, $\mathbf{A}'=0$ at the current-free core. However, ϕ has still to be taken into account in the boundary conditions far away from the superconductor. Explicitly, $\mathbf{A}'\approx\nabla\phi$ and $\mathbf{A}'\approx-\mu_0 I\ln r/(2\pi)+\nabla\phi$ for 3-D and infinitely long 2-D geometries, respectively, whereas in the Coulomb gauge, the boundary conditions are $\mathbf{A}=0$ and $\mathbf{A}'\approx-\mu_0 I\ln r/(2\pi)$, respectively ($r$ is the radial distance from the superconductor electrical center). In this case, ϕ is the electrostatic potential generated by the current source in order to keep a constant current I. The physical source of ϕ is the surface electrical charges at both ends of the superconductor wire and on the lateral surfaces.

Second, ϕ is necessary when a multifilamentary body with isolated filaments is submitted to a changing applied magnetic field. In order to ensure a zero net current in all filaments, scalar potential ϕ between the filaments is needed. The reason is as follows. The electric field in the current-free zone is zero (see Fig. 10 for a typical current distribution in this case). In order to achieve zero electric field there, it is necessary to have $\nabla\phi$ because $\partial\mathbf{A}/\partial t$ is nonzero at the current-free zone. The cause is that there is a net flux between the filaments, which is equal to $\oint\mathbf{A}\cdot d\mathbf{r}$. A similar situation appears when the filaments are connected by a normal conducting material.

Finally, the scalar potential is necessary for the general 3-D case and for 2-D thin surfaces. A general body submitted to a magnetic field created by a round winding produces $\mathbf{A}$ with cylindrical symmetry (in the Coulomb gauge). Then, if the superconducting body does not match this cylindrical symmetry, e.g., because it has corners, a certain $\nabla\phi$ that "corrects" the direction of $\mathbf{E}$ is needed, in order to allow currents parallel to the superconductor surface [48]. This is clear when $\mathbf{E}$ and $\mathbf{J}$ are parallel, but a certain $\nabla\phi$ should also be present for an arbitrary tensor relation between $\mathbf{E}$ and $\mathbf{J}$.

The meaning of the $\mathbf{T}$ and Ω potentials is as follows. The $\mathbf{T}$ potential is such that $\mathbf{J}=\nabla\times\mathbf{T}$. Although it follows that $\mathbf{J}=\nabla\times\mathbf{H}$, $\mathbf{T}$ is not necessarily $\mathbf{H}$. Since $\nabla\times(\mathbf{T}-\mathbf{H})=0$, the quantity $\mathbf{T}-\mathbf{H}$ can be written as a gradient of a scalar function, i.e., $\mathbf{T}-\mathbf{H}=\nabla\Omega$ and $\mathbf{H}=\mathbf{T}-\nabla\Omega$. Note that $\mathbf{T}$ is subjected to gauge invariance. That is, $\mathbf{T}'=\mathbf{T}-\nabla\varphi$ generates the same current density $\mathbf{J}=\nabla\times\mathbf{T}=\nabla\times\mathbf{T}'$, where φ is any scalar function. As a consequence, the meaning of Ω depends on the gauge of $\mathbf{T}$. When the gauge function φ is zero, $\nabla\cdot\mathbf{H}=-\nabla^2\Omega$; hence, Ω is the magnetic scalar potential due to the magnetic pole density. For this gauge, $\mathbf{T}$ is the magnetic field created by the currents. In addition, other gauges are also used in computations [21], [22].

3) Methods for 2-D Surfaces: An obviously mathematically 2-D geometry is thin films with finite length.

The advantage of flat 2-D surfaces is that the current density can be written as a function of a scalar field, i.e., $\mathbf{J}(x,y)=\nabla\times\hat{\mathbf{z}}g(x,y)$, where the z-direction is perpendicular to the surface [52]. g is the z component of the current potential $\mathbf{T}$ since $\mathbf{J}=\nabla\times\mathbf{T}$. It could be also regarded as an effective density of magnetic dipoles $\mathbf{M}$. For a smooth $E(J)$ relation, this quantity can be computed by numerically inverting the integral equation for the vector potential in (57) [52] or the Biot–Savart law [53]. Naturally, FEM models based on the $\mathbf{T}$ formulation are useful for these surfaces [54], which is the same with those based on the $\mathbf{H}$ formulation [55], [56]. Variational principles can solve the situation of the CSM [57], [58].

A more complex situation is when the surfaces are bent in three dimensions, such as twisted wires, spiral cables, and Roebel cables (this latter with important simplifications). The models developed so far use the FEM with the $\mathbf{T}$ [54], [59], [60] and $\mathbf{H}$ formulations [56].

4) Methods for Fully 3-D Problems: We define a fully 3-D situation as the case when the body of study is a 3-D domain, and the problem cannot be reduced to a mathematically 2-D domain. Thus, we exclude problems with cylindrical symmetry, as well as thin surfaces with 3-D bending (see Section II-B3).

For a fully 3-D situation (and flat surfaces in 3-D bending), the magnetic field is not perpendicular to the current density in certain parts of the sample. Then, the modeling should take flux cutting [61] into account. This can be done by using the dependence of J_c on the angle between the electric field, i.e., $\mathbf{E}$, and the current density, i.e., $\mathbf{J}$ [41], [62], [63]. Experimental evidence reveals elliptical dependence [64].

The implementation of 3-D models can be done as follows. In principle, variational methods can describe the CSM in 3-D [4], although this has not yet been brought into practice. FEM models have successfully calculated several 3-D situations, although in all cases, the model assumes that $\mathbf{J}$ is parallel to $\mathbf{E}$ and a smooth $E(J)$ relation. These calculations are for the $\mathbf{T}-\Omega$ [32], $\mathbf{A}-\phi$ [32], [65], [48], or $\mathbf{H}$ [55], [56] formulations. An alternative model based on the $\mathbf{H}$ formulation that does not use the Garlekin method for the FEM can be found in [66].

References for examples of 3-D calculations are in Section II-D12.

C. How to Calculate AC Losses Once the Electromagnetic Quantities are Known

This section deduces several formulas to calculate ac losses in superconductors once the electromagnetic quantities are known. These can be obtained by any method described in Section II-B.

First, Section II-C1 justifies that the density of local dissipation is $p = \mathbf{J} \cdot \mathbf{E}$. Section II-C2 outlines how to calculate the ac losses for the CSM. Section II-C3 presents simplified formulas for the magnetization ac losses. Finally, Section II-C4 discusses how to calculate the ac losses from the energy delivered by the power sources.

1) Local Instantaneous Dissipation in Type-II Superconductors: The local instantaneous power dissipation p in a type-II superconductor is

$$p = \mathbf{J} \cdot \mathbf{E}. \tag{9}$$

In the following, we summarize the mechanisms that lead to this relation [12], [67], [68]. The driving force per unit length $\mathbf{F}_d$ on a vortex is $\mathbf{F}_d = \mathbf{J} \times \mathbf{\Phi}_0$, where $|\mathbf{\Phi}_0|$ is the vortex flux quantum, with value $\pi\hbar/e$, and the direction of $\mathbf{\Phi}_0$ follows the direction of the vortex. Then, the local rate of work per unit volume p on the vortices is

$$p = (\mathbf{J} \times \mathbf{\Phi}_0 n) \cdot \mathbf{v} = (\mathbf{\Phi}_0 n \times \mathbf{v}) \cdot \mathbf{J} \tag{10}$$

where n and $\mathbf{v}$ are the vortex density and velocity, respectively. From electromagnetic analysis, it can be shown that the moving vortices with speed $\mathbf{v}$ create an electric field (see Appendix A), i.e.,

$$\mathbf{E} = \mathbf{\Phi}_0 n \times \mathbf{v} = \mathbf{B} \times \mathbf{v}. \tag{11}$$

The given fields $\mathbf{E}$ and $\mathbf{B}$ are the average in a volume containing several vortices. Finally, by inserting (11) into (10), we obtain (9).

Equation (9) also applies to normal conductors [6, pp. 258]. Then, this equation is also valid to calculate the loss due to the eddy and coupling currents. However, the loss mechanism in normal conductors and superconductors is very different. In normal conductors, $\mathbf{E}$ creates work on the charge carriers and induces movement in them, and this movement manifests in $\mathbf{J}$. In contrast, in superconductors, $\mathbf{J}$ is the quantity that exerts work and induces movement on the vortices. This vortex movement manifests in $\mathbf{E}$.

For a given local $\mathbf{J}$, $\mathbf{E}$ does not change in time, which means that $\mathbf{v}$ is constant. This is because several dissipation mechanisms cause a viscous flow of the vortices [12], [68]. For power applications, the relation between E and J does not depend on the speed of the change of the current density. Kötzler *et al.* experimentally showed that the response to ac fields for a wide range of frequencies, i.e., 3 mHz to 50 MHz, is consistent with a unique $E(J)$ relation of the studied sample [68], [70].

2) Application to the CSM: The application of (9) for the local loss dissipation requires to know $\mathbf{J}$ and $\mathbf{E}$. Once the state variable is known, the current density can be found by means of one of the following relations: $\nabla \times \mathbf{H} = \mathbf{J}$, $\nabla \times \mathbf{T} = \mathbf{J}$, and $\nabla \times (\nabla \times \mathbf{A}) = \mathbf{J}$. Then, by assuming a smooth $\mathbf{E}(\mathbf{J})$ relation for the superconductor, $\mathbf{E}$ is simply obtained from that relation. For the CSM, the relation between $\mathbf{E}$ and $\mathbf{J}$ is multivalued; hence, $\mathbf{E}$ cannot be found in this way.

For the CSM, $\mathbf{E}$ is calculated from

$$\mathbf{E} = -\partial\mathbf{A}/\partial t - \nabla\phi. \tag{12}$$

The vector potential in the Coulomb gauge is obtained from J by using (57). For this gauge, ϕ becomes the electrostatic potential (see Appendix B). The electrostatic potential can be solved as a variable during the computation of $\mathbf{J}$ [38], [39] or can be calculated from $\mathbf{A}$ from the following relation [42], [46]:

$$\nabla\phi(t) = -\frac{\partial \mathbf{A}(t, \mathbf{r}_0)}{\partial t} \tag{13}$$

where $\mathbf{r}_0$ is a position in the superconductor where $|\mathbf{J}| < J_c$; hence, $\mathbf{E} = 0$ [see (3)]. In long conductors and bodies with cylindrical symmetry, the single component of $\mathbf{J}$, i.e., J, vanishes at the current-free core and at the current fronts (boundaries between $J = +J_c$ and $J = -J_c$). In the thin-film approximation, $|J| < J_c$ in the under-critical region. It should be noted that the time derivative in (13) is the *partial* time derivative; thus, the time dependence of $\mathbf{r}_0$ should not be taken into account in evaluating the time derivative. From (9) and (13), the instantaneous power loss density is

$$p(t, \mathbf{r}) = J\left[\frac{\partial A(t, \mathbf{r}_0)}{\partial t} - \frac{\partial A(t, \mathbf{r})}{\partial t}\right]. \tag{14}$$

The given equation can be simplified for monotonic penetration of the current fronts, constant J_c, and infinitely long conductors or cylindrical symmetry. The deduction in the following follows the concepts from [5], [71], and [42]. Next, we present a deduction assuming any combination of a transport current and a uniform applied field proportional to each other. With monotonic penetration of the current fronts, the current density in the reverse and returning curves in an ac cycle, i.e., J_{rev} and

$J_{\rm ret}$, are related to the one in the initial curve, i.e., $J_{\rm in}$, [2], [3], [72] as

$$J_{\rm rev}(u) = J_{{\rm in},m} - 2J_{\rm in}\left[(1-u)/2\right]$$
$$J_{\rm ret}(u) = -J_{{\rm in},m} + 2J_{\rm in}\left[(1+u)/2\right] \quad (15)$$

where $J_{{\rm in},m}$ is the current distribution at the end of the initial curve, and u is defined as follows. For a transport current, $u(t)$ is such that $I(t) = u(t)I_m$, where I_m is the amplitude of the transport current. If there is no transport current but the applied field is created by a winding with a linear current–field characteristic, we define $u(t)$ as $\mathbf{H}_a(t,\mathbf{r}) = u(t)\mathbf{H}_m(\mathbf{r})$, where $\mathbf{H}_m(\mathbf{r})$ is the maximum applied field at position $\mathbf{r}$. This relation is also valid for the simultaneous action of a transport current and an in-phase applied field. For monotonic current penetration, there is always at least one point, which is called a kernel, where $J = 0$ in the whole cycle. Then, $\mathbf{r}_0$ in (14) becomes constant. Integrating the loss power density of (14) in the volume and integrating by parts for the time variable, we find that

$$Q = -\oint dt \int_V \frac{\partial J}{\partial t}\left[A(t,\mathbf{r}_0) - A(t,\mathbf{r})\right] d^3\mathbf{r} \quad (16)$$

where we took into account that J in each position changes once in each half-cycle and that this change is instantaneous from J_c to $-J_c$ (or *vice versa*). The time derivative of this discontinuous dependence is $\partial J(t,\mathbf{r})/\partial t = -2J_c\delta[t - t_c(\mathbf{r})]$, where δ is the Dirac delta, and $t_c(\mathbf{r})$ is the time of the shift of J at position $\mathbf{r}$. The time integration results in

$$Q = 4\int_V J_{{\rm in},m}(\mathbf{r})\left\{A\left[t_c(\mathbf{r}),\mathbf{r}_0\right] - A\left[t_c(\mathbf{r}),\mathbf{r}\right]\right\} d^3\mathbf{r}. \quad (17)$$

The relation of (15) is also valid for the vector potential A in the Coulomb gauge. Then

$$A(\mathbf{r},t) = \pm A_{{\rm in},m}(\mathbf{r}) \mp 2A_{\rm in}\left[\mathbf{r},\left(1 \mp u(t)\right)/2\right] \quad (18)$$

where the top sign is for the reverse curve, and the bottom sign is for the returning curve. The current density shifts its sign at the current front (see Fig. 2). For the initial curve, the current front encloses the flux-free region, where $\mathbf{B} = \mathbf{J} = 0$; hence, A is uniform. Then, A at the current front is the same as in the kernel. By taking this into account and using (18), the loss per cycle from (17) becomes

$$Q = 4\int_V J_{{\rm in},m}(\mathbf{r})\left[A_{{\rm in},m}(\mathbf{r}_0) - A_{{\rm in},m}(\mathbf{r})\right] d^3\mathbf{r}. \quad (19)$$

For a pure transport current, the given equation turns into

$$Q = 4J_c\int_V \left[A_{{\rm in},m}(\mathbf{r}_0) - A_{{\rm in},m}(\mathbf{r})\right] d^3\mathbf{r} \quad (20)$$

because, at the zone where $J_{{\rm in},m}$ vanishes, $A_{{\rm in},m}(\mathbf{r}) = A_{{\rm in},m}(\mathbf{r}_0)$. Equation (20) corresponds to the original formula from Norris [5]. The general equation (19) reduces to the one given by Rhyner for a uniform applied field [71].

3) Magnetization Loss: When the only time-dependent excitation is the applied magnetic field $\mathbf{H}_a(t,\mathbf{r})$, the expression for the ac losses per cycle can be simplified. Next, we take into account the ac losses in the *superconductor only*. In the following, we deduce several formulas for the magnetization loss. From (9), the density of the instantaneous power dissipation in the whole superconductor is

$$p = \mathbf{J}_s \cdot \mathbf{E} \quad (21)$$

where $\mathbf{J}_s$ is the current distribution in the superconductor. Then, the instantaneous power dissipation is $P = \int_V \mathbf{J}_s \cdot \mathbf{E}\ d^3\mathbf{r}$, where V is any volume containing the superconductor, and $d^3\mathbf{r}$ is the volume differential. The loss per cycle Q is the time integration in one cycle.

Using $\nabla \times \mathbf{H}_s = \mathbf{J}_s$, $\nabla \times \mathbf{E} = -\partial\mathbf{B}/\partial t$, the differential vector relation $(\nabla \times \mathbf{H}_s)\cdot\mathbf{E} = \nabla\cdot(\mathbf{H}_s \times \mathbf{E}) + (\nabla \times \mathbf{E})\cdot\mathbf{H}_s$, and the divergence theorem, we find that

$$P = -\int_V \mathbf{H}_s \cdot \frac{\partial \mathbf{B}}{\partial t}\, d^3\mathbf{r} + \oint_{\partial V} \mathbf{H}_s \times \mathbf{E} \cdot ds \quad (22)$$

where $\mathbf{H}_s$ is the magnetic field created by the superconductor currents, ∂V is the surface of the volume V, and ds is the surface differential. When the volume V contains not only the superconductor but also the sources of the applied magnetic field (the current or magnetic pole densities) and V approaches infinity, the second term of (22) vanishes. This can be seen as follows. Let us take V as a sphere of radius r. With large r, the largest contribution to the fields is their dipolar component. Then, $|\mathbf{H}_s| \sim 1/r^3$, and since $\mathbf{E} = -\partial\mathbf{A}/\partial t - \nabla\phi$ with $|\mathbf{A}| \sim 1/r^2$ and $|\nabla\phi| \sim 1/r^3$, it follows that $|\mathbf{H}_s \times \mathbf{E}| \sim 1/r^5$. Since the surface only increases as r^2, the integration vanishes with $r \to \infty$. Then, the instantaneous power loss is

$$P = -\int_{V_\infty} \mathbf{H}_s \cdot \frac{\partial \mathbf{B}}{\partial t}\, d^3\mathbf{r} \quad (23)$$

where V_∞ is the whole space. Note that (23) for the total power loss is general, although its integrand is no longer the local rate of power dissipation.

The ac losses per cycle Q as a response to a periodic ac field can be further simplified. If the whole system is in the void, $\mathbf{B} = \mu_0\mathbf{H} = \mu_0(\mathbf{H}_a + \mathbf{H}_s)$, and $\mathbf{H}_s \cdot \partial\mathbf{B}/\partial t = \mu_0[\mathbf{H}_s \cdot \partial\mathbf{H}_a/\partial t + (1/2)\partial|\mathbf{H}_s|^2/\partial t]$. When integrating in one cycle, the second term trivially vanishes, resulting in

$$Q = -\mu_0 \oint dt \int_{V_\infty} \mathbf{H}_s \cdot \frac{\partial \mathbf{H}_a}{\partial t}\, d^3\mathbf{r}. \quad (24)$$

Note that the applied field $\mathbf{H}_a(t,\mathbf{r})$ in the given equation is not necessarily uniform, and it may rotate during the cycle. In addition, the volume integral in (24) is not the instantaneous power loss.

For uniform $\mathbf{H}_a$, we can use the fact that $\int_{V_\infty} \mathbf{H}_s d^3\mathbf{r} = (1/2)\int_{V_\infty} \mathbf{r} \times \mathbf{J}_s d^3\mathbf{r} = \mathbf{m}$; hence, (24) becomes

$$Q = -\mu_0 \oint \mathbf{m} \cdot \frac{\partial \mathbf{H}_a}{\partial t}\, dt \quad (25)$$

where $\mathbf{H}_a$ may still rotate in one cycle. For an applied field in a constant direction, the ac losses per cycle are

$$Q = -\mu_0 \oint m_z dH_a \tag{26}$$

where we choose the direction of the z-axis as the direction of the applied field.

Next, we rewrite (24) in a more useful way for calculations using the $\mathbf{J}$ or $\mathbf{A}$ formulations. Using $\mu_0 \mathbf{H}_s = \nabla \times \mathbf{A}_s$, differential vector equality $(\nabla \times \mathbf{A}_s) \cdot \mathbf{H}_a = \nabla \cdot (\mathbf{A}_s \times \mathbf{H}_a) + (\nabla \times \mathbf{H}_s) \cdot \mathbf{A}_a$, and the divergence theorem, we find that

$$Q = -\oint dt \int_{V_\infty} \mathbf{J}_s \cdot \frac{\partial \mathbf{A}_a}{\partial t}\, d^3\mathbf{r} + \oint_{\partial V_\infty} \mathbf{A}_s \times \frac{\partial \mathbf{H}_a}{\partial t} \cdot ds. \tag{27}$$

Using the same arguments as for (22), the term with the surface integral vanishes. Note that, even if the applied field may be uniform in the superconductor, far away from its sources, it has to decay with the distance. Then, (27) becomes

$$Q = -\oint dt \int_{V_\infty} \mathbf{J}_s \cdot \frac{\partial \mathbf{A}_a}{\partial t}\, d^3\mathbf{r}. \tag{28}$$

For magnetic materials originated by a microscopic density of magnetic dipoles $\mathbf{M}$, it is practical to use formulas independent of the loss mechanism associated to the change of the local density of dipoles because they can be applied to any magnetic material. The variation of the free energy of a magnetic material is $\delta \mathcal{F} = -\int_V \mathbf{M} \cdot \delta \mathbf{H}_a$ [6, pp. 116]. The loss per cycle is the integration of the free energy in a cycle, i.e.,

$$Q = -\mu_0 \oint dt \int_V \mathbf{M} \cdot \frac{\partial \mathbf{H}_a}{\partial t}\, d^3\mathbf{r}. \tag{29}$$

From this formula, it is trivial to reproduce (25) and (26) for uniform applied fields. This formula can be also written in terms of the total magnetic field $\mathbf{H}$, i.e., $Q = -\mu_0 \oint d\mathbf{t}\ t \int_V \mathbf{M} \cdot \partial \mathbf{H}/\partial t$. For soft magnetic materials, $\mathbf{M}$ is practically parallel to $\mathbf{H}$. By taking this into account and neglecting the loss due to a rotation in the magnetic field, the loss per cycle is

$$Q \approx -\mu_0 \int_V \oint M dH = \mu_0 \int_V q(H_m, H_{\text{bias}})\, d^3\mathbf{r}. \tag{30}$$

The given equation assumes that the magnitude of the local magnetic field oscillates with amplitude H_m around H_{bias}. The quantity $q(H_m, H_{\text{bias}})$ is the density of hysteresis loss corresponding to this amplitude, which can be experimentally obtained. If the applied magnetic field oscillates with no dc component, $H_{\text{bias}} = 0$ for the whole volume. The density of hysteresis loss can be also written as a function of the magnetic flux density, i.e., B_m and B_{bias}.

For infinitely long wires and tapes, the power loss and the loss per cycle per unit length, i.e., P_l and Q_l, follow (23), (24), (28)–(30), after the replacement of the volume integration with the cross-sectional surface integration. The same applies to (25) and (26) but with the replacement of the magnetic moment $\mathbf{m}$ with the magnetic moment per unit length $\mathbf{m}_l$.

4) AC Losses From the Point of View of the Power Source: By continuity of the energy flow, the loss per cycle dissipated in the superconductor equals the energy per cycle supplied by the current sources. In general, a superconductor may be under the effect of a transport current or a magnetic field created by an external winding, which implies two current sources [74], [75].

If the model solves a single conductor in pure transport current or a complete superconducting coil, there is only one power source. The voltage delivered by the power source corresponds to the difference of the electrostatic potential $\Delta\phi$. Then, the ac losses per cycle in the coil are

$$Q = -\oint I \Delta\phi\, dt. \tag{31}$$

For the CSM, the drop of the electrostatic potential in each turn can be calculated from the scalar potential from (13) and by multiplying by the length of the conductor [76], [43]. The total voltage drop is the sum of the drop in all the turns.

Although (31) for the loss per cycle is valid, the instantaneous power dissipation in the coil not necessarily equals the instantaneous power delivered by the source, i.e., $I(t)\Delta\phi(t)$. The cause is the (nonlinear) inductance of the coil. This can be seen as follows. From (12) and (21), the instantaneous power ac losses are

$$P(t) = -\int_V \left(\mathbf{J}_s \cdot \nabla_\phi + \mathbf{J}_s \cdot \frac{\partial \mathbf{A}}{\partial t} \right) d^3\mathbf{r}. \tag{32}$$

Since there are no external sources of magnetic field, $\mathbf{A}$ in the Coulomb gauge only depends on $\mathbf{J}_s$ through (57). As a consequence, $\int_V \mathbf{J}_s \cdot \partial \mathbf{A}/\partial t\, d^3\mathbf{r} = \int_V \partial \mathbf{J}_s/\partial t \cdot \mathbf{A}\, d^3\mathbf{r}$. Then, $\int_V \mathbf{J}_s \cdot \partial \mathbf{A}/\partial t\, d^3\mathbf{r}$ is the time derivative of the magnetic energy $U = (1/2) \int_V \mathbf{J}_s \cdot \mathbf{A}\, d^3\mathbf{r}$. Thus, the time integral in one cycle of the second term in (32) vanishes. The remaining term is (31) because, in straight conductors, $\nabla\phi$ is uniform [77], as well as in each turn of circular coils [76].

If there is also an applied magnetic field, the total loss per cycle from (12) and (21) becomes

$$Q = -\oint I \Delta\phi\, dt - \oint dt \int_{V_\infty} \mathbf{J}_s \cdot \frac{\partial \mathbf{A}_a}{\partial t}\, d^3\mathbf{r} \tag{33}$$

where we follow the same steps as the reasoning after (32). The second term of (33) is the magnetization loss from (28). That formula is equivalent to (24), which reduces to (25) for uniform applied fields *in the superconductor*. Under this condition, the total loss in the superconductor is

$$Q = -\oint I \Delta\phi\, dt - \mu_0 \oint \mathbf{m} \cdot \frac{\partial \mathbf{H}_a}{\partial t}\, dt. \tag{34}$$

The first term is usually called "transport loss," whereas the second term is called "magnetization loss." If the applied magnetic field and the transport current are in phase, the transport and magnetization losses correspond to the loss covered by the transport and magnetization sources, respectively. This is because the sources are only coupled inductively; hence, the energy transfer from one source to the other in one cycle vanishes. Equation (34) is universal; thus, it is also valid when

the sources are not in phase to each other. However, in that case, the two terms in (34) cannot be always attributed to the loss covered by each source separately [75].

D. Solutions for Particular Cases

The purpose of this section is to gather a reference list of the hysteresis loss classified by topics. The number of published papers in the field is vast. Although we made the effort of making justice to the bulk of published works, a certain degree of omission is inevitable, and we apologize in advance to the concerned authors. Readers interested in a particular topic may go directly to the section of interest according to its title. In the following, we do not regard the case of [78]. A review on that problem can be found in another paper of this issue [78].

1) AC Applied Magnetic Field: The response to an applied magnetic field strongly depends on the geometry of the superconducting body, as discussed in [8] and [9].

The first works were for geometries that are infinitely long in the field direction because there are no demagnetizing effects. Bean introduced the CSM for slabs [1] and cylinders [3], and calculated the magnetization and the ac losses in certain limits. Later, Goldfarb *et al.* and Clem obtained formulas for the ac susceptibility for any field amplitude [79], [80]. The formula for the ac losses per unit volume is

$$\begin{aligned} Q_v &= \frac{2\mu_0 H_m^3}{3H_p} && \text{if } H_m < H_p \\ &= \frac{\mu_0 H_p}{3}\left(6H_m - 4H_p\right) && \text{if } H_m \geq H_p \\ &\approx 2\mu_0 H_p H_m && \text{if } H_m \gg H_p. \end{aligned} \quad (35)$$

In the given equation, H_m is the amplitude of the applied magnetic field, and $H_p = J_c w/2$, where w is the thickness of the slab. To obtain this equation, we used the fact that the ac losses per unit volume Q_v are related to the imaginary part of the ac susceptibility χ'' as $Q_v = \mu_0 \pi H_m^2 \chi''$. The imaginary part of the ac susceptibility (and the loss factor Q/H_m^2) presents a peak at an amplitude, i.e.,

$$H_{\text{peak}} = \frac{2}{3} J_c w. \quad (36)$$

This formula is useful to obtain J_c from magnetization ac loss measurements.

There are extensive analytical results for the critical state with magnetic field dependence of the critical current density $J_c(B)$ for infinite geometries. Most papers only calculate the current distribution and magnetization in slabs [81], [82]. The most remarkable analytical work for the ac losses is from Chen and Sanchez [83], who studied rectangular bars.

Comparisons between the CSM and a power-law $E(J)$ relation are in [84] for a slab and in [85] for a cylinder. The latter paper also finds that the frequency for which the ac susceptibility from the CSM and a power-law $E(J)$ relation is the most similar, at least for field amplitudes above that of the peak in χ''. This frequency is

$$f_c = E_c/(2\pi\mu_0 a^2 J_c) \quad (37)$$

where a is the radius of the cylinder. This frequency is based on an extension of the scaling law by Brandt [86]. This scaling law applied to χ'' reads

$$\chi''_{\text{PL}}(H_m, f) = \chi''_{\text{PL}}\left(H_m C^{\frac{1}{n-1}}, Cf\right) \quad (38)$$

where χ''_{PL} is χ'' for a power-law $E(J)$ relation, C is any arbitrary constant, and n is the exponent of the power law. Combining the scaling law in (38) with (37), one can find a relation between χ'' for the CSM, i.e., χ''_{CSM}, and that for the power law, i.e.,

$$\begin{aligned} \chi''_{\text{PL}}(H_m, f) &= \chi''_{\text{PL}}\left[H_m\left(\frac{f_c}{f}\right)^{\frac{1}{n-1}}, f_c\right] \\ &\approx \chi''_{\text{CSM}}\left[H_m\left(\frac{f_c}{f}\right)^{\frac{1}{n-1}}\right]. \end{aligned} \quad (39)$$

The first geometries with demagnetizing effects to be solved were thin strips and cylinders. For these geometries, conformal mapping techniques allowed to find analytical solutions for the CSM. Halse and Brandt *et al.* obtained the case of a thin strip in a perpendicular applied field [6], [72], although an earlier work from Norris developed the conformal mapping technique for a transport current [5]. The ac losses per unit volume are

$$\begin{aligned} Q_v &= \mu_0 w J_c H_m \left(\frac{2}{x}\ln\cosh\, x - \tanh x\right) \\ &\approx \mu_0 w J_c H_m \qquad \text{if } \mathrm{H_m} \gg \mathrm{H_c} \end{aligned} \quad (40)$$

where x is defined as $x = H_m/H_c$ with $H_c = J_c d/\pi$, and d and w are the thickness and width of the strip, respectively. For the same dimension w and low H_m, the ac losses per unit volume in a slab are smaller than in a thin film. However, the limit of high applied field amplitudes is the same for the strip and the slab, i.e., $Q_v \approx \mu_0 w J_c H_m$ [from (35) and (40)]. The peak of χ'' (and Q/H_m^2) is at an amplitude [87]

$$H_{\text{peak}} = 0.7845 J_c d. \quad (41)$$

The ac losses in a thin disk with constant J_c were obtained by Clem and Sanchez [88]. The solutions of the current and field distributions (as well as the magnetization) are analytical, although the expression for ac losses is in integral form.

In general, to solve the geometries with intermediate thickness requires numerical techniques. In the following, we first summarize the works on geometries for wires in a transverse applied field (rectangular, circular, elliptical, and tubular); then, the works on several of these wires parallel to each other (multiple conductors); afterward, the works on the case of wires under an arbitrary angle with the surface of the wires; and finally, the works on the solutions for several cases with rotational symmetry subjected to a magnetic field in the axial direction (cylinders, rings, spheres, spheroids, etc.).

Rectangular wires were studied in detail by Brandt, who calculated the current distribution and other electromagnetic quantities for a power-law $E(J)$ relation [23]. For the CSM, Prigozhin computed the current distribution [38], and

Pardo *et al.* discussed the ac susceptibility and presented tables in [87].

Circular and elliptical wires are geometries often met in practice. The main papers for the CSM are the following. The earliest work is from Ashkin, who numerically calculated the current fronts and the ac losses in round wires [10]. Later, several authors calculated the elliptical wire by analytical approximations, either by assuming elliptical flux fronts [8], [89], [90] or very low thickness [91]. Numerical solutions beyond these assumptions are in [40], [90], and [92], with the latter containing tables for ac susceptibility. Earlier work already solved this situation for a power-law $E(J)$ relation [93], [94].

The most complete work on tubular wires is from Mawatari [95]. This paper presents analytical solutions for the current and flux distribution, as well as the ac losses, in a thin tubular wire. The current distribution in a tube with finite thickness had previously been published in [40].

For the hysteresis loss in multiple conductors, it is necessary to distinguish between the uncoupled and fully coupled cases. These cases are the following. If several superconducting conductors (wires or tapes) are connected to each other by a normal conductor, either at the ends or along their whole length, coupling currents appear, and as a consequence, the ac losses per cycle depend on the frequency (see Section IV). The ac losses become hysteretic not only for the limit of high interconductor resistance (or low frequency) but also for low resistance (or high frequency), as shown by measurements [96] and simulations [54]. These limits are the "uncoupled" and "fully coupled" cases that we have introduced earlier. It is possible to simulate these two cases by setting different current constraints: For the uncoupled case, the net current is zero in all the conductors, whereas the fully coupled one allows the current to freely distribute among all the tapes [97]. For thin strips, there exist analytical solutions. Mawatari found the ac losses in vertical and horizontal arrays of an infinite number of strips [98] for the uncoupled case, and Ainbinder and Maksimova solved two parallel strips for both the uncoupled and fully coupled cases in [99]. The study of an intermediate number of tapes requires numerical calculations. Simulations for vertical arrays can be found in [100] and [101] for a power-law $E(J)$ relation and in [97] for the CSM. Complicated cross sections for the fully coupled case can be found in [102]. Matrix arrays for both the coupled and uncoupled cases are in [97] and [103]. A wire with uncoupled filaments is in [104]. A systematic study of the initial susceptibility in multifilamentary tapes with uncoupled filaments is in [105].

All the given results for single and multiple conductors are for applied magnetic fields parallel to either the thin or wide dimension of the conductor cross section. Solutions for intermediate angles can be found in the following papers. Mikitik *et al.* analytically studied a thin strip, but they did not calculate the ac losses [106], [107]. The ac losses in single conductors are in [25] and [108]–[110] for a power-law $E(J)$ relation and in [46] and [111] for the CSM. Solutions for arrays of strips for both a power-law $E(J)$ relation and the CSM are in [112]. The latter reference also reports that the ac losses in a thin strip with magnetic field dependence of J_c may depend on both the parallel and perpendicular components of the applied field; therefore, the ac loss analysis cannot be always reduced to only the variation on the perpendicular component of the applied field.

Next, we list the works for bodies with rotational symmetry. Apart from the analytical solutions in [88] and [113] for thin disks, the main works for cylinders subjected to a uniform applied field are the following. Brandt studied in detail several electromagnetic properties of cylinders with finite thickness in [24] and the ac susceptibility in [114] for a power-law $E(J)$ relation. Later, Sachez and Navau studied the same geometry for the CSM [44], and Chen *et al.* discussed the ac susceptibility and publish tables [92]. For cylindrical rings, the ac susceptibility and ac losses were calculated in [86] for thin rings and, in [115], for finite thickness. Pioneering works on the current distribution and ac losses in spheres and spheroids in the CSM can be found in [116]–[118]. Finally, the current distribution for several bodies of revolution can be found in [38] and [40].

All the numerical models discussed in Section II-A can solve the general situation of a conductor with an arbitrary cross section, either infinitely long or with rotational symmetry.

2) AC Transport Current: The effect of an alternating transport current in a superconducting wire (or tape) also depends on the wire geometry.

The simplest situation is a round wire because of symmetry. London calculated this situation in the CSM [2]. London ideated the CSM in parallel to Bean [1]. The ac losses per unit length Q_l in a round wire is

$$\frac{2\pi Q_l}{\mu_0 I_c^2} = (2-i_m)i_m + 2(1-i_m)\ln(1-i_m) \approx \frac{i_m^3}{3} \qquad \text{if } i_m \ll 1 \tag{42}$$

where the expression on the left is adimensional, $i_m = I_m/I_c$, and I_m is the current amplitude. Norris found that this formula is also valid for wires with an elliptical cross section (elliptical wires), which is based on complex mathematical arguments [5]. He also developed the technique of conformal mapping to calculate the current distribution in thin strips [5]. The resulting ac losses in a thin strip are

$$\frac{2\pi Q_l}{\mu_0 I_c^2} = 2\left[(1+i_m)\ln(1+i_m) + (1-i_m)\ln(1-i_m) - i_m^2\right] \approx \frac{i_m^4}{3} \qquad \text{if } i_m \ll 1. \tag{43}$$

Later, Clem *et al.* calculated the magnetic flux outside the strip [119]. They found the key result that it is necessary to use C-shaped loops closing at least the width of the strip in order to measure properly the ac loss. Contrary to the case of an applied magnetic field, thin films cannot be simplified as a slab with critical current density penetrating in a uniform depth across the film width. The formula for a slab from Hancox [120] can only be applied to estimate the ac losses due to the current penetration from the wide surfaces of the film, also known as "top" and "bottom" losses. Curiously, the formula for a slab exactly corresponds to the limit of low current amplitudes in (42).

Numerical methods are usually necessary to calculate the ac losses for other geometries or an $E(J)$ relation.

For an elliptical wire, Amemiya *et al.* compared the ac loss for the CSM and a power-law $E(J)$ relation [93]. Later, Chen and Gu further discussed this kind of comparison for round wires in [121], where tables for the ac losses are presented. They also found a scaling law for the ac losses, as for the magnetization case. The scaling law for the loss per unit length $Q_{l,\mathrm{PL}}$ is

$$\frac{Q_{l,\mathrm{PL}}}{I_m^2}(I_m, f) = \frac{Q_{l,\mathrm{PL}}}{I_m^2}\left(I_m C^{\frac{1}{n-1}}, Cf\right) \tag{44}$$

where I_m is the amplitude of the current, and C is an arbitrary constant. A study of the effect of the field dependence in an elliptical wire can be found in [94].

The effect of nonhomogeneity in the cross section of a round wire and a thin strip are discussed in [18] and [122], respectively. In summary, degraded superconductor at the edges of the conductor increases the ac loss and *vice versa*. A similar effect appears if the strips are thinner close to the edges [123].

The main results for rectangular wires with finite thickness are the following. Norris was the first to numerically calculate the current fronts and ac losses for the CSM [124]. Later, several authors published more complete works [87], [125], [126], where [87] also presents tables and a fitting formula. Results for a power-law $E(J)$ relation can be found in [127].

The following papers calculate the current distribution and ac losses in multiple wires and tapes connected in parallel; thus, the current can freely distribute among the conductors (the case of wires connected in series corresponds to coils, which is discussed in Section II-D6). The only analytical solution is for two coplanar thin strips in the critical state [99]. Numerical results that are always in the critical state for Bi-2223 multifilamentary tapes with several geometries are in [128] and [129]. The effect of arranging rectangular tapes in horizontal, vertical, and rectangular arrays is studied in [130]. A comparison between the CSM and a power-law $E(J)$ relation in a matrix array of coated conductors is in [103]. Valuable earlier work using a power law for several kinds of multifilamentary wires and tapes is in [102] and [131].

We review cables transporting alternating current in Sections II-D4 and II-D5.

3) Simultaneous Alternating Transport Current and Applied Field: This section outlines the results for superconducting tapes under the action of both an alternating transport current and a uniform applied field. First, we summarize the case of in-phase current and field and, afterward, with an arbitrary phase shift.

For a current and a field in phase with each other, analytical solutions only exist for slabs and strips in the CSM. Carr solved the situation of a slab and presented a formula for the ac losses [132]. (The reader can find the same formula in SI units in [42].) Later, Brandt and Indenbom and Zeldov *et al.* simultaneously obtained the magnetic field and current distributions for a thin strip [133], [134], and Schonborg deduced the ac losses from them [135]. However, as discussed in the original two papers [133], [134], the formulas are only valid when the critical region monotonically penetrates in the initial curve. This is ensured at least for the high-current–low-field regime, which appears for $I \geq I_c \tanh(H_a/H_c)$ with $H_c = J_c d/\pi$. The range

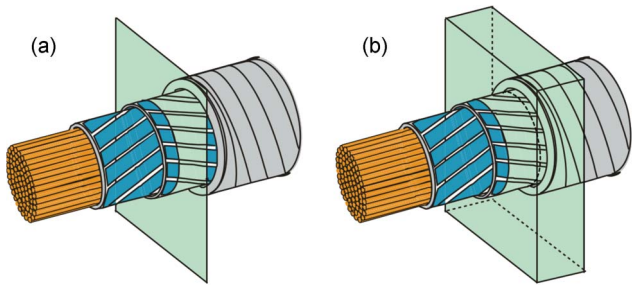

Fig. 5. Schematic view of a two-layer HTS power cable and of 2-D and 3-D regions to be considered for simulation. Figure taken from [59] and reproduced with permission from Institute of Physics (IOP).

of applicability of the slab and strip formulas compared with numerical calculations is discussed in [42]. In that reference, the current penetration process in a rectangular wire with finite thickness is studied in detail. However, the earliest numerical calculations are for a power-law $E(J)$ relation [26]. Elliptical wires with a power law are computed and discussed in detail by several authors [93], [27], [35], [136]. The latter reference also compares different shapes: round, elliptical, and rectangular wires. The main features for the thin geometry of a coated conductor is discussed in [31].

In electrical machines, the current and the magnetic field are not always in phase with each other. Analytical solutions for an arbitrary phase shift only exist for slabs [137] and strips [138] in the CSM and for low applied magnetic fields. These calculations predict that the ac loss maximum is when the alternating current and the field are in phase with each other. However, simulations for slabs [139] and elliptical wires [75], [140] show that, for large applied fields, the ac loss maximum is at intermediate phase shifts for both a power-law $E(J)$ relation and the CSM. Experiments confirm this fact [75], [140].

4) Power-Transmission Cables: The cross section of state-of-the-art power-transmission cables is of superconducting tapes lying on a cylindrical former, in order to minimize the ac loss. These tapes are spirally wound on the former, allowing the cable to bend (see Fig. 5). To estimate the loss, the cross section is often approximated as a cylindrical shell (or monoblock) because its solution in the CSM is analytical [120]. However, other analytical approximations may also be applicable [141].

Most of the models for the real cross section assume that the tapes are straight, neglecting the effect of the spiral shape; this corresponds to considering just the cross section in Fig. 5(a) and to assuming that it extends straight along the cable's axis. The error of this approximation is negligible for single-layer cables. Moreover, due to symmetry, the cross section in the computations can be reduced to a single circular sector [142]–[144]. Simulations for tapes with a ferromagnetic substrate show that its presence always increases the ac losses [145], [146]. In multilayer cables, the twist pitch of the tapes strongly influences the current sharing between layers [147]. One reasonable approximation is to assume that the twist pitch is optimum, so that all the tapes carry the same current independently of the layer that they belong to [148]–[150]. All the given numerical calculations are for a smooth $E(J)$ relation, although it is also possible to assume the CSM [151]. These computations show that nonuniformity in the tapes increases ac losses [151].

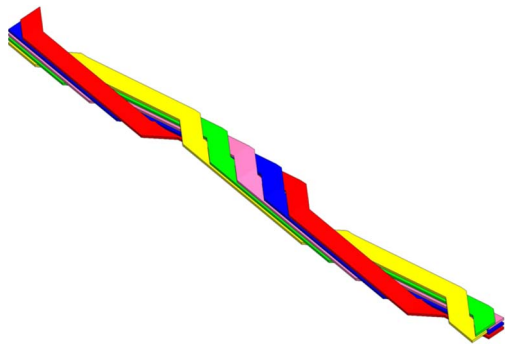

Fig. 6. Typical structure of a Roebel cable composed of meander-shaped strands obtained from ReBCO-coated conductors. Only half of the stands are shown for clarity.

Analytical solutions are more recent than numerical ones, due to the complexity of the deductions. These have been found for cables made of thin strips in the CSM. They show that, if the tapes are bent and, hence, the cable cross section is a tube with slits, the ac losses are lower than if the tapes are straight, forming a polygon [152].

The real spiral geometry is more complicated to compute. The first step has been to calculate the critical current [153]. AC loss calculations for cables made of Bi-2223 tapes require 3-D models [see Fig. 5(b)], resulting in high computing complexity, so that only coarse meshes are considered [32], [154]. More recent models for coated conductors improve the accuracy by reducing the problem to a mathematically 1-D [155] or 2-D [55], [59] one.

5) Roebel Cables: Roebel cables are compact transposed cables for windings that require high currents (see Fig. 6). Due to transposition, coupling loss is minimized.

The complicated structure of Roebel cables can be simplified with a 2-D approximation. If the transposition length is much larger than the cable width, the loss in the crossed strands is much smaller than in the straight parts. As a consequence, the cable can be modeled as a matrix of tapes (see [103] and [156] for more details). For an applied magnetic field, the computations distinguish between the "uncoupled" and "fully coupled" cases, as for multiple tapes (see Section II-D1), not only if the applied field is perpendicular to the strand surface [103] [156] but also for an arbitrary angle [112]. The equivalent can be also done for the transport loss, with the interpretation that the "uncoupled" and "fully coupled" cases are for transposed and untransposed strands [103], [156], [157]. The "uncoupled" case requires that the net current in all the strands is the same, whereas the "fully coupled" one allows the current to distribute freely among strands.

Until now, only two papers have taken the real 3-D bending into account [60], [158]. The work by Nii *et al.* is based on the T formulation and assumes the strands to be infinitely thin [60]. The authors calculate the current density and ac loss distribution in the "uncoupled case" for one example of transport current, applied magnetic field, and a combination of both. That work shows that there appear points of high loss density close to the crossing strands. This increases the ac loss comparing to cross-sectional models. The increase is important for low ac applied fields (and no transport current) because the current penetration in the crossed strands is much larger than in the straight parts. Otherwise, cross-sectional models do not introduce an error larger than 10% concerning the total loss. Zermeno *et al.* used the H formulation to develop a full 3-D electromagnetic model of a Roebel cable [158]. The use of periodic boundary conditions allowed simulating a periodic cell, keeping the number of degrees of freedom at a manageable level in this way. This model also reveals high-loss-density regions near the crossing strands in the case of applied perpendicular field. In the transport current case, the losses are mostly localized along the long edges of the strands, which supports the possibility of using a 2-D model for this case. Results are also compared with experimental data, showing a fairly good agreement; the observed mismatch for the magnetization losses is probably due to different reasons: for example, the fact that the experimental setup does not grant the perfect uncoupling of the strands (assumed in the simulations) and that the model does not take into account the dependence of J_c on the magnetic field.

6) Coils: The ac losses in the tape (or wire) that composes a superconducting coil is subjected to both a transport current and a magnetic field created by the rest of the turns. Since real coils are made of hundreds or thousands of turns, computations are complex.

Early calculations computed only the critical current, which already provided valuable information [159].

One possible simplification for the ac losses is to approximate that the effect of the whole coil in a certain turn is the same as an applied magnetic field. This applied field is computed by assuming that the current density is uniform in the rest of the turns. Afterward, the ac losses in the turn of study are estimated by either measurements in a single tape [160], [161] or by numerical calculations [162]. The problem of this approximation is that the neighboring turns shield the magnetic field from the coil [97], [101]. This situation is the worst if the winding consists of stacks of pancake coils because the whole pancake shields the magnetic field, as it is the case for stacks of tapes [97], [101].

There are several ways to take into account the nonuniform current distribution in all the turns simultaneously. The first way is to assume infinite stacks of tapes, describing only the ac losses at the center of a single pancake coil, either by analytical calculations for the CSM [163] or by numerical ones for a smooth $E(J)$ relation [164]. The second is to simply solve all the turns simultaneously for single pancake coils (pancakes) [39], [43], [76], [165], [166], double pancakes [167], and stacks of pancakes [112]. For this, it is possible to calculate the circular geometry [43], [76], [112], [165], [166] or assume stacks of infinitely long tapes [39], [167]. Finally, for closely packed turns, it is possible to approximate the pancake cross section as a continuous object [39], [168]. Semi-analytical approaches assume that the region with critical current is the same for all the turns [169], [170]. This condition can be relaxed by assuming a parabolic shape of the current front [168]. However, advanced numerical simulations do not require any assumption about the shape of these current fronts [39].

The presence of ferromagnetic materials strongly influences the ac losses in the superconductor. Magnetic diverters reduce

the ac losses in pancake coils [171], [172], whereas a ferromagnetic substrate increases it [167], [173].

7) Noninductive Windings: Noninductive windings are the typical configurations for resistive superconducting fault current limiters (SFCLs). The reason is the low inductance and low ac losses.

Modeling of this situation starts with two parallel tapes on top of each other transporting opposite current (antiparallel tapes). For thin strips, it is possible to obtain approximated analytical formulas because the ac losses are dominated by the penetration from the edges [5]. However, if the thickness of the rectangular wire is finite, numerical computations show that, for low current amplitudes, the ac losses is dominated by the flux penetration from the wide surfaces [124]. This contribution of the ac losses is called "top and bottom" loss [174]. For practical superconductors, the aspect ratio is high (at least 15 and 1000 for Bi-2223 and ReBCO tapes, respectively). For this cases, the ac losses for antiparallel tapes is much lower than if the tapes are placed far away from each other. Most of this ac loss reduction is lost if the tapes are not well aligned [175]. Degradation at the edges of the coated conductors also worsens the low-loss performance of the antiparallel configuration [176].

Bifilar windings (windings made of antiparallel tapes) reduce even further the ac loss if they are either made of elliptical wires [177] or coated conductors [174], [176]. The most favorable situation concerning ac losses is for bifilar pancake coils [176]. For strips in this configuration, there exist valuable analytical formulas [174]. There also exist analytical formulas for the equivalent of a bifilar coil but with all the strips on the same plane [178]. The ac losses for this configuration are larger than if the tapes are far away from each other, which is opposite to bifilar pancake coils.

8) Rotating Fields: Modeling the effect of rotating fields is very different if the magnetic field is either perpendicular to the current density or not.

For infinitely long wires or tapes in a transverse applied magnetic field, the local current density is always perpendicular to the magnetic field. All the numerical methods from Section II-B1 can solve this situation. The main feature of the current distribution is that it becomes periodic only after the first half-cycle that follows from the initial curve, as seen for cylinders [40], square bars [40], and rectangular bars [37]. This feature has an effect on the magnetization [179]. If the sample has been previously magnetized, a rotating field partially demagnetizes the sample after a few cycles [179], [180].

If the magnetic field is not perpendicular to the current density in part of the ac cycle, there appear flux cutting mechanisms in addition to vortex depinning; thus, the situation is more complex. This situation can be described by a double CSM with two characteristic critical current densities: one for depinning and another one for flux cutting [181]. This model allows calculating analytical solutions of the whole electromagnetic process, including the ac losses, for a slab submitted to a rotating magnetic field parallel to its surface [182]. An extension of this model takes into account a continuous variation of the critical current density as a function of the orientation of the electric field with respect to the current density [41], [183]. This model requires numerical methods to solve the current distribution [41], [183], [184]. Experimental evidence suggests elliptical dependence between the electric field and the critical current density [64].

9) Pulsed Applied Field: This section first summarizes the main modeling issues for bulk applications (slabs and cylinders) and, afterward, for coils in pulse mode.

Calculations for slabs show that, essentially, the response to a pulsed applied field is very similar to a periodic ac field [185], [186]. If the pulse starts from a zero applied field, then increases to a certain maximum H_m, and finally decreases to zero again, the response for the periodic case in the increasing and decreasing parts of the pulses is the same as the initial and reverse curves for a periodic ac field, respectively. For the CSM, the response is exactly the same, although for a smooth $E(J)$ relation, the instantaneous current and flux distribution depends on the shape of the pulse, as seen for slabs [185]. In case that there is a bias dc field superimposed to the pulse, the movement of the current fronts is exactly the same as for an ac field, except for the first increase in current. In addition, as a consequence of the dc field, there is a region with critical current density inside the sample. This has been analytically studied in [186].

The geometry of finite cylinders is more realistic to model bulk samples, but it requires numerical computations. The process of the current and flux penetration has been studied for the CSM [187] and for a power-law $E(J)$ relation [188]. The latter work also takes into account the self-heating effects caused by the changing magnetic field.

For the design of dc magnets, it is essential to consider the dissipation in pulse mode [189], [190]. There are several ways to model the loss in pulse mode. The first one is to use the measured ac losses of the cable in a pulsed applied field as a function of the peak field. The total energy loss is calculated from computations of the magnetic field of the coil by assuming uniform current density in the superconductor and by taking the corresponding measured loss in the cable into account [189]. The second way is to assume the slab model for the wire [190], which is a good approximation for large magnetic fields. The last way is to calculate the detailed current distribution in the whole magnet, as explained in Section II-D6.

10) AC Ripple on DC Background: The problems that a researcher can encounter in the modeling of the ac losses in a dc background are very different if the dc background is a transport current or an applied magnetic field. The case of a dc applied magnetic field perpendicular to the ac excitation is outlined in Section II-D11.

The situation of an ac applied magnetic field superimposed to a dc component in the same direction is basically the same as pulsed applied fields (see Section II-D9). After the increase in the applied field to the peak, the process of flux penetration is the same as a pure ac field. The only difference is that the critical current density is lower because of the presence of the dc component, as seen for slabs [186] and stacks of tapes in perpendicular applied field [191]. This concept is exploited to estimate the magnetization ac losses in complex coils due to current fluctuations around the working current. One possibility is to use analytical approximations for the ac losses in one wire [192].

An interesting case is when the dc applied field is in the same direction as a certain alternating transport current. For this situation, the ac transport current overwhelms the dc magnetization, approaching to the reversible value after a few cycles [193]. These calculations require advanced models because the magnetic field has a parallel component to the current density (see Section II-D8).

For a wire with a dc transport current and a transverse applied ac field, the most interesting feature is the appearance of a dynamic resistance [194]. This dynamic resistance appears for amplitudes of the applied magnetic field above a certain threshold. Analytical formulas exist for slabs with either a constant J_c [194] or a field-dependent one [195]. This case has also been numerically calculated for stacks of tapes, in the modeling of a pancake coil [191]. However, the applied fields are small compared with the penetration field of the stack; hence, the dynamic resistance may not be present.

A dc transport current may increase the loss due to an ac oscillation, as shown by analytical approximations for slabs and strips in the CSM [196]. These formulas also take an alternating applied field into account. Extended equations including also the effect of a dc magnetic field can be found in [197], where they are applied to optimize the design of a dc power-transmission cable.

11) AC Applied Magnetic Field Perpendicular to DC Background Field: Given a superconductor magnetized by a dc magnetic field, a relatively small ac magnetic field perpendicular to the dc one strongly reduces the magnetization (collapse of magnetization), as experimentally shown in [198]. The explanation is different if the sample is slab-like, with both applied fields parallel to the surface or if either the dc field is perpendicular to the sample surface or the sample has a finite thickness.

For a slab with both applied fields parallel to the surface, the collapse of the magnetization can only be explained by flux cutting mechanisms [198]. By assuming the double CSM, solutions can be analytically found for a limited amplitude of the ac field [198]. General solutions for continuous angular dependence between the critical current density and the electric field require numerical methods [62], [199].

For infinitely long wires in a transverse applied field, the current density is always perpendicular to the magnetic field independently of the angle with the surface. Then, flux cutting cannot occur. The collapse of magnetization is explained by the flux penetration process. This can be seen by physical arguments and analytical solutions for thin strips [200] and by numerical calculations for rectangular wires [201]. Collapse of magnetization is also present when the ac applied field is parallel to the infinite direction of a strip (and the dc one is perpendicular to the surface) [202].

12) 3-D Calculations: In this paper, we consider 3-D calculations as those where the superconductor is a 3-D object that cannot be mathematically described by a 2-D domain. A summary of the requirements and existing models for the 3-D situation is in Section II-B4.

The calculated examples are power-transmission cables made of tapes with finite thickness [32], [56], [154], multifilamentary twisted wires [55], two rectangular prisms connected by a normal metal [32], a permanent magnet moving on a thick superconductor [66], a finite cylinder in a transverse applied field [48], a cylinder with several holes [65], and an array of cylinders or rectangular prisms [56].

III. Eddy Currents

Eddy-current computations go beyond problems involving superconductivity. They are important for modeling electric machines, induction heaters, eddy-current brakes, electromagnetic launching, and biomedical apparatus, to name just a few applications [203]. Thus, we begin this section by shortly reviewing the key research done by the computational electromagnetism community. Then, we discuss the specific numerical methods to solve eddy-current problems and derive losses. Finally, we review some of the numerical loss computations related to nonsuperconducting and nonmagnetic but conducting parts present in technical superconductors.

A. Eddy Currents and Conventional Electromagnetism

Numerical simulations of eddy-current problems in conventional computational electromagnetism have been under investigation since the early 1970s [204], [205]. With the exception of some work done at the very beginning [206], [207], most of the early research concentrated on 3-D computations [205], [208], [209], and theoretical background for numerical eddy-current simulations is mostly established in 3-D space [210]–[213]. The need for 3-D modeling comes from practical electrotechnical devices, such as electric motors. It is necessary to model them in three dimensions to guarantee accurate simulations, which also include end effects [209], [214], [215].

In order to compute the eddy currents, the majority of researchers solved partial differential equations with the FEM [216]. However, since the computing capacity in the 1980s was relatively low, hybrid methods, combining the good sides of integral equation and FEMs, have also been widely utilized from various perspectives [208], [217]–[220].

The trend to analyze only 3-D geometries in conventional eddy-current problems characteristically differs from the approaches to model hysteresis losses in superconductors by treating them as conventional electric conductors with nonlinear power-law resistivity in two dimensions [51]. Typically, a 2-D analysis of superconductors is adequate to solve a wide class of problems, but in certain cases, a new and more accurate analysis also requires modeling in three dimensions in the case of superconductors [59], [221].

The analysis of a 2-D geometry results in simpler formalism and program implementation than the analysis in a 3-D one since, for a solution of eddy-current problem in two dimensions, it is not mandatory to solve all the components of a vector field [214]. However, edge elements for vector-valued unknowns have been used for more than twenty years [222]–[225], and their usability in 3-D eddy-current problems based on the vector potential is well known and demonstrated [226], [227], as well as in 2-D problems based on the H-formulation [228]. Nowadays, there are several publicly available or commercial software packages for eddy-current simulations

[229]–[232], and the visualization in postprocessing, skills to use the software, and the computation time are the major differences between 2-D and 3-D eddy-current simulations.

However, in 3-D eddy-current computations of conventional conductor materials, such as copper, not much attention is typically paid to the conductivity, which is expected to be constant. Naturally, this is a modeling decision since, for example, copper suffers from anisotropic magnetoresistance [233], [234]. Thus, the problem is closer to the problem of utilizing power law in 3-D geometries for superconductor resistivity than what the literature related to computations suggests. Anyhow, the good correspondence between the simulations and the experiments still suggests that the approximation of constant conductivity does not lead to severe errors in loss computations as it would in the case of superconductor simulations [235], [236].

B. Computation Methods for Eddy Currents

The methods to compute eddy-current losses from solved current density and/or magnetic field distributions do not differ from the methods used to solve superconductor hysteresis loss from a solution obtained with an eddy-current solver utilizing nonlinear resistivity for the superconductor. Thus, the main methods are the utilization of Joule heating and domain integrals and the integration of Poynting vector through surfaces surrounding the domain under consideration [228], [237], [238]. However, when one needs to separate the magnetization loss in the superconductor from the eddy-current loss, it is difficult to use the Poynting vector approach since these two domains are typically in direct contact with each other.

The main numerical methods for eddy-current simulations are the FEM, the integral equation method (IEM), and their combinations [203]. IEMs can be combined with FEMs in two ways: The boundary terms are computed either by the volume integration method [239] or by the boundary integration method [240]. Integration methods typically suffer from dense system matrices, but fast multipole acceleration considerably increases their speed [241]. However, to the best of our knowledge, these sophisticated methods are not available in commercial software packages.

All these methods can work with several formulations. Within these formulations, there is often the possibility to make different modeling decisions: For example, in the so-called $T-\Omega$ formulation, the field T can be solved by Biot–Savart integration [227] or by using the so-called cotree gauge [242]. Table I summarizes the main formulations used for eddy-current simulations with the most typical methods. Several other formulations with slight variations have been reviewed in [222].

C. Computation of Eddy-Current Losses in Superconductors

Although the primary concern for the computation of losses in technical superconductors is the hysteresis loss of superconducting materials, a numerical estimation of eddy-current losses is also important. Furthermore, methods to reduce eddy-current losses, at the expense of stability, are however well known, and low ac loss conductors have thus increased matrix resistivity [243], [244]. The contribution of eddy-current loss at power frequencies (below 200 Hz) to the total loss of a superconductor [245], [246] or a superconducting coil [247] is generally reported to be low, and many studies neglect these losses [248], [249]. This applies to both the silver-sheathed Bi-based conductors [245], [247] as well as to copper-stabilized layered YBCO-coated conductors [250], [163].

TABLE I
MOST COMMON FORMULATIONS AND SOLUTION METHODS FOR NUMERICAL EDDY-CURRENT COMPUTATIONS

Formulation	Solution method	Notes
$A-V$	FEM [216], [226], [227] FEM-BEM [219]	
$T-\Omega$	FEM [243], [22] FEM-BEM [208]	Two different gauges for T-field: co-tree and Biot-Savart
H	FEM [228] FEM-VIM [240] VIM [217]	Primarily used only in superconductivity community and with hysteresis loss computations of superconductors, not eddy current computations in normal metals

For a 1-cm-wide YBCO tape having YBCO layer thickness of 0.9 μm, copper stabilization of 50 μm, and self-field critical current of 260 A at 77 K, the hysteresis loss at 60-Hz sinusoidal current with peak current of critical current is 380 mW/m. The corresponding eddy-current loss in the copper stabilizer can be estimated to be in the order of 5 mW/m [250]. However, if the tape is brought to 4.2 K, the copper resistivity still decreases, and the eddy-current loss increases. The eddy-current power per unit length P_{eddy} in a copper stabilizer layer of a YBCO tape can be estimated as [163]

$$P_{\mathrm{eddy}} = \frac{4\mu_0^2}{\pi}\frac{twf^2}{\rho}I_c^2 h(i) \tag{45}$$

where t, w, and ρ are the copper stabilizer thickness, width, and resistivity, respectively. h is a complex function of normalized operation current i. At $i=1$, it receives a value of 0.03 and, at $i=0.5$, a value of 10^{-5} (see details in [163]). Thus, from this formula, we can conclude that the eddy-current loss in the stabilizer or the matrix is proportional to the second power of the frequency and inversely proportional to the resistivity of the normal metal; in addition, it also largely depends on the current amplitude.

If one wants to go a bit deeper in the analysis, one should note that a realistic operation current is considerably below the critical current; thus, the eddy-current losses can be on the level of hysteresis losses. In Bi-based Ag-sheathed tapes, the contribution of eddy-current losses is from 30% down to 1% when the operation current increases from $0.1I_c$ to $0.8I_c$ at a frequency of 60 Hz and a temperature of 77 K [251]. In addition, it should be noted that, at low currents, the filament arrangement can change the contribution of eddy-current losses at least from 5% to 30% of the overall losses. Thus, one should keep in mind that eddy-current losses in the matrix cannot be totally forgotten, although in many cases, they seem to give little contribution to the overall losses at power frequencies [252].

Eddy-current losses can be estimated from the overall loss measurements since their frequency dependence is different from hysteretic and resistive losses. The measured total average

loss power $P_{\rm tot}$ of a superconductor under periodic excitation can be expressed as

$$P_{\rm tot} = \underbrace{P_{\rm res}}_{RI_{\rm rms}^2} + \underbrace{P_{\rm hyst}}_{fQ_{\rm hyst}} + \underbrace{P_{\rm eddy}}_{\propto f^2} \tag{46}$$

where $P_{\rm res}$ and $P_{\rm hyst}$ are the average contributions of resistive and hysteretic losses in the sample, respectively; R is the sample's resistance along resistive paths where part of the current flows; $I_{\rm rms}$ is the RMS value of the excitation current; and $Q_{\rm hyst}$ is the superconductor hysteresis loss over one cycle. Thus, the loss in one cycle $Q_{\rm cycle}$ can be expressed as [253]

$$Q_{\rm cycle}(f) = Q_{\rm hyst} + \frac{P_{\rm res}}{f} + C_{\rm eddy} f \tag{47}$$

where $C_{\rm eddy}$ is a frequency-independent eddy-current loss constant (in joules per hertz). The constants $C_{\rm hyst}$, $P_{\rm res}$, and $P_{\rm eddy}$ can be extracted from measurements performed with the same amplitudes but varying frequencies.

In YBCO- and Bi-based tapes, materials with high conductivity, such as silver, need to be used to allow high-quality superconducting regions. Then, the eddy-current loss in these materials can pose a real challenge. In [253], the authors measured Bi-2223/Ag tapes with filaments from 1 to 55 and extracted the $C_{\rm eddy}$ factor of (47). They studied frequency range of 59–2500 Hz. Additionally, FEM modeling was performed to estimate the losses in the silver matrix. The modeling resulted in a prediction for eddy-current loss at least four times smaller than that extracted from simulations using (47). However, the measured eddy-current loss had negligible contribution to $Q_{\rm cycle}$ when the frequency was below 200 Hz, and the operation current was below 0.3 of the critical one.

IV. Coupling Losses

There is no wide consensus about what loss components are to be put under the term coupling loss [254]. This is because coupling losses and eddy-current losses have similar nature since they both arise from currents in nonsuperconducting parts of the conductor [255]. Additionally, filament coupling influences the current penetration profiles inside a superconductor; thus, it changes the hysteresis loss [103]. In this paper, with the term coupling loss, we indicate the loss that arises in normal conducting regions when a current loop going from a filament to another via normal metal is formed due to a time-varying applied magnetic field. Here, we discuss first about performing numerical simulations from which it is possible to extract the coupling loss. Then, we review how filamentary coupling affects hysteresis losses and how this can be simulated.

A. Simulating Filament Coupling Effects

Coupling loss simulations that take into account the real conductor geometry need in general to be performed with models having three spatial dimensions [256]. Important characteristics for the simulations that represent real-world cases are, at a minimum, the modeling of superconducting domain, the modeling of the normal metal matrix, and the modeling of the contact resistance between these two [255], [257].

For estimating coupling loss, there is no easy way to use analytical formulas, which work in general cases. The reason for this is that the actual filament distribution largely determines the coupling loss. Additionally, separation of coupling loss from other loss components, such as eddy-current loss, is difficult from measurement results since these losses have similar nature. However, in general, one can say that a short twist pitch in conductors results in low coupling loss, and low transverse resistivity results in increased coupling loss. For a given conductor, the coupling loss increases with the second power of frequency. Analytical approaches to coupling losses are reviewed in [258].

So far, FEM-like tools have been less frequently used to model coupling losses than hysteresis losses in superconductors. There are three main reasons for this. First, when the magnetic field is not perpendicular to the current density, it is uncertain what kind of a model or a constitutive law should be adopted to model currents in the superconductor [259]. This case is usual in 3-D geometries. The CSM does not work in this case; thus, it is doubtful to use also its power-law approximation. Although power law works in some simulations of simple geometries in three dimensions [32], [260], [262]–[264], experimental verification of these studies are missing. However, currently, there is ongoing interest in solving this problem [64], [183], [264]. Second, in three dimensions, it is not possible to obtain the same discretization level and, thus, accuracy, as in two dimensions. Since superconductor modeling is highly nonlinear, even solving small problems takes a considerable amount of time [32]. In three dimensions, real-world problems with low accuracy still typically require several tens of thousands of degrees of freedoms. Finally, methods to reduce coupling losses are very well known for filamentary superconductors [265]. These methods include twisting the conductor, increasing the matrix transverse resistivity, and using highly resistive barriers around filaments. Thus, particularly in LTSs, the coupling losses are small, and from the perspective of wire development and applications, the establishment of methods for coupling loss simulations has not been crucial. However, utilization of these manufacturing methods with a filamentary HTS, such as Bi-based or MgB_2 wires, is still an unknown issue. Additionally, these methods are not applicable for striated YBCO conductors as such, and there are many recent developments aiming at reducing YBCO ac losses by filamentarizing the end product [257], [266]–[269]. This effort must also include considerations on coupling losses; thus, their modeling is important since, even in the 10 Hz regime, the coupling loss in striated YBCO can be important [270].

An alternative way of modeling coupling losses in a program that solves directly Maxwell's field equations is the utilization of equivalent circuit models [269]. This kind of models have been mainly developed for LTS cables, such as cable-in-conduit conductors (CICC) [271]. These models are fairly complicated (as shown in Fig. 7) and require measurement of contact resistance between many points. However, they are still applicable to coupling loss simulations of Roebel cables [272], which also have a loose cable structure such as many CICCs [273].

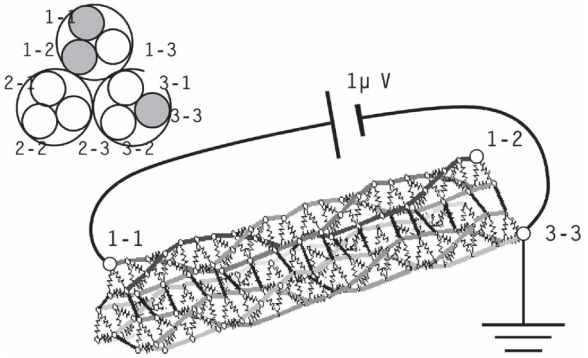

Fig. 7. Circuit analysis model for coupling loss computation of CICC. Reprinted with permission from Elsevier [271].

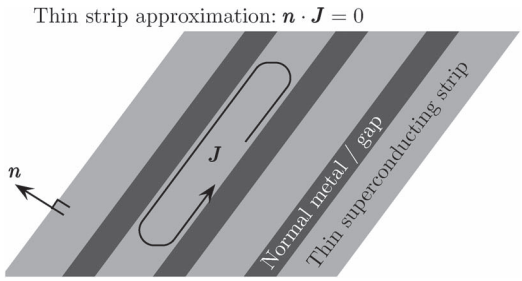

Fig. 8. Schematic view of the thin strip approximation of a striated YBCO tape. One magnetization current loop is shown for the case of uncoupled filaments.

In addition, when FEM-type simulations target high accuracy, the laborious characterization of interface contact resistance becomes mandatory anyway.

When coupling losses are modeled in thin conductors by directly solving the fields, it is possible to take 2-D approaches. It can be estimated that there is no current flow from the bottom of the tape to the top or *vice versa* [274]. This modeling decision is generally called thin strip approximation [257] (see Fig. 8). Striated YBCO conductors are examples of geometries that can be simulated with such approximation. Thus, although the tape can have complicated 3-D geometry, at every cross section, in local coordinates, one current density component always vanishes [59]. Since superconductor hysteresis losses are computed simultaneously to coupling losses, we will review this method more deeply in the following.

B. Influence of Filamentary Coupling on Hysteresis Losses

In 2-D hysteresis loss simulations of a multifilamentary conductor or a cable consisting of several conductors, it is necessary to make a modeling decision concerning filament coupling effects when a magnetic field is applied. However, typical programs consider only two extreme cases: Either the filaments are perfectly coupled or not coupled at all [103]. Full coupling means that the filaments interact together similarly to a single larger filament. Uncoupled situation means that filaments operate completely individually, although the fields that they generate can alter current distributions in the other filaments [274], [275].

Three-dimensional simulations are typically mandatory to study the intermediate cases, e.g., the effect of matrix resistivity and filament-to-matrix contact resistance on the current distribution in a superconductor [55]. Naturally, these 3-D simulations also consider actual sample sizes and do not require infinite long samples. However, for high-aspect-ratio tapes, such as YBCO, it is possible to assume that the current density is always parallel to the tape's wide surface. Then, the problem reduces to a 2-D one, which allows different solutions with intermediate coupling where the resistivity between the filaments is varied [274]. Naturally, in this model, coupling currents can only flow from the edges of the superconductor to the normal metal, which limits the use of this model to the study of in-plane coupling currents (see Fig. 8). The field problem in this thin strip approximation is formulated in terms of current density vector potential such that $\boldsymbol{J} = \nabla \times (\boldsymbol{n}T)$, where $\boldsymbol{n}$ is the unit normal to the computation surface, and T is a scalar field. The governing equation includes also integral terms since the field generated by the surface currents is computed by integral equations. Power-law resistivity has been used to model the electric behavior of the superconductor [274].

In [274], the influence of the resistance between striations of a multifilamentary YBCO tape on hysteresis loss and coupling loss was studied with the thin strip approximation. The striated YBCO tape had 20 filaments. When the frequency was below 5000 Hz, coupling loss increased with decreasing resistance between the filaments. Roughly, one order of magnitude increase in contact resistance between filaments decreased the coupling loss by one order of magnitude. In addition, the variation of hysteresis loss as a function of filament-to-filament contact resistance was studied. The difference of losses in the fully coupled case and the uncoupled case was a bit more than one order of magnitude. Losses computed with different values of contact resistance fell between these two limits. At 50 Hz, the coupling loss was still, in every case, much lower than the hysteresis loss, and the most important factor of the filamentary coupling was the change in hysteresis loss and not the amount of coupling loss. Naturally, these results depend largely on the number of filaments as well as on the presence of a stabilization layer. Additionally, in practical applications, the end of the YBCO tape needs to be soldered to current lead. Then, the filaments are well coupled, and introduction of filament transposition becomes mandatory.

In Figs. 9 and 10, we present typical current distributions for the two extreme case of fully coupled and uncoupled filaments, when an external magnetic field is applied. In these 2-D simulations, the current density is a scalar quantity, and it flows perpendicular to the modeling plane. We had two filaments, both having a radius of 0.5 mm and separated by 1 mm. The matrix eddy-current losses were neglected in this study. We applied vertical magnetic flux density $50\sin(2\pi ft)$ mT. We had field independent J_c of 127 A/mm^2. We utilized $A-V$ formulation for the simulation [36]. As shown, in the case of uncoupled filaments, the current density distributions look similar to one filament alone at the applied field. For the coupled case, the interaction of filaments is clearly visible. This leads to higher magnetization of the superconductor and, thus, to higher losses. Similar simulations for the cross section of YBCO Roebel cable were presented in [103].

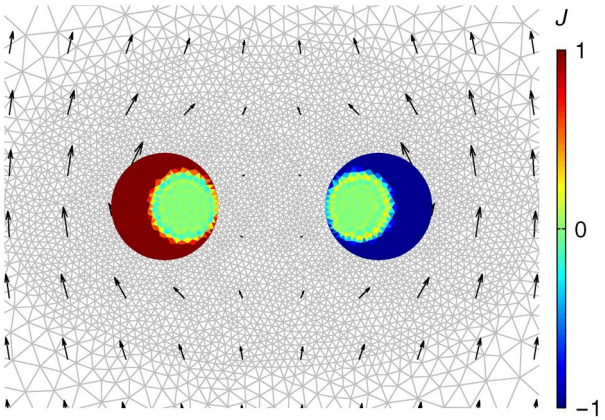

Fig. 9. Current penetration simulation of the coupled case. Red and blue represent currents toward and from the plane, respectively. Black arrows represent magnetic flux density vectors. Gray background presents the mesh for numerical computation. View is displayed from the time when applied field reaches its maximum.

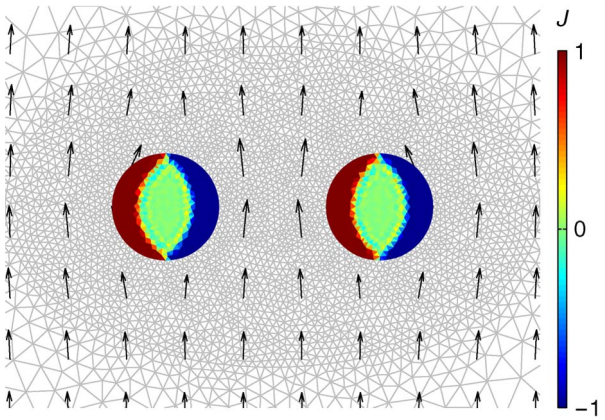

Fig. 10. Current penetration simulation of the uncoupled case. Details correspond to those in Fig. 9.

V. Influence of Magnetic Parts

The presence of magnetic materials in superconducting systems is not uncommon because magnetic materials can be a part of superconducting wires or a component of superconducting devices. YBCO-coated conductors manufactured by the Rolling-assisted Biaxially Textured Substrates (RABiTS) technique typically have a ferromagnetic substrate. First-generation HTS tapes (Bi-2223) or MgB_2 wires can be manufactured with magnetic stabilizer/reinforcing layers. Superconductors and magnetic cores are the primary components of many power applications, such as generators, transformers, and motors. The magnetic components can influence the ac losses in superconducting systems in two ways: 1) They change the magnetic profile inside the superconductor (thereby affecting the superconductor losses); and 2) they contribute additional hysteretic losses to the system. Therefore, the prediction of the effect of magnetic components on the total ac losses in a superconducting system is essential and has attracted significant effort from the research community.

In general, two types of approaches can be distinguished: analytical and numerical models. Analytical models provide relatively simple formulas to compute the losses in the superconductor; their main limitations concern the type of analyzed

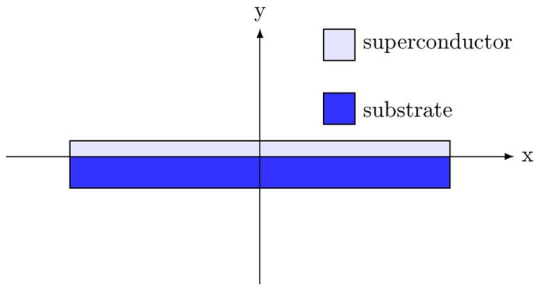

Fig. 11. Schematic view of the cross section of a YBCO-coated conductor with a magnetic substrate. Not drawn to scale.

geometries of the superconductor and/or the magnetic parts, the physical properties of the material (typically, CSM for the superconductor and infinite magnetic permeability for the magnetic material), and the fact that they neglect the losses in the magnetic material. On the other hand, numerical methods can overcome these limitations, although they generally require a larger computational effort.

In the following, we shortly review the main methods found in the literature. All of these models are usually solved for the 2-D cross section of a conductor or a device, which is perpendicular to the direction of the transport current. For example, these models can be used to calculate the magnetic and current density distribution in the xy plane for the cross section of a superconductor with ferromagnetic substrate, as shown in Fig. 11.

A. Analytical Models

Genenko *et al.* pioneered analytical calculations of ferromagnetic/superconductor heterostructures by investigating the effect of an infinite magnetic barrier placed next to a current-carrying superconducting strip [276]. It was found that the effects on the current density distribution inside the superconductor mostly depend on the barrier's shape and distance from the superconductor and only marginally on its magnetic permeability. The method was later used to propose configurations aiming at increasing the transport capability [277] and reducing the ac losses [278] of superconducting strips. The aforementioned models, however, consider magnetic domains that are not embedded in the structure of the tape or wire, and as such, they are not suitable to describe technical conductors used in applications, e.g., coated conductors with magnetic substrate or MgB_2 wires with magnetic material.

An analytical model to calculate the magnetic distribution and ac loss of an isolated YBCO tape with magnetic substrate of infinite permeability μ was proposed in [279]. This analytical model derives formulas to calculate the magnetic field, current distribution, and ac loss in a superconducting strip with a magnetic substrate (SC/FM strip conductors) for some special simple cases. In the model, a 2-D magnetic field, $H = (H_x, H_y)$ was considered as a complex field $H(\zeta) = H_{ay} + iH_{ax}$, where ζ is a complex variable $\zeta = x + iy$. The primary idea of the model is to solve the generalized Biot–Savart law for a SC/FM strip [279]:

$$H(\zeta) = H_{ay} + iH_{ax}) + \frac{1}{2\pi}\int_{-a}^{a} dx' \frac{K_z(x') + i\sigma_m(x')}{\zeta - x'} \quad (48)$$

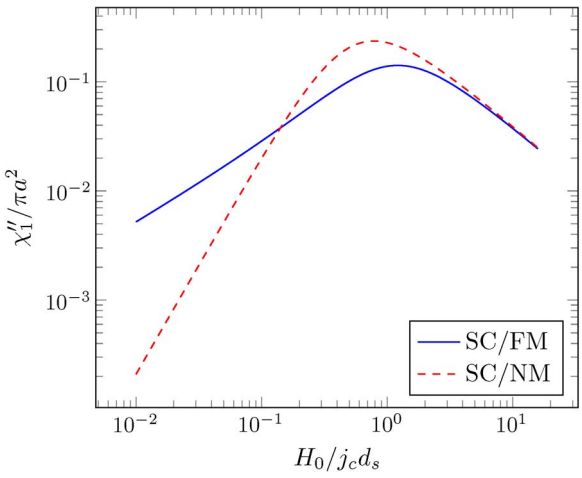

Fig. 12. Normalized imaginary part of ac susceptibility as a function of normalized applied magnetic field.

where $\mathbf{H}_a = H_{ax}\hat{\mathbf{x}} + H_{ay}\hat{\mathbf{y}}$ is a uniform applied magnetic field, $K_z(x)$ is the sheet current in the superconducting strip, and $\sigma(x)$ is the effective sheet magnetic charge in the ferromagnetic substrate. Both $K_z(x)$ and $\sigma(x)$ can be determined from Faraday's laws [6, Eqs. (4) and (5)] and must satisfy the following constraints: The total net current in the superconducting strip must be equal to the transport current, and the total net magnetic charge in the substrate is zero.

In order to be able to derive the explicit results for the current and magnetic field distribution, the model must assume that the ferromagnetic substrate is an ideal soft magnet with infinite permeability, i.e., $\mu \to \infty$. With this approximation, the outside of the magnetic substrate has only the perpendicular component on its surface. This determines the boundary condition at the surface of a ferromagnetic substrate.

First, the model was solved for a SC/FM strip conductor in the ideal Meissner state and exposed to either a perpendicular or parallel magnetic field, or a transport current. In the ideal Meissner state, the perpendicular magnetic field component on the surface of the superconducting strip must be zero.

Based on the CSM, formulas for the case of the SC/FM strip conductor exposed in a perpendicular dc or ac field were also derived. In ac perpendicular applied field $H_a(t) = H_0\cos(\omega t)$, the time dependence of magnetic moment per unit length $m_y(t)$ is derived explicitly and can be expressed as the Fourier series to determine the complex ac susceptibility $\chi_n' + i\chi_n''$ at the nth harmonics. The superconducting ac loss Q generated per unit length of a SC/FM strip in an ac perpendicular field can be therefore calculated from the imaginary part of the first harmonic χ_1'' as follows [88]:

$$Q(H_0) = \pi\mu_0 H_0^2 \chi''(H_0) \tag{49}$$

Fig. 12 plots the normalized imaginary part $\chi_1''/\pi a^2$ (a is the half width of the conductor) for the fundamental frequency $(n = 1)$ of the ac susceptibility as a function of normalized applied field $H_0/j_c d_s$ (j_c and d_s are the critical current density and thickness of the superconducting strip, respectively) for strip superconductors with ferromagnetic substrate (SC/FM) and without magnetic substrate (SC/NM).

Experimental results reported by Suenaga *et al.* in [280] indicated that, in perpendicular applied field, the ferromagnetic hysteresis loss in the Ni–W substrate of a RABiTS tape would be significantly lower than that in the superconducting layer and can be therefore negligible in the total magnetization losses. The model given predicted that magnetization losses in the SC/FM conductor are higher than those in the SC/NM counterpart at low applied fields, i.e., $\mu_0 H_0 < 0.14 j_c d_s$. For a conductor with $j_c = 1.2 \cdot 10^{10}$ A/m^2 and $d_s = 2.5$ μm, the crossing point $\mu_0 H_0 = 0.14 j_c d_s = 4.9$ mT is consistent with the experimental results reported in [280] for a YBCO tape with a Ni–W substrate. That quantitative agreement suggests that the model with infinite permeability can be used to quantitatively predict ac losses for a superconducting strip with a magnetic substrate of large but finite permeability exposed to a perpendicular applied magnetic field. However, this model currently does not apply for other important cases, which represent better for the real operating conditions of HTSs in devices, such as a SC/FM strip carrying an ac transport current or/and exposed to a perpendicular/parallel applied magnetic field. In addition, as already pointed out, this model does not provide a way to predict the ferromagnetic losses in the magnetic substrate, which may be significant in some situations [281], [282]. Thus, the accurate prediction of the total ac losses in an SC/FM system is difficult to be obtained with this analytical model, and numerical methods are therefore needed.

B. Numerical Models

Two numerical models have been widely used to compute losses in superconducting devices with magnetic parts, and they both employ the FEM. While those FEM models are supposed to be suitable with soft magnetic materials whose $\mu(H)$ is considered to be approximately the same for both the upper and the lower branches of a $B-H$ loop, they may be also applied for a system with hard magnetic materials by using $\mu(H)$ approximately determined from the virgin magnetization curve. An accurate model for hard magnetic materials that is capable of considering the hysteresis in $B-H$ loop would be very complicated and has not been developed yet.

1) H-Formulation FEM Model: The H-formulation FEM model to compute ac losses for superconducting systems with magnetic materials was first proposed in [281] and [282]. This model is capable of taking the field dependence of permeability and ferromagnetic loss of the magnetic materials into account. With respect to the standard version of the H-formulation [29], [228], the writing of Faraday's equation need to be modified to take into account that μ_r depends on H and, hence, on time. As a consequence, μ_r cannot be taken out of the time derivative in the governing equation

$$\frac{\partial(\mu_r\mu_0\mathbf{H})}{\partial t} + \rho\nabla\times\mathbf{J} = 0 \tag{50}$$

and the equation needs to be expanded. The details of the new formulations can be found in [281] and [282].

The hysteresis loss in the magnetic material Q_{fe} is the area of the $B-H$ loop and is usually a function of B_m, which is the maximum magnetic field of that loop. The hysteretic loss

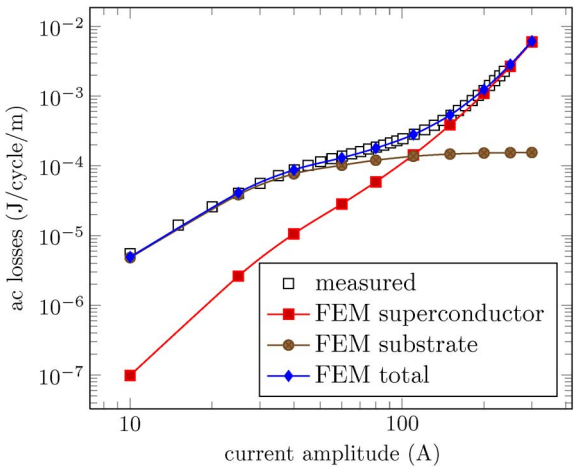

Fig. 13. FEM and experimental results for the ac loss components in a 1-cm-wide RABiTS YBCO tape ($I_c = 330$ A) carrying an ac transport current.

at each location inside the magnetic material can be therefore calculated from the maximum value of the induction field B_m at that location during an ac cycle. Therefore, based on the $Q_{\rm fe}(B_m)$ relation fitted from the experimental data, the total magnetic loss $q_{\rm fe}$ can be estimated by taking the integral of $Q_{\rm fe}(x, y)$ over the cross section $A_{\rm SUB}$ of the magnetic material [281], [282], i.e.,

$$q_{\rm fe} = \int_{A_{\rm SUB}} Q_{\rm fe}(B_m(x, y))dxdy. \tag{51}$$

This model is quite versatile and can be used for HTS devices with complicated geometries, as long as the field dependence of μ_r and $Q_{\rm fe}$ for the magnetic materials in the device are known. In fact, the model has been used extensively to calculate ac losses for superconducting systems using RABiTS-coated conductors with an Ni–W substrate. For this type of conductors, the field dependence of μ_r and $Q_{\rm fe}$ of the substrate material was determined experimentally and published in [283]. The functions fitting the experimentally observed field dependence of μ_r and $Q_{\rm fe}$ were entered in the model and used for the calculation of ac losses [281], [282]. As an example, Fig. 13 shows the comparison between calculated and measured total transport losses in a RABiTS tape as a function of transport current. In the simulation, the superconducting loss in the YBCO layer and ferromagnetic loss in the substrate were calculated separately, and the sum of these loss components provides the total self-field loss in this sample. In general, the modeled total self-field loss agrees well with that obtained from the measurement. The good agreement between simulations and experiments was also observed for other cases of RABiTS conductors with Ni–W substrates, such as the total ac loss in parallel applied field [281], the total ac losses for stacks of two parallel tapes [282], bifilar coils [284], racetrack coils [167], pancake coils [285], [286], or cables [287].

2) A-Formulation FEM Method: This method is based on the following general equation:

$$\nabla \times \left(\frac{1}{\mu}\nabla \times \mathbf{A}\right) = \mathbf{j} = -\sigma\left(\frac{\partial \mathbf{A}}{\partial}t + \nabla\phi\right) \tag{52}$$

where $\mathbf{A}$ is the magnetic vector potential, and ϕ is the scalar potential. For infinitely long conductors and circular rings, ϕ is constant in the cross section. Miyagi proposed a 2-D edge-based hexahedral finite-element modeling technique to solve that equation with constant and variable μ. At the beginning, (52) was solved for conductors with a substrate of constant μ, but a considerable discrepancy between calculated results and experimental data was observed [288]. The model was therefore improved to take the field dependence of permeability into account for better accuracy [289]. The authors used the Newton–Raphson method to handle the nonlinearity of permeability of the substrate. The detailed algorithm and techniques used to solve (52) with nonlinear $\sigma(j)$ and $\mu(B)$ can be found in [289]. This model, however, has not been validated against experiment. Although authors did not use this method to predict the ferromagnetic loss in the substrate material, this can be done by a similar way as presented in the H-formulation technique.

Another numerical technique to solve (52) was introduced in [45]. This method is based on the CSM and two assumptions: 1) There exists a "neutral zone" inside the conductor where the current density j (or the electric field E) vanishes during the entire cycle; and 2) the magnetic flux monotonically penetrates from the surface when the applied current or magnetic field increases monotonically. Because the electric field is zero, the vector potential A_c in the neutral zone must be uniform and satisfies $\nabla\phi = -\partial\mathbf{A}_c/\partial t$. Then, the authors introduced a new variable, the so-called calibrated vector potential $\mathbf{A}' = \mathbf{A} - \mathbf{A_c}$, which is zero in the neutral zone. The electric field can then be calculated by the following simple equation:

$$\mathbf{E} = \partial\mathbf{A}'/\partial t. \tag{53}$$

Since $\mathbf{A}'$ in the neutral zone is zero, $\mathbf{A}'(x, y, t)$ is the magnetic flux per unit length between the neutral zone and the point (x, y). Thus, based on the CSM, the current density from one time step can be analytically calculated from the calibrated vector potential of the previous time step. The ferromagnetic hysteretic loss in the magnetic material was estimated by a similar technique, as described in the H-formulation method. The details of the calculation procedures can be found in [45].

The authors employed the model to calculate ac losses in a Bi-2223 conductor with an elliptical cross section for two cases: 1) a conductor carrying an ac transport current; and 2) a conductor exposed to a perpendicular applied ac field. The edges of the conductor are covered with ferromagnetic material (Ni) for ac loss reduction. As an example, Fig. 14 depicts the calculated evolution of magnetic and current density profiles in that conductor when the applied field changes from 5 to 50 mT. The theoretical results of ac losses in this conductor were then compared with the experimental data [45]. The quite good agreement between the theoretical prediction and the experimental data has validated this numerical method, and it can provide another option to calculate ac loss and electromagnetic behavior in a SC/FM system [290].

3) Other FEM-Based Models: Other numerical models, based on the FEM, have recently been developed to study the interaction of superconducting and magnetic materials.

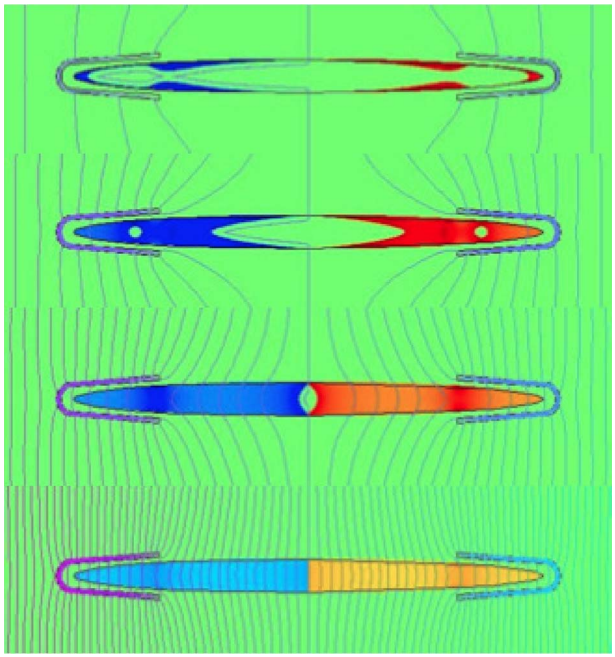

Fig. 14. Evolution of magnetic and current density profiles calculated for the initial increase in the perpendicular magnetic field. From top to bottom, the applied fields are 5, 12, 22 and 50 mT, respectively. Density of electrical current is characterized by the darkness of the color, the magnetic field is represented by the lines of constant vector potential. Figure taken from [45] and reprinted with permission from IOP.

TABLE II
IDEAL AND PRACTICAL CARNOT SPECIFIC POWER FOR OPERATING TEMPERATURE FROM 4.2 TO 273 K

Operating temperature T_{op} (K)	Carnot specific power	Realistic specific power (when heat load > 100 W)
273	0.11	0.4
77	2.94	12-20
50	5.06	25-35
20	14.15	100-200
4.2	71.14	11000

TABLE III
SUMMARY OF THE ESTIMATED HEAT LOAD OF HTS DEVICES AT THE OPERATING TEMPERATURE

HTS Component	BSCCO Heat load	YBCO Heat load
Cables (per phase)	3-5 kW/km at 65-80 K	3-5 kW/km at 65-80 K
Transformers (5-100 MVA)	50-100 W at 25-45 K or at 65-80 K	50-100 W at 60-80 K
Motors (1-10 MW)	50-200 W at 25-40 K	50-200 W at 50-65 K
Generators (10-500) MW	100-500 W at 25-40 K	100-500 W at 50-65 K
FCLs	10's W at 30 K 750 W at 80 K	1kW at 50-80 K
SMES	10's W at 20-30 K	10-100 W at 50-65 K

Genenko *et al.* [291] studied the influence of the shape of magnetic shields to reduce the ac losses in a superconducting strip. It was found that not only the shape of the shield but also the magnetic permeability of the magnetic material plays a key role for that purpose if the size of the shield is comparable to or less than that of the superconductor. The same group also developed a model to simulate superconducting strips with magnetic substrate in applied ac field based on an electrostatic–magnetostatic equivalence [292].

Farinon *et al.* extended their adaptive resistivity algorithm [293] to take into account magnetic materials [294].

VI. AC LOSSES IN HTS POWER APPLICATIONS

Calculation of ac losses is essential for HTS power applications since the design of the cooling systems needs to take into account the thermal loads. The cooling system maintains the required cryogenic temperatures during the operation of HTS devices. AC loss is a contribution source of the heat load; thus, the importance of ac loss lies in two aspects: The calculation is essential for the engineering design of cooling systems, and the calculation acts as a guide to explore methods for minimizing ac losses. This section discusses the impact of the ac losses in the most important power applications and the main contribution of the ac loss for each case.

A. Cryogenic Considerations

One important reason why HTSs are very attractive is that they can operate without liquid helium, which is a very expensive type of cryogen. Both BSCCO- and YBCO-based superconductors can operate at 77 K; the price per liter of liquid nitrogen is 20–100 times lower than that of liquid helium depending on the purchase location [295]. The latent heat of liquid nitrogen is 161 kJ/L at one atmosphere [296].

In order to achieve a larger critical current and higher magnetic field, HTS devices are operated at temperatures lower than 77 K with the aid of cryocoolers. One important parameter in determining the efficiency of cryocoolers is Carnot efficiency. The inverse of the Carnot efficiency is called the Carnot specific power and is the number of watts required at ambient temperature to provide 1 watt of refrigeration at the lower operating temperature. Column 2 in Table II presents the ideal Carnot specific power (watt input per watt lifted) [297]. However, commercial refrigerators run only at a fraction of Carnot efficiency; thus, column 3 gives a more realistic value for the specific power (watt input at 303 K per watt lifted at $T_{\rm op}$). Thus, in the cryogenic system design, the cooling power required for removing the heat load due to the ac losses can be calculated using Table II. Table III summarizes the estimated heat load of HTS devices at the operating temperature [297].

B. Techniques for AC Loss Reduction

Ac loss calculation can be used to find solutions to reduce ac losses of HTS power devices.

As it has been described in this paper, ac losses have different components: hysteretic, ferromagnetic, eddy-current, and coupling current losses. Hysteresis losses can be reduced by decreasing the filament size [243]. Eddy-current losses can be

reduced by increasing the stabilizer resistivity. Coupling current losses can be reduced by increasing the matrix resistivity. Ferromagnetic losses can be eliminated by avoiding ferromagnetic materials.

There are a few general methods for reducing ac losses of HTS applications. Controlling the amplitude and magnetic field orientation are effective ways for reducing ac losses [298], [299]. Using flux diverters or shielding layers are common means to reduce the magnetic field, which in turn reduces ac losses. Since HTS-coated conductors produce significantly higher ac losses in a perpendicular magnetic field, reducing the perpendicular component is an effective way to lower the ac losses.

The large cross-sectional aspect ratio of HTS-coated conductors leads to a large hysteresis loss in external fields. Filamentization of the coated conductor proved to be effective in reducing hysteresis losses [300], [301]. Sumption *et al.* pointed out that the losses for a coated conductor subdivided into ten filaments is shown to be reduced significantly [301]. However, filamentarization introduces coupling losses, caused by the relatively good conductivity of nonsuperconducting barriers and remnant superconducting "bridges" between neighboring strips [302]. Another contribution of losses in a striated conductor comes from magnetic flux coupling between filaments because magnetic field distribution inside the superconducting filaments is influenced by the field concentration in the nonsuperconducting region [302].

C. Electrical Power Applications

In this section, ac losses in various applications of HTS power applications are briefly reviewed. Typical techniques for reducing losses in different applications are described.

1) Rotating Machines: In an ac synchronous machine, superconducting coils can either be used as armature coils or rotor coils. If used as stator coils, superconductors will carry an ac and will be exposed to a rotating field, thus producing large ac losses [303], [304]. If used as the rotor coils, the magnetic field of the superconducting coils is phase-locked with the stator field. Under balanced load conditions, the rotor experiences a dc field from the armature. However, nonsynchronous disturbances, which are usually a result of unbalanced loads, transient events caused by system faults, and noise from the grid, can produce nonsynchronous ac effects that affect the superconducting coils on the rotor. The induced time-varying fields in the armature at frequencies other than the synchronous frequency induce compensating ac in the field windings, which in turn causes ac losses in the superconducting coils on the rotor. In a synchronous superconducting wind generator design, the superconducting coil windings on the rotor will also experience external ripple field from the power electronics excitation ripple and wind turbulence. This effect is investigated in [305].

In the Siemens 4-MW demonstration motor experiment [306], superconducting coils are used as rotor coils, whereas conventional copper coils are used in the armature. The experiment shows that the associated rotor losses, including ac losses, are smaller than 120 W, which would cost 10-kW compressor power; thus, the cooling system would decrease the system efficiency by $10\ \text{kW}/4\ \text{MW} = 0.25\%$, which is quite small for a large-scale application [306]. This power requirement is encouraging because it shows that the cooling system to remove the heat load is not a significant barrier for a large superconducting machine.

2) Power-Transmission Cables: In HTS power-transmission cables, superconducting tapes are usually helically wound around a cylindrical former. A very simple but useful model for calculating ac loss is the "monoblock" model in which the cable is considered as a tube of superconductor [141]. Although the monoblock model does not take into account the interaction between phases and the geometry of the tapes, it constitutes a frequently used engineering estimation for large-scale applications [307].

Another useful model is the electrical circuit model [308], [309], which models cables with resistance and inductance connected in series and in parallel. The resistance values are calculated from Norris equation, whereas the inductance values are calculated from self-inductance and mutual inductance formulas. This model is able to take into account the interaction between the conductor layers, the insulation layer, and the shielding layer.

Clem *et al.* proposed that the ac loss of HTS power-transmission cables could be broken down into six different mechanisms [310]: Bean model losses as in a Bean slab, losses in helically wound phase conductors arising from finite gaps between adjacent tapes, losses arising from the polygonal configuration of the conductor cross section if the tapes do not conform to the cylindrical former, flux cutting loss, losses when the current exceeds the critical current, and losses in the possible magnetic substrates.

The key parameters affecting ac losses in power-transmission cables are the number of conductors, the conductor's width, the gap size between adjacent tapes, and the radius of the former and the current distribution. One common design of superconducting cables is the monolayer design. AC losses in a monolayer cable do not significantly increase over one single tape since most of the flux lines lie outside the superconducting layers in the cable. It has been found that using narrower tapes and/or decreasing gaps between adjacent tapes are effective solutions for ac loss reduction [257], [311]. Due to the mechanical requirements and architecture of the conductor, a monolayer cable consisting of 2.5–4-mm-wide tape would have minimized ac losses [312], [313].

In a two-layer counter-wound cable using coated conductors, gap, and polygonal losses, flux transfer losses in imbalanced two-layer cables and ferromagnetic losses for conductors with magnetic substrates are the major contribution to ac losses [310]. Current imbalance and ferromagnetic losses can be minimized by orienting the substrates of the inner winding inward and the outer winding outward [310].

In multilayer cables, the ac losses behave differently. It has been found that ac losses in cables with many layers are hardly affected by gaps between adjacent coated conductors, as well as a lateral critical current distribution [313].

3) Compact High-Current Cables: Different from power-transmission cables, superconductors are often required to be

parallel or stack placed to create a high-current-density cable for applications in high-field magnets and busbars. Several kiloampere to tens of kiloampere cables are expected in these applications.

Twisting and transposition are typical methods for reducing ac losses in parallel and stack-placed superconducting cables [103], [243], [301]. This is because magnetic flux coupling can be reduced by transposing the conductors. However, it is not easy for HTSs be transposed as LTS wires since, often, HTSs are made into flat tapes. Recently, significant effort has been devoted to develop HTS Roebel cables, Rutherford cables, and other types of a twisted stack of coated conductors for high-current applications [314]–[316]. Filamentarization is another technique to reduce ac losses in high-current cables [252]. In addition, decreasing the aspect ratio (width/thickness) of the cable by assembling stacks of strands instead of individual strands in cables can also reduce ac losses [156].

4) Fault Current Limiters: For resistive-type SFCLs, it is preferable to contain a long length of superconductors in a small volume. One type of SFCLs uses an array or a matrix of superconducting tapes [317]–[319]. Fo. For ac loss calculation, a stack of superconductors can be modeled for this type of SFCLs [319]. Another design is to use a noninductive superconducting coil [174], [284]. To calculate ac losses of this type of SFCL, HTS coils need to be studied [174], [284]. In the dc-biased iron-core-type SFCL, superconducting coils carry dc; thus, there are no ac losses [320]. To calculate losses in the shielded iron-core-type SFCL, one needs to analyze the ac losses of a superconducting bulk cylinder or a tape.

An effective way to reduce ac losses in a resistive SFCL is the bifilar design [174]. This design can significantly reduce the inductance and also ac losses by decreasing the magnetic field volume [321]. Another technique for reducing ac losses is to use the two-in-hand structured wire [284]. The loss of a coil using two-in-hand structure wire is only half of that generated in an isolated tape per unit length. The ferromagnetic losses can be minimized by orienting the substrates of the inner winding layer inward and the outer winding outward (face-to-face configuration [310]).

In a commercial 12-kV resistive SFCL, ac losses account for 60% of the total thermal load [321].

5) Transformers: From the point of view of engineering design, ac losses in transformers can be regarded as ac losses in HTS coils. AC losses come from the transport losses in the primary and secondary windings and the magnetization losses due to the magnetic fields, in particular, the leakage magnetic field in the end region of superconducting windings. One technique for reducing losses is to use a compensation coil to cancel the unwanted magnetic field, particularly the perpendicular component. Heydari *et al.* discussed how to use auxiliary windings to reduce the leakage magnetic field, hence, the ac losses [322]. Another way of reducing leakage magnetic field is by using flux diverters to shape the field. Al-Mosawi *et al.* examined the validity of this method and proved that ac losses are reduced by 40% in a 10-kVA superconducting transformer using Bi-2223 conductors [323]. Low-ac-loss conductor designs, e.g., Roebel cables, are also proposed to be used in transformers for carrying a large transport current [315]. In an example study, it is estimated that the losses only reduces the efficiency by 0.2% in a 800-kVA transformer using BSCCO-2223 tapes, with a penalty factor of 20 taken into account [324], [325]. This shows that, such as in a large superconducting machine, the cooling power is only a fraction of the total output power of superconducting transformers.

6) Superconducting Energy Storage: The energy storage devices in superconducting energy storage systems (SMES) are superconducting magnets. The ac loss associated with changing currents and magnetic fields are nearly zero if the magnets operate in storage mode. The two significant continuous energy losses for HTS magnets are the joint resistance of HTSs [326] and the normal resistance in the power electronics transistors. However, ac losses may occur in the system as a result of variation in the operating current and magnetic field due to the charging or discharging of energy [327]. The ac loss per unit time might be significantly higher than in normal conditions during a discharge process since a SMES is expected to react quickly in response to a grid incident, i.e., a quick discharge to maintain grid stability [328]–[330]. In certain discharge circumstances, the ac loss per unit time will be much larger than a cryocooler capacity. An example study shows that, for 1 s of the discharging time in a 600-kJ SMES system, the total ac loss is 167.2 W, which is a large amount of heat, increasing the system temperature by 3 K [331]. Thus, the temperature rise during a discharge process should be analyzed in the design work. The ac loss calculation is also essential for a SMES cyclic efficiency estimation.

VII. Conclusion and Outlook

We have presented a review of the literature on ac loss computation in HTS tapes, wires, and devices. Two-dimensional calculations by different methods are now fully developed to the point that ac losses in superconductors with geometries of arbitrary complexity can be quickly computed with good accuracy. Magnetic materials can be also taken into account, and at least with certain models, their nonlinear magnetic characteristics can be modeled. In addition, situations different from pure ac excitations (such as ramps, pulses, and combination of ac and dc field and currents) can be handled. We are confident to say that all the situations relevant for realistic applications can be modeled in 2-D.

The most challenging step for the scientific community will be the extension to 3-D calculations. The challenge resides not only in the numerical difficulties related to 3-D modeling (choice of the mesh, increase in memory requirements, and computation time, etc.) but also in the choice of an appropriate constitutive relation for modeling the different types of superconductors in 3-D and in its implementation in the numerical codes.

AC losses in different electrical power applications are investigated and summarized. It can be concluded that ac loss calculation in such applications is important for cooling system design and examining innovative methods for heat load reduction.

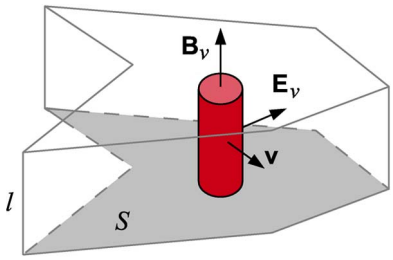

Fig. 15. Vortex moving at velocity $\mathbf{v}$ creates an electric field $\mathbf{E}_v$ due to its magnetic field $\mathbf{B}_v$. The cylinder represents the magnetic core of the vortex. The wire figure is an arbitrary integration volume (see Appendix A).

Appendix A
Electric Field Created by Moving Vortices

This appendix outlines the main steps to obtain the macroscopic electric field created by moving vortices, i.e., (11).

The electric field created by a moving vortex, i.e., $\mathbf{E}_v$, at a certain speed $\mathbf{v}$ is as follows. This electric field is $\mathbf{E}_v = -\partial \mathbf{A}_v/\partial t - \nabla \phi_v$, where $\mathbf{A}_v$ is the vector potential in the Coulomb gauge, and ϕ_v is the scalar potential. The time dependence is due to the movement of the vortex. Then, $\mathbf{A}_v(t, \mathbf{r}) = \mathbf{A}_v[\mathbf{r} - \mathbf{r}_v(t)]$, where $\mathbf{r}_v$ is the position of the center of the vortex. Thus, $\mathbf{E}_v = (\mathbf{v} \cdot \nabla)\mathbf{A}_v - \nabla \phi_v$. By means of differential vector relations, this equation becomes $\mathbf{E}_v = \mathbf{B}_v \times \mathbf{v} + \nabla(\mathbf{v} \cdot \mathbf{A}_v - \phi_v)$. For a long straight vortex, the average in a volume V of height l and base surface S (see Fig. 15) containing a portion of the vortex is $\mathbf{E}_{\mathrm{av},v} = [1/(lS)] \int_V \mathbf{E}_v \, d^3\mathbf{r}$, where the volume integral is

$$\int_V \mathbf{E}_v d^3\mathbf{r} = \int_V \mathbf{B}_v \times \mathbf{v} d^3\mathbf{r} + \oint_{\partial V} (\mathbf{v} \cdot \mathbf{A} - \phi_v) ds. \tag{54}$$

In the given equation, ∂V is the surface of the volume V. The second term in the equation vanishes. This is because of two reasons. First, both $\mathbf{A}_v$ and ϕ_v vanish far away from the vortex center. Second, the integral contributions for the portion close to the vortex center cancel by symmetry. This reasoning also applies if the volume V is the cell of the vortex lattice. Both the vector and scalar potentials created by the vortices in the lattice vanish on the border of the cell [68], [332]. The integral of $\mathbf{v} \cdot \mathbf{A}_v$ and ϕ_v on the top and bottom surfaces also vanishes by symmetry. Then, the electric field created by one vortex is $\mathbf{E}_{\mathrm{av},v} = (\mathbf{\Phi}_0 \times \mathbf{v})/S$; hence, for n vortices per unit surface, the average electric field is

$$\mathbf{E} = \Phi_0 n \times \mathbf{v} = \mathbf{B} \times \mathbf{v}. \tag{55}$$

Equation (55) for the average electric field assumes that the dimensions of the base of the volume (see Fig. 15) are larger than the vortex separation. In practice, the vortex separation is often much smaller than the sample dimensions. Thus, $\mathbf{E}$ is approximately the local electric field in a "differential" volume of the sample. For thin films in a perpendicular field, the vortices become Pearl vortices [333], but the above analysis is still valid.

Appendix B
Properties of the Vector and Scalar Potentials and Coulomb Gauge

Several calculation methods assume the Coulomb gauge for the vector and scalar potentials $\mathbf{A}$ and ϕ. In this paper, the discussions in Sections II-C2 and II-C4 assume the Coulomb gauge. For the reader's convenience, this appendix lists the main properties of the Coulomb gauge and summarizes their deduction.

Since $\nabla \cdot \mathbf{B} = 0$, the flux density can be written as a rotational of function $\mathbf{A}$ as $\mathbf{B} = \nabla \times \mathbf{A}$. This defines the vector potential $\mathbf{A}$. From the differential Ampère's law with negligible displacement current, i.e., $\nabla \times \mathbf{B} = \mu_0 \mathbf{J}$, the vector potential is

$$\mathbf{A}(t, \mathbf{r}) = \frac{\mu_0}{4\pi} \int_{V'} \frac{\mathbf{J}(t, \mathbf{r}')}{|\mathbf{r} - \mathbf{r}'|} d^3\mathbf{r}' + \nabla \Psi(t, \mathbf{r}) \tag{56}$$

where the function $\Psi(t, \mathbf{r})$ is an arbitrary scalar function. The equation above can be deduced by differential vector analysis, as in [69, pp. 179–181]. The choice of this arbitrary function defines the gauge. The Coulomb gauge is defined as $\Psi = 0$. Then, the vector potential in Coulomb gauge, i.e., $\mathbf{A}_c$, is

$$\mathbf{A}_c(t, \mathbf{r}) = \frac{\mu_0}{4\pi} \int_{V'} \frac{\mathbf{J}(t, \mathbf{r}')}{|\mathbf{r} - \mathbf{r}'|} d^3\mathbf{r}'. \tag{57}$$

As a consequence, $\nabla \cdot \mathbf{A}_c = 0$ because $\nabla \cdot \mathbf{J} = 0$. In addition, $\mathbf{A}_c$ approaches zero as $\mathbf{r}$ approaches infinity, except if there is current at infinity. Another property of $\mathbf{A}$ in the Coulomb gauge is that it only depends on the current density.

The scalar potential is defined as follows. Faraday's law and $\mathbf{B} = \nabla \times \mathbf{A}$ imply that $\nabla \times (\mathbf{E} + \partial \mathbf{A}/\partial t) = 0$. Then, $\mathbf{E} + \partial \mathbf{A}/\partial t$ can be written as the gradient of a scalar function ϕ; hence, $\mathbf{E} = -\partial \mathbf{A}/\partial t - \nabla \phi$. Inserting this equation into the Gauss law, i.e., $\nabla \cdot \mathbf{E} = \rho/\epsilon_0$ and using equation (56) results in $\nabla^2(\phi + \partial \Psi/\partial t) = -\rho/\epsilon_0$, where ρ is the charge density and Ψ is the function that defines the gauge of the vector potential. The unique solution of this Laplace equation, under the assumption that $\phi + \partial \Psi/\partial t$ vanishes at the infinity, is

$$\phi(t, \mathbf{r}) = \frac{1}{4\pi\epsilon_0} \int_{V'} \frac{\rho(t, \mathbf{r}')}{|\mathbf{r} - \mathbf{r}'|} d^3\mathbf{r}' - \frac{\partial \Psi}{\partial t}. \tag{58}$$

The Coulomb gauge for $\mathbf{A}$ is defined as $\Psi = 0$. With this gauge, the scalar potential becomes the electrostatic potential as follows:

$$\phi_c(t, \mathbf{r}) = \frac{1}{4\pi\epsilon_0} \int_{V'} \frac{\rho(t, \mathbf{r}')}{|\mathbf{r} - \mathbf{r}'|} d^3\mathbf{r}'. \tag{59}$$

For infinitely long conducting wires, the vector potential in the Coulomb gauge is the integral along the length of the wire of (57), resulting in

$$\mathbf{A}_c(t, \mathbf{r}) = -\frac{\mu_0}{2\pi} \int_{V'} \mathbf{J}(t, \mathbf{r}') \ln |\mathbf{r} - \mathbf{r}'| d^3\mathbf{r}'. \tag{60}$$

ACKNOWLEDGMENT

The authors would like to thank Prof. A. Campbell, Dr. S. Pamidi, and Dr. J. Kvitkovic for their helpful comments.

REFERENCES

[1] C. P. Bean, "Magnetization of hard superconductors," *Phys. Rev. Lett.*, vol. 8, no. 6, pp. 250–253, Mar. 1962.

[2] H. London, "Alternating current losses in superconductors of the second kind," *Phys. Lett.*, vol. 6, no. 2, pp. 162–165, Sep. 1963.

[3] C. P. Bean, "Magnetization of high-field superconductors," *Rev. Mod. Phys.*, vol. 36, no. 1, pp. 31–39, Jan.–Mar. 1964.

[4] A. Bossavit, "Numerical modelling of superconductors in three dimensions: A model and a finite element method," *IEEE Trans. Magn.*, vol. 30, no. 5, pp. 3363–3366, Sep. 1994.

[5] W. Norris, "Calculation of hysteresis losses in hard superconductors carrying AC: Isolated conductors and edges of thin sheets," *J. Phys. D, Appl. Phys.*, vol. 3, no. 4, pp. 489–507, Apr. 1970.

[6] M. R. Halse, "AC face field losses in a type II superconductor," *J. Phys. D, Appl. Phys.*, vol. 3, no. 5, pp. 717–720, May 1970.

[7] A. M. Campbell, "A general treatment of losses in multifilamentary superconductors," *Cryogenics*, vol. 22, no. 1, pp. 3–16, Jan. 1982.

[8] M. N. Wilson, *Superconducting Magnets*. Oxford, U.K.: Clarendon, 1983.

[9] W. J. Carr, *AC Loss and Macroscopic Theory of Superconductors*. New York, NY, USA: Gordon and Breach, 1983.

[10] M. Ashkin, "Flux distribution and hysteresis loss in a round superconducting wire for the complete range of flux penetration," *J. Appl. Phys.*, vol. 50, no. 11, pp. 7060–7066, Nov. 1979.

[11] Y. Yeshurun and A. P. Malozemoff, "Giant flux creep and irreversibility in an Y-Ba-Cu-0 crystal: An alternative to the superconducting-glassmodel," *Phys. Rev. Lett.*, vol. 60, no. 21, pp. 2202–2205, May 1988.

[12] Y. B. Kim, C. F. Hempstead, and A. R. Strnad, "Flux-flow resistance in type-II superconductors," *Phys. Rev.*, vol. 139, no. 4A, pp. A1163–A1172, Aug. 1965.

[13] F. Gömöry, J. Šouc, M. Vojenèiak, and B. Klinèok, "Phenomenological description of flux pinning in non-uniform high-temperature superconductors in magnetic fields lower than the self-field," *Supercond. Sci. Technol.*, vol. 20, no. 9, pp. S271–S277, Sep. 2007.

[14] M. Majoros, B. A. Glowacki, and A. M. Campbell, "Critical current anisotropy in Ag/$(Pb,Bi)_2Sr_2Ca_2Cu_3O_{10+x}$ multifilamentary tapes: Influence of self-magnetic field," *Supercond. Sci. Technol.*, vol. 14, no. 6, pp. 353–362, Jun. 2001.

[15] E. Pardo, M. Vojenèiak, F. Gömöry, and J. Šouc, "Low-magnetic-field dependence and anisotropy of the critical current density in coated conductors," *Supercond. Sci. Technol.*, vol. 24, no. 6, p. 065007, Jun. 2011.

[16] A. E. Pashitski, A. Polyanskii, A. Gurevich, J. Parrell, and D. C. Larbalestier, "Suppression of magnetic granularity by transport current in $(Bi,Pb)_2Sr_2Ca_2Cu_3O_x$ tapes," *Appl. Phys. Lett.*, vol. 67, no. 18, pp. 2720–2722, Oct. 1995.

[17] G. Grasso, B. Hensel, A. Jeremie, and R. Flükiger, "Distribution of the transport critical current density in Ag sheathed $(Bi,Pb)_2Sr_2Ca_2Cu_3O_x$ tapes produced by rolling," *Phys. C, Supercond.*, vol. 241, no. 1/2, pp. 45–52, Jan. 1995.

[18] O. Tsukamoto, "AC losses in a type II superconductor strip with inhomogeneous critical current distribution," *Supercond. Sci. Technol.*, vol. 18, no. 5, pp. 596–605, May 2005.

[19] T. Nishioka, N. Amemiya, N. Enomoto, Z. Jiang, Y. Yamada, T. Izumi, Y. Shiohara, T. Saitoh, Y. Iijima, and K. Kakimoto, "AC loss of YBCO coated conductors fabricated by IBAD/PLD method," *IEEE Trans. Appl. Supercond.*, vol. 15, no. 2, pp. 2843–2846, Jun. 2005.

[20] F. Grilli, R. Brambilla, and L. Martini, "Modeling high-temperature superconducting tapes by means of edge finite elements," *IEEE Trans. Appl. Supercond.*, vol. 17, no. 2, pp. 3155–3158, Jun. 2007.

[21] C. J. Carpenter, "Comparison of alternative formulations of 3-dimensional magnetic-field and eddy-current problems at power frequencies," *Proc. Inst. Elect. Eng.*, vol. 124, no. 11, pp. 1026–1034, Nov. 1977.

[22] T. W. Preston and A. B. J. Reece, "Solution of 3-dimensional eddy current problems: The $T-\Omega$ method," *IEEE Trans. Magn.*, vol. MAG-18, no. 2, pp. 486–491, Mar. 1982.

[23] E. H. Brandt, "Superconductors of finite thickness in a perpendicular magnetic field: Strips and slabs," *Phys. Rev. B*, vol. 54, no. 6, pp. 4246–4264, Aug. 1996.

[24] E. H. Brandt, "Superconductor disks and cylinders in an axial magnetic field. I. Flux penetration and magnetization curves," *Phys. Rev. B*, vol. 58, no. 10, pp. 6506–6522, Sep. 1998.

[25] J. Rhyner, "Calculation of AC losses in HTSC wires with arbitrary current voltage characteristics," *Phys. C, Supercond.*, vol. 310, no. 1–4, pp. 42–47, Dec. 1998.

[26] T. Yazawa, J. J. Rabbers, B. ten Haken, H. H. J. ten Kate, and Y. Yamada, "Numerical calculation of current density distributions in high temperature superconducting tapes with finite thickness in self field and external field," *Phys. C, Supercond.*, vol. 310, no. 1–4, pp. 36–41, Dec. 1998.

[27] S. Stavrev, B. Dutoit, and N. Nibbio, "Geometry considerations for use of Bi-2223/Ag tapes and wires with different models of $J_c(B)$," *IEEE Trans. Appl. Supercond.*, vol. 12, no. 3, pp. 1857–1865, Sep. 2002.

[28] K. Kajikawa, T. Hayashi, R. Yoshida, M. Iwakuma, and K. Funaki, "Numerical evaluation of AC loss in HTS wires with 2D FEM formulated by self magnetic field," *IEEE Trans. Appl. Supercond.*, vol. 13, no. 2, pp. 3630–3633, Jun. 2003.

[29] Z. Hong, A. M. Campbell, and T. A. Coombs, "Numerical solution of critical state in superconductivity by finite element software," *Supercond. Sci. Technol.*, vol. 19, no. 12, pp. 1246–1252, Dec. 2006.

[30] N. Amemiya, S. Murasawa, N. Banno, and K. Miyamoto, "Numerical modelings of superconducting wires for AC loss calculations," *Phys. C, Supercond.*, vol. 310, no. 1–4, pp. 16–29, Dec. 1998.

[31] N. Enomoto and N. Amemiya, "Electromagnetic field analysis of rectangular high T_c superconductor with large aspect ratio," *Phys. C, Supercond.*, vol. 412–414, pp. 1050–1055, Oct. 2004.

[32] F. Grilli, S. Stavrev, Y. Le Floch, M. Costa-Bouzo, E. Vinot, I. Klutsch, G. Meunier, P. Tixador, and B. Dutoit, "Finite-element method modeling of superconducors: From 2-D to 3-D," *IEEE Trans. Appl. Supercond.*, vol. 15, no. 1, pp. 17–25, Mar. 2005.

[33] A. Stenvall and T. Tarhasaari, "Programming finite element method based hysteresis loss computation software using non-linear superconductor resistivity and $T-\varphi$ formulation," *Supercond. Sci. Technol.*, vol. 23, no. 7, p. 075010, Jul. 2010.

[34] A. O. Hauser, "Calculation of superconducting magnetic bearings using a commercial FE-program (ANSYS)," *IEEE Trans. Magn.*, vol. 33, no. 2, pp. 1572–1575, Mar. 1997.

[35] H. Tonsho, S. Fukui, T. Sato, M. Yamaguchi, S. Torii, T. Takao, and K. Ueda, "Theoretical and experimental study on AC loss in HTS tape in AC magnetic field carrying AC transport current," *IEEE Trans. Appl. Supercond.*, vol. 13, no. 2, pp. 2368–2371, Jun. 2003.

[36] A. Stenvall and T. Tarhasaari, "An eddy current vector potential formulation for estimating hysteresis losses of superconductors with FEM," *Supercond. Sci. Technol.*, vol. 23, no. 12, p. 125013, Dec. 2010.

[37] M. Maslouh, F. Bouillault, A. Bossavit, and J. C. Vérité, "From Bean's model to the HM characteristic of a superconductor: Some numerical experiments," *IEEE Trans. Appl. Supercond.*, vol. 7, no. 3, pp. 3797–3801, Sep. 1997.

[38] L. Prigozhin, "Analysis of critical-state problems in type-II superconductivity," *IEEE Trans. Appl. Supercond.*, vol. 7, no. 4, pp. 3866–3873, Dec. 1997.

[39] L. Prigozhin and V. Sokolovsky, "Computing AC losses in stacks of high-temperature superconducting tapes," *Supercond. Sci. Technol.*, vol. 24, no. 7, p. 075012, Jul. 2011.

[40] L. Prigozhin, "The Bean model in superconductivity: Variational formulation and numerical solution," *J. Comput. Phys.*, vol. 129, no. 1, pp. 190–200, Nov. 1996.

[41] A. Badia and C. López, "Vector magnetic hysteresis of hard superconductors," *Phys. Rev. B*, vol. 65, no. 10, pp. 104514-1–104514-12, Mar. 2002.

[42] E. Pardo, F. Gömöry, J. Šouc, and J. M. Ceballos, "Current distribution and AC loss for a superconducting rectangular strip with in-phase alternating current and applied field," *Supercond. Sci. Technol.*, vol. 20, no. 4, pp. 351–364, Apr. 2007.

[43] J. Šouc, E. Pardo, M. Vojenèiak, and F. Gömöry, "Theoretical and experimental study of AC loss in high temperature superconductor single pancake coils," *Supercond. Sci. Technol.*, vol. 22, no. 1, p. 015006, Jan. 2009.

[44] A. Sanchez and C. Navau, "Magnetic properties of finite superconducting cylinders. I. Uniform applied field," *Phys. Rev. B*, vol. 64, no. 21, pp. 214506-1–214506-10, Dec. 2001.

[45] F. Gömöry, M. Vojenèiak, E. Pardo, and J. Šouc, "Magnetic flux penetration and AC loss in a composite superconducting wire with ferromagnetic parts," *Supercond. Sci. Technol.*, vol. 22, no. 3, p. 034017, Mar. 2009.

[46] F. Gömöry, M. Vojenèiak, E. Pardo, M. Solovyov, and J. Šouc, "AC losses in coated conductors," *Supercond. Sci. Technol.*, vol. 23, no. 3, p. 034012, Mar. 2010.

[47] A. M. Campbell, "A new method of determining the critical state in superconductors," *Supercond. Sci. Technol.*, vol. 20, no. 3, pp. 292–295, Mar. 2007.

[48] A. M. Campbell, "A direct method for obtaining the critical state in two and three dimensions," *Supercond. Sci. Technol.*, vol. 22, no. 3, p. 034005, Mar. 2009.

[49] G. Barnes, M. McCulloch, and D. Dew-Hughes, "Computer modelling of type II superconductors in applications," *Supercond. Sci. Technol.*, vol. 12, no. 8, pp. 518–522, Aug. 1999.

[50] N. Takeda, M. Uesaka, and K. Miya, "Computation and experiments on the static and dynamic characteristics of high T_c superconducting levitation," *Cryogenics*, vol. 34, no. 9, pp. 745–752, 1994.

[51] F. Sirois, "Numerical methods for modeling high-temperature superconductors," *IEEE Trans. Appl. Supercond.*, 2013, submitted for publication.

[52] E. H. Brandt, "Square and rectangular thin superconductors in a transverse magnetic field," *Phys. Rev. Lett.*, vol. 74, no. 15, pp. 3025–3028, Apr. 1995.

[53] J. I. Vestgården, D. V. Shantsev, Y. M. Galperin, and T. H. Johansen, "Flux distribution in superconducting films with holes," *Phys. Rev. B*, vol. 77, no. 1, pp. 014521-1–014521-7, Jan. 2008.

[54] N. Amemiya, S. Sato, and T. Ito, "Magnetic flux penetration into twisted multifilamentary coated superconductors subjected to AC transverse magnetic fields," *J. Appl. Phys.*, vol. 100, no. 12, pp. 123907-1–123907-7, Dec. 2006.

[55] F. Grilli, R. Brambilla, F. Sirois, A. Stenvall, and S. Memiaghe, "Development of a three-dimensional finite-element model for high-temperature superconductors based on the H-formulation," *Cryogenics*, vol. 53, pp. 142–147, Jan. 2013.

[56] M. Zhang and T. A. Coombs, "3D modeling of high- T_c superconductors by finite element software," *Supercond. Sci. Technol.*, vol. 25, no. 1, p. 015009, Jan. 2012.

[57] L. Prigozhin, "Solution of thin film magnetization problems in type-II superconductivity," *J. Comput. Phys.*, vol. 144, no. 1, pp. 180–193, Jul. 1998.

[58] C. Navau, A. Sanchez, N. Del-Valle, and D. X. Chen, "Alternating current susceptibility calculations for thin-film superconductors with regions of different critical-current densities," *J. Appl. Phys.*, vol. 103, no. 11, pp. 113907-1–113907-8, Jun. 2008.

[59] K. Takeuchi, N. Amemiya, T. Nakamura, O. Maruyama, and T. Ohkuma, "Model for electromagnetic field analysis of superconducting power transmission cable comprising spiraled coated conductors," *Supercond. Sci. Technol.*, vol. 24, no. 8, p. 085014, Aug. 2011.

[60] M. Nii, N. Amemiya, and T. Nakamura, "Three-dimensional model for numerical electromagnetic field analyses of coated superconductors and its application to Roebel cables," *Supercond. Sci. Technol.*, vol. 25, no. 9, p. 095011, Sep. 2012.

[61] A. M. Campbell and J. E. Evetts, "Flux vortices and transport currents in type II superconductors," *Adv. Phys.*, vol. 21, no. 90, pp. 199–428, Mar. 1972.

[62] C. Romero-Salazar and F. Pérez-Rodríguez, "Elliptic flux-line-cutting critical-state model," *Appl. Phys. Lett.*, vol. 83, no. 25, pp. 5256–5258, Dec. 2003.

[63] A. Badía-Majós, C. López, and H. S. Ruiz, "General critical states in type-II superconductors," *Phys. Rev. B*, vol. 80, no. 14, pp. 144509-1–144509-21, Oct. 2009.

[64] J. R. Clem, M. Weigand, J. H. Durrell, and A. M. Campbell, "Theory and experiment testing flux-line cutting physics," *Supercond. Sci. Technol.*, vol. 24, no. 6, p. 062002, Jun. 2011.

[65] G. P. Lousberg, M. Ausloos, C. Geuzaine, P. Dular, P. Vanderbemden, and B. Vanderheyden, "Numerical simulation of the magnetization of high-temperature superconductors: A 3D finite element method using a single time-step iteration," *Supercond. Sci. Technol.*, vol. 22, no. 5, p. 055005, May 2009.

[66] M. Zehetmayer, M. Eisterer, and H. W. Weber, "Simulation of the current dynamics in a superconductor induced by a small permanent magnet: Application to the magnetoscan technique," *Supercond. Sci. Technol.*, vol. 19, no. 7, pp. S429–S437, Jul. 2006.

[67] G. Blatter, M. V. Feigelman, V. B. Geshkenbein, A. I. Larkin, and V. M. Vinokur, "Vortices in high-temperature superconductors," *Rev. Mod. Phys.*, vol. 66, no. 4, pp. 1125–1388, Oct.–Dec. 1994.

[68] E. H. Brandt, "The flux-line lattice in superconductors," *Rep. Progr. Phys.*, vol. 58, no. 11, pp. 1465–1594, Nov. 1995.

[69] J. D. Jackson, *Classical Electrodynamics*, 3rd ed. Hoboken, NJ, USA: Wiley, 1999.

[70] J. Kötzler, G. Nakielski, M. Baumann, R. Behr, F. Goerke, and E. H. Brandt, "Universality of frequency and field scaling of the conductivity measured by AC susceptibility of a $YBa_2Cu_3O_{7-\delta}$ film," *Phys. Rev. B*, vol. 50, no. 5, pp. 3384–3391, Aug. 1994.

[71] J. Rhyner, "Vector potential theory of AC losses in superconductors," *Phys. C, Supercond.*, vol. 377, no. 1/2, pp. 56–66, Aug. 2002.

[72] E. H. Brandt, M. V. Indenbom, and A. Forkl, "Type-II superconducting strip in perpendicular magnetic field," *Europhys. Lett.*, vol. 22, no. 9, pp. 735–740, Jun. 1993.

[73] L. D. Landau, E. M. Lifshitz, and L. P. Pitaevskii, *Electrodynamics of Continuous Media*. Amsterdam, The Netherlands: Elsevier Butterworth Heinemann, 2008.

[74] S. P. Ashworth and M. Suenaga, "Measurement of AC losses in superconductors due to AC transport currents in applied AC magnetic fields," *Phys. C, Supercond.*, vol. 313, no. 3/4, pp. 175–187, Feb. 1999.

[75] M. Vojenciak, J. Šouc, J. Ceballos, F. Gömöry, B. Klinèok, E. Pardo, and F. Grilli, "Study of AC loss in Bi-2223/Ag tape under the simultaneous action of AC transport current and AC magnetic field shifted in phase," *Supercond. Sci. Technol.*, vol. 19, no. 4, pp. 397–404, Apr. 2006.

[76] E. Pardo, "Modeling of coated conductor pancake coils with a large number of turns," *Supercond. Sci. Technol.*, vol. 21, no. 6, p. 065014, Jun. 2008.

[77] W. J. Carr, Jr., "Hysteresis loss in a coated conductor subject to a combined applied magnetic field and transport current," *Supercond. Sci. Technol.*, vol. 19, no. 6, pp. 454–458, Jun. 2006.

[78] C. Navau, N. Del-Valle, and A. Sanchez, "Macroscopic modeling of magnetization and levitation of hard type-II superconductors: The critical-state model," *IEEE Trans. Appl. Supercond.*, vol. 23, no. 1, p. 8201023, Feb. 2013.

[79] R. B. Goldfarb, M. Lelental, and C. Thompson, *Magnetic Susceptibility of Superconductors and Other Spin Systems*, R. A. Hein, Ed. New York, NY, USA: Plenum, 1991, p. 49.

[80] J. R. Clem, *Magnetic Susceptibility of Superconductors and Other Spin Systems*, R. A. Hein, Ed. New York, NY, USA: Plenum, 1991, p. 177.

[81] W. A. Fietz, M. R. Beasley, J. Silcox, and W. W. Webb, "Magnetization of superconducting Nb-25% Zr wire," *Phys. Rev.*, vol. 136, no. 2A, pp. A335–A345, Oct. 1964.

[82] J. H. P. Watson, "Magnetization of synthetic filamentary superconductors. B. The dependence of the critical current density on temperature and magnetic field," *J. Appl. Phys.*, vol. 39, no. 7, pp. 3406–3413, Jun. 1968.

[83] D. X. Chen and A. Sanchez, "Theoretical critical-state susceptibility spectra and their application to high- T_c superconductors," *J. Appl. Phys.*, vol. 70, no. 10, pp. 5463–5477, Nov. 1991.

[84] N. Amemiya, K. Miyamoto, N. Banno, and O. Tsukamoto, "Numerical analysis of AC losses in high Tc superconductors based on $E-j$ characteristics represented with n-value," *IEEE Trans. Appl. Supercond.*, vol. 7, no. 2, pp. 2110–2113, Jun. 1997.

[85] D. X. Chen and E. Pardo, "Power-law $E(J)$ characteristic converted from field-amplitude and frequency dependent AC susceptibility in superconductors," *Appl. Phys. Lett.*, vol. 88, pp. 222505-1–222505-3, May 2006.

[86] E. H. Brandt, "Susceptibility of superconductor disks and rings with and without flux creep," *Phys. Rev. B*, vol. 55, no. 21, pp. 14 513–14 526, Jun. 1997.

[87] E. Pardo, D.-X. Chen, A. Sanchez, and C. Navau, "The transverse critical-state susceptibility of rectangular bars," *Supercond. Sci. Technol.*, vol. 17, no. 3, pp. 537–544, Mar. 2004.

[88] J. R. Clem and A. Sanchez, "Hysteretic AC losses and susceptibility of thin superconducting disks," *Phys. Rev. B*, vol. 50, no. 13, pp. 9355–9362, Oct. 1994.

[89] V. M. Krasnov, V. A. Larkin, and V. V. Ryazanov, "The extended Bean critical state model for superconducting 3-axes ellipsoid and its application for obtaining the bulk critical field H_{c1} and the pinning current J_c in high- T_c superconducting single crystals," *Phys. C, Supercond.*, vol. 174, no. 4–6, pp. 440–446, Mar. 1991.

[90] F. Gömöry, R. Tebano, A. Sanchez, E. Pardo, C. Navau, I. Husek, F. Strycek, and P. Kovac, "Current profiles and AC losses of a superconducting strip with an elliptic cross-section in a perpendicular magnetic field," *Supercond. Sci. Technol.*, vol. 15, no. 9, pp. 1311–1315, Sep. 2002.

[91] K. V. Bhagwat and P. Chaddah, "Flux penetration in thin elliptic superconducting cylinders subjected to transverse magnetic fields," *Phys. C, Supercond.*, vol. 254, no. 1/2, pp. 143–150, Nov. 1995.

[92] D. X. Chen, E. Pardo, and A. Sanchez, "Transverse AC susceptibility of superconducting bars with elliptical cross-section and constant

critical-current density," *Supercond. Sci. Technol.*, vol. 18, no. 7, pp. 997–1002, Jul. 2005.

[93] N. Amemiya, K. Miyamoto, S. Murasawa, H. Mukai, and K. Ohmatsu, "Finite element analysis of AC loss in non-twisted Bi-2223 tape carrying AC transport current and/or exposed to DC or AC external magnetic field," *Phys. C, Supercond.*, vol. 310, no. 1–4, pp. 30–35, Dec. 1998.

[94] N. Nibbio, S. Stavrev, and B. Dutoit, "Finite element method simulation of AC loss in HTS tapes with B-dependent E-J power law," *IEEE Trans. Appl. Supercond.*, vol. 11, no. 1, pp. 2631–2634, Mar. 2001.

[95] Y. Mawatari, "Superconducting tubular wires in transverse magnetic fields," *Phys. Rev. B*, vol. 83, no. 13, pp. 134512-1–134512-8, Apr. 2011.

[96] Y. Fukumoto, H. J. Wiesmann, M. Garber, M. Suenaga, and P. Haldar, "Alternating-current losses in silver-sheathed $(Bi,Pb)_2Sr_2Ca_2Cu_3O_{10}$ tapes II: Role of interfilamentary coupling," *Appl. Phys. Lett.*, vol. 67, no. 21, pp. 3180–3182, Nov. 1995.

[97] E. Pardo, A. Sanchez, and C. Navau, "Magnetic properties of arrays of superconducting strips in a perpendicular field," *Phys. Rev. B*, vol. 67, no. 10, pp. 104517-1–104517-18, Mar. 2003.

[98] Y. Mawatari, "Critical state of periodically arranged superconducting-strip lines in perpendicular fields," *Phys. Rev. B*, vol. 54, no. 18, pp. 13 215–13 221, Nov. 1996.

[99] R. M. Ainbinder and G. M. Maksimova, "Hysteretic characteristics of a double stripline in the critical state," *Supercond. Sci. Technol.*, vol. 16, no. 8, pp. 871–878, Aug. 2003.

[100] R. Tebano, F. Gömöry, E. Seiler, and F. Strycek, "Numerical investigations of the mutual magnetic coupling in superconducting tapes in z-stack arrangement with external AC magnetic field," *Phys. C, Supercond.*, vol. 372–376, pp. 998–1000, Aug. 2002.

[101] F. Grilli, S. P. Ashworth, and S. Stavrev, "Magnetization AC losses of stacks of YBCO coated conductors," *Phys. C, Supercond.*, vol. 434, no. 2, pp. 185–190, Feb. 2006.

[102] S. Stavrev, B. Dutoit, and P. Lombard, "Numerical modelling and AC losses of multifilamentary Bi-2223/Ag conductors with various geometry and filament arrangement," *Phys. C, Supercond.*, vol. 384, no. 1/2, pp. 19–31, Jan. 2003.

[103] F. Grilli and E. Pardo, "Simulation of AC loss in Roebel coated conductor cables," *Supercond. Sci. Technol.*, vol. 23, no. 11, p. 115018, Nov. 2010.

[104] L. Rostila, E. Demencèík, J. Šouc, S. Brisigotti, P. Kováè, M. Polak, G. Grasso, M. Lyly, A. Stenvall, A. Tumino, and L. Kopera, "Magnesium diboride wires with nonmagnetic matrices—AC loss measurements and numerical calculations," *IEEE Trans. Appl. Supercond.*, vol. 21, no. 3, pp. 3338–3341, Jun. 2011.

[105] P. Fabbricatore, S. Farinon, S. Innocenti, and F. Gömöry, "Magnetic flux shielding in superconducting strip arrays," *Phys. Rev. B*, vol. 61, no. 9, pp. 6413–6421, Mar. 2000.

[106] G. P. Mikitik, E. H. Brandt, and M. Indenbom, "Superconducting strip in an oblique magnetic field," *Phys. Rev. B*, vol. 70, no. 1, pp. 014520-1–014520-11, Jul. 2004.

[107] E. H. Brandt and G. P. Mikitik, "Anisotropic superconducting strip in an oblique magnetic field," *Phys. Rev. B*, vol. 72, no. 2, pp. 024516-1–024516-7, Jul. 2005.

[108] Y. Ichiki and H. Ohsaki, "Numerical analysis of AC losses in YBCO coated conductor in external magnetic field," *Phys. C, Supercond.*, vol. 412–414, pp. 1015–1020, Oct. 2004.

[109] N. Enomoto, T. Izumi, and N. Amemiya, "Electromagnetic field analysis of rectangular superconductor with large aspect ratio in arbitrary orientated magnetic fields," *IEEE Trans. Appl. Supercond.*, vol. 15, no. 2, pp. 1574–1577, Jun. 2005.

[110] S. Stavrev, F. Grilli, B. Dutoit, and S. Ashworth, "Comparison of the AC losses of BSCCO and YBCO conductors by means of numerical analysis," *Supercond. Sci. Technol.*, vol. 18, no. 10, pp. 1300–1312, Oct. 2005.

[111] D. Karmakar and K. V. Bhagwat, "Magnetization of hard superconductor samples subjected to oblique fields," *Phys. Rev. B*, vol. 65, no. 2, pp. 024518-1–024518-7, Dec. 2001.

[112] E. Pardo and F. Grilli, "Numerical simulations of the angular dependence of magnetization AC losses: Coated conductors, Roebel cables and double pancake coils," *Supercond. Sci. Technol.*, vol. 25, no. 1, p. 014008, Jan. 2012.

[113] J. Zhu, J. Mester, J. Locldaart, and J. Turneaure, "Critical states in 2D disk-shaped type-II superconductors in periodic external magnetic field," *Phys. C, Supercond.*, vol. 212, no. 1/2, pp. 216–222, Jul. 1993.

[114] E. H. Brandt, "Superconductor disks and cylinders in an axial magnetic field: II. Nonlinear and linear AC susceptibilities," *Phys. Rev. B*, vol. 58, no. 10, pp. 6523–6533, Sep. 1998.

[115] C. Navau, A. Sanchez, E. Pardo, D. X. Chen, E. Bartolomé, X. Granados, T. Puig, and X. Obradors, "Critical state in finite type-II superconducting rings," *Phys. Rev. B*, vol. 71, no. 21, pp. 214507-1–214507-9, Jun. 2005.

[116] R. Navarro and L. J. Campbell, "Magnetic-flux profiles of high- T_c superconducting granules: Three-dimensional critical-state-model approximation," *Phys. Rev. B*, vol. 44, no. 18, pp. 10 146–10 157, Nov. 1991.

[117] R. Navarro and L. J. Campbell, "Three dimensional solution of critical state models: AC hysteresis losses," *Supercond. Sci. Technol.*, vol. 5, no. 1S, pp. S200–S203, Jan. 1992.

[118] K. L. Telschow and L. S. Koo, "Integral-equation approach for the Bean critical-state model in demagnetizing and nonuniform-field geometries," *Phys. Rev. B*, vol. 50, no. 10, pp. 6923–6928, Sep. 1994.

[119] J. R. Clem, M. Benkraouda, and J. McDonald, "Penetration of magnetic flux and electrical current density into superconducting strips and disks," *Chin. J. Phys.*, vol. 34, no. 2-11, pp. 284–290, Apr. 1996.

[120] R. Hancox, "Calculation of AC losses in a type-II superconductor," *Proc. Inst. Elect. Eng.*, vol. 113, no. 7, pp. 1221–1228, Jul. 1966.

[121] D. X. Chen and C. Gu, "Alternating current loss in a cylinder with power-law current–voltage characteristic," *Appl. Phys. Lett.*, vol. 86, no. 25, pp. 252504-1–252504-3, Jun. 2005.

[122] F. Gömöry and L. Gherardi, "Transport AC losses in round superconducting wire consisting of two concentric shells with different critical current density," *Phys. C, Supercond.*, vol. 280, no. 3, pp. 151–157, Jul. 1997.

[123] K. Kajikawa, Y. Mawatari, T. Hayashi, and K. Funaki, "AC loss evaluation of thin superconducting wires with critical current distribution along width," *Supercond. Sci. Technol.*, vol. 17, no. 3, pp. 555–563, Mar. 2004.

[124] W. T. Norris, "Calculation of hysteresis losses in hard superconductors: Polygonal-section conductors," *J. Phys. D, Appl. Phys.*, vol. 4, no. 9, pp. 1358–1364, Sep. 1971.

[125] T. Fukunaga, R. Inada, and A. Oota, "Field-free core, current distribution, and alternating current losses in self fields for rectangular superconductor tapes," *Appl. Phys. Lett.*, vol. 72, no. 25, pp. 3362–3364, Jun. 1998.

[126] M. Däumling, "AC power loss for superconducting strips of arbitrary thickness in the critical state carrying a transport current," *Supercond. Sci. Technol.*, vol. 11, no. 6, pp. 590–593, Jun. 1998.

[127] C. Gu and Z. Han, "Calculation of AC losses in HTS tape with FEA program ANSYS," *IEEE Trans. Appl. Supercond.*, vol. 15, no. 2, pp. 2859–2862, Jun. 2005.

[128] T. Fukunaga, R. Inada, and A. Oota, "Current distributions and AC losses in self-fields for superconductor tapes and cables," *IEEE Trans. Appl. Supercond.*, vol. 9, no. 2, pp. 1057–1060, Jun. 1999.

[129] A. Oota, R. Inada, N. Inagaki, P. X. Zhang, and H. Fujimoto, "A progress in reducing AC transport losses of Ag-sheathed Bi2223 tapes by a rectangular deformation using two-axial rollers," *Phys. C, Supercond.*, vol. 386, pp. 100–105, Apr. 2003.

[130] E. Pardo, A. Sanchez, D.-X. Chen, and C. Navau, "Theoretical analysis of the transport critical-state AC loss in arrays of superconducting rectangular strips," *Phys. Rev. B*, vol. 71, no. 13, pp. 134517-1–134517-12, Apr. 2005.

[131] S. Stavrev, B. Dutoit, and P. Lombard, "AC losses of multifilamentary Bi-2223/Ag conductors with different geometry and filament arrangement," *IEEE Trans. Appl. Supercond.*, vol. 13, no. 2, pp. 3561–3565, Jun. 2003.

[132] W. J. Carr, Jr., "AC Loss from the combined action of transport current and applied field," *IEEE Trans. Magn.*, vol. MAG-15, no. 1, pp. 240–243, Jan. 1979.

[133] E. H. Brandt and M. Indenbom, "Type-II-superconductor strip with current in a perpendicular magnetic field," *Phys. Rev. B*, vol. 48, no. 17, pp. 12 893–12 906, Nov. 1993.

[134] E. Zeldov, J. Clem, M. McElfresh, and M. Darwin, "Magnetization and transport currents in thin superconducting films," *Phys. Rev. B*, vol. 49, no. 14, pp. 9802–9822, Apr. 1994.

[135] N. Schonborg, "Hysteresis losses in a thin high-temperature superconductor strip exposed to AC transport currents and magnetic fields," *J. Appl. Phys.*, vol. 90, no. 6, pp. 2930–2933, Sep. 2001.

[136] S. Zannella, L. Montelatici, G. Grenci, M. Pojer, L. Jansak, M. Majoros, G. Coletta, R. Mele, R. Tebano, and F. Zanovello, "AC losses in transport current regime in applied AC magnetic field: Experimental analysis and modeling," *IEEE Trans. Appl. Supercond.*, vol. 11, no. 1, pp. 2441–2444, Mar. 2001.

[137] S. Takacs, "Hysteresis losses in superconductors with an out-of-phase applied magnetic field and current: Slab geometry," *Supercond. Sci. Technol.*, vol. 20, no. 12, pp. 1093–1096, Dec. 2007.

[138] Y. Mawatari and K. Kajikawa, "Hysteretic AC loss of superconducting strips simultaneously exposed to AC transport current and phase-different AC magnetic field," *Appl. Phys. Lett.*, vol. 90, no. 2, pp. 022506-1–022506-3, Jan. 2007.

[139] K. Kajikawa, A. Takenaka, K. Kawasaki, M. Iwakuma, and K. Funaki, "Numerical simulation for AC losses of HTS tapes in combined alternating transport current and external AC magnetic field with phase shift," *IEEE Trans. Appl. Supercond.*, vol. 11, no. 1, pp. 2240–2243, Mar. 2001.

[140] D. N. Nguyen, P. V. Sastry, D. C. Knoll, G. Zhang, and J. Schwartz, "Experimental and numerical studies of the effect of phase difference between transport current and perpendicular applied magnetic field on total AC loss in Ag-sheathed (Bi, Pb) SrCaCuO tape," *J. Appl. Phys.*, vol. 98, no. 7, pp. 073902-1–073902-6, Oct. 2005.

[141] G. Vellego and P. Metra, "An analysis of the transport losses measured on HTSC single-phase conductor prototypes," *Supercond. Sci. Technol.*, vol. 8, no. 6, pp. 476–483, Jun. 1995.

[142] F. Grilli, S. Stavrev, B. Dutoit, and S. Spreafico, "Numerical modeling of a HTS cable," *IEEE Trans. Appl. Supercond.*, vol. 13, no. 2, pp. 1886–1889, Jun. 2003.

[143] F. Grilli and M. Sjöström, "Prediction of resistive and hysteretic losses in a multi-layer high-T_c superconducting cable," *Supercond. Sci. Technol.*, vol. 17, no. 3, pp. 409–416, Mar. 2004.

[144] B. Klinèok and F. Gömöry, "Influence of gaps in monolayer superconducting cable on AC losses," *J. Phys., Conf. Ser.*, vol. 43, no. 43, pp. 897–900, 2006.

[145] D. Miyagi, M. Umabuchi, N. Takahashi, and O. Tsukamoto, "Study of AC transport current loss of assembled HTS coated-conductors with ferromagnetic substrate using FEM," *Phys. C, Supercond.*, vol. 463–465, pp. 785–789, Oct. 2007.

[146] N. Amemiya, Z. Jiang, Z. Li, M. Nakahata, T. Kato, M. Ueyama, N. Kashima, S. Nagaya, and S. Shiohara, "Transport losses in single and assembled coated conductors with textured-metal substrate with reduced magnetism," *Phys. C, Supercond.*, vol. 468, no. 15–20, pp. 1718–1722, Sep. 2008.

[147] L. Rostila, S. Suuriniemi, J. Lehtonen, and G. Grasso, "Numerical minimization of AC losses in coaxial coated conductor cables," *Phys. C, Supercond.*, vol. 470, no. 3, pp. 212–217, Feb. 2010.

[148] Z. Jiang, N. Amemiya, and M. Nakahata, "Numerical calculation of AC losses in multi-layer superconducting cables composed of coated conductors," *Supercond. Sci. Technol.*, vol. 21, no. 2, p. 025013, Feb. 2008.

[149] J. Nakahata and N. Amemiya, "Electromagnetic field analyses of two-layer power transmission cables consisting of coated conductors with magnetic and non-magnetic substrates and AC losses in their superconductor layers," *Supercond. Sci. Technol.*, vol. 21, no. 1, p. 015007, Jan. 2008.

[150] N. Amemiya, M. Nakahata, N. Fujiwara, and Y. Shiohara, "Ac losses in two-layer superconducting power transmission cables consisting of coated conductors with a magnetic substrate," *Supercond. Sci. Technol.*, vol. 23, no. 1, p. 014022, Jan. 2010.

[151] R. Inada, Y. Nakamura, and A. Oota, "Numerical analysis for AC losses in single-layer cables composed of rectangular superconducting strips with various lateral J_c distributions," *J. Phys., Conf. Ser.*, vol. 97, no. 1, p. 012324, 2008.

[152] Y. Mawatari, A. Malozemoff, T. Izumi, K. Tanabe, N. Fujiwara, and Y. Shiohara, "Hysteretic AC losses in power transmission cables with superconducting tapes: Effect of tape shape," *Supercond. Sci. Technol.*, vol. 23, no. 2, p. 025031, Feb. 2010.

[153] K. Ohmatsu, K. Muranaka, K. Fujino, M. Konishi, and K. Yasuda, "Design study of model cable conductor by using HoBCO thin film tape," *IEEE Trans. Appl. Supercond.*, vol. 14, no. 2, pp. 620–625, Jun. 2004.

[154] T. Nakamura, H. Kanzaki, K. Higashikawa, T. Hoshino, and I. Muta, "Analysis of shielding layers in HTS cable taking account of spiral structure," *IEEE Trans. Appl. Supercond.*, vol. 15, no. 2, pp. 1747–1750, Jun. 2005.

[155] M. Siahrang, F. Sirois, D. N. Nguyen, S. Babic, and S. P. Ashworth, "Fast numerical computation of current distribution and AC losses in helically wound thin tape conductors: Single-layer coaxial arrangement," *IEEE Trans. Appl. Supercond.*, vol. 20, no. 6, pp. 2381–2389, Dec. 2010.

[156] S. Terzieva, M. Vojenciak, E. Pardo, F. Grilli, A. Drechsler, A. Kling, A. Kudymow, F. Gömöry, and W. Goldacker, "Transport and magnetization AC losses of ROEBEL assembled coated conductor cables: Measurements and calculations," *Supercond. Sci. Technol.*, vol. 23, no. 1, p. 014023, Jan. 2010.

[157] Z. Jiang, K. P. Thakur, M. Staines, R. A. Badcock, N. J. Long, R. G. Buckley, A. D. Caplin, and N. Amemiya, "The dependence of AC loss characteristics on the spacing between strands in YBCO Roebel cables," *Supercond. Sci. Technol.*, vol. 24, no. 6, p. 065005, Jun. 2011.

[158] V. Zermeno, F. Grilli, and F. Sirois, "A full 3-D time-dependent electromagnetic model for Roebel cables," *Supercond. Sci. Technol.*, vol. 26, no. 5, p. 052001, May 2013.

[159] J. Pitel, A. Korpela, J. Lehtonen, and P. Kovac, "Mathematical model of voltage–current characteristics of Bi(2223)/Ag magnets under an external magnetic field," *Supercond. Sci. Technol.*, vol. 15, no. 11, pp. 1499–1506, Nov. 2002.

[160] M. P. Oomen, R. Nanke, and M. Leghissa, "Modelling and measurement of AC loss in BSCCO/Ag-tape windings," *Supercond. Sci. Technol.*, vol. 16, no. 3, pp. 339–354, Mar. 2003.

[161] A. Kawagoe, F. Sumiyoshi, T. Mito, H. Chikaraishi, T. Baba, K. Okumura, M. Iwakuma, T. Hemmi, K. Hayashi, R. Abe, T. Ushiku, and K. Miyoshi, "Winding techniques for conduction cooled LTS pulse coils for 100 kJ class UPS-SMES as a protection from momentary voltage drops," *IEEE Trans. Appl. Supercond.*, vol. 14, no. 2, pp. 727–730, Jun. 2004.

[162] H. Tonsho, M. Toyoda, S. Fukui, M. Yamaguchi, T. Sato, M. Furuse, H. Tanaka, K. Arai, and M. Umeda, "Numerical evaluation of AC loss in high temperature superconducting coil," *IEEE Trans. Appl. Supercond.*, vol. 14, no. 2, pp. 674–677, Jun. 2004.

[163] K.-H. Müller, "AC power losses in flexible thick-film superconducting tapes," *Phys. C, Supercond.*, vol. 281, no. 1, pp. 1–10, Jul. 1997.

[164] R. Brambilla, F. Grilli, D. N. Nguyen, L. Martini, and F. Sirois, "AC losses in thin superconductors: The integral equation method applied to stacks and windings," *Supercond. Sci. Technol.*, vol. 22, no. 7, p. 075018, Jul. 2009.

[165] F. Grilli and S. P. Ashworth, "Measuring transport AC losses in YBCO-coated conductor coils," *Supercond. Sci. Technol.*, vol. 20, no. 8, pp. 794–799, Aug. 2007.

[166] M. Zhang, J.-H. Kim, S. Pamidi, M. Chudy, W. Yuan, and T. A. Coombs, "Study of second generation, high-temperature superconducting coils: Determination of critical current," *J. Appl. Phys.*, vol. 111, no. 8, pp. 083902-1–083902-8, Apr. 2012.

[167] M. D. Ainslie, V. M. Rodriguez-Zermeno, Z. Hong, W. Yuan, T. J. Flack, and T. A. Coombs, "An improved FEM model for computing transport AC loss in coils made of RABiTS YBCO coated conductors for electric machines," *Supercond. Sci. Technol.*, vol. 24, no. 4, p. 045005, Apr. 2011.

[168] W. Yuan, A. M. Campbell, and T. A. Coombs, "A model for calculating the AC losses of second-generation high temperature superconductor pancake coils," *Supercond. Sci. Technol.*, vol. 22, no. 7, p. 075028, Jul. 2009.

[169] J. H. Claassen, "An approximate method to estimate AC loss in tape-wound superconducting coils," *Appl. Phys. Lett.*, vol. 88, no. 12, pp. 122512-1–122512-3, Mar. 2006.

[170] J. R. Clem, J. H. Claassen, and Y. Mawatari, "AC losses in a finite Z stack using an anisotropic homogeneous-medium approximation," *Supercond. Sci. Technol.*, vol. 20, no. 12, pp. 1130–1139, Dec. 2007.

[171] O. A. Shevchenko, J. J. Rabbers, A. Godeke, B. ten Haken, and H. H. J. ten Kate, "AC loss in a high-temperature superconducting coil," *Phys. C, Supercond.*, vol. 310, no. 1–4, pp. 106–110, Dec. 1998.

[172] E. Pardo, J. Šouc, and M. Vojenèiak, "AC loss measurement and simulation of a coated conductor pancake coil with ferromagnetic parts," *Supercond. Sci. Technol.*, vol. 22, no. 7, p. 075007, Jul. 2009.

[173] M. D. Ainslie, T. J. Flack, and A. M. Campbell, "Calculating transport AC losses in stacks of high temperature superconductor coated conductors with magnetic substrates using FEM," *Phys. C, Supercond.*, vol. 472, no. 1, pp. 50–56, Jan. 2012.

[174] J. R. Clem, "Field and current distributions and AC losses in a bifilar stack of superconducting strips," *Phys. Rev. B*, vol. 77, no. 13, pp. 134506-1–134506-7, Apr. 2008.

[175] D. N. Nguyen, F. Grilli, S. P. Ashworth, and J. O. Willis, "AC loss study of antiparallel connected YBCO coated conductors," *Supercond. Sci. Technol.*, vol. 22, no. 5, p. 055014, May 2009.

[176] J. Šouc, F. Gömöry, and M. Vojenèiak, "Coated conductor arrangement for reduced AC losses in a resistive-type superconducting fault current limiter," *Supercond. Sci. Technol.*, vol. 25, no. 1, p. 014005, Jan. 2012.

[177] M. Majoros, L. Ye, A. M. Campbell, T. A. Coombs, M. D. Sumption, and E. W. Collings, "Modeling of transport AC losses in superconducting arrays carrying anti-parallel currents," *IEEE Trans. Appl. Supercond.*, vol. 17, no. 2, pp. 1803–1806, Jun. 2007.

[178] Y. Mawatari and H. Yamasaki, "Alternating current loss in coplanar arrays of superconducting strips with bidirectional currents," *Appl. Phys. Lett.*, vol. 75, no. 3, pp. 406–408, Jul. 1999.

[179] A. Badía-Majós and C. López, "Critical-state analysis of orthogonal flux interactions in pinned superconductors," *Phys. Rev. B*, vol. 76, no. 5, pp. 054504-1–054504-8, Aug. 2007.

[180] P. Vanderbemden, Z. Hong, T. A. Coombs, M. Ausloos, N. H. Babu, D. A. Cardwell, and A. M. Campbell, "Remagnetization of bulk high-temperature superconductors subjected to crossed and rotating magnetic fields," *Supercond. Sci. Technol.*, vol. 20, no. 9, pp. S174–S183, Sep. 2007.

[181] J. R. Clem, "Flux-line-cutting losses in type-II superconductors," *Phys. Rev. B*, vol. 26, no. 5, pp. 2463–2473, Sep. 1982.

[182] J. R. Clem and A. Perez-Gonzalez, "Flux-line-cutting and flux-pinning losses in type-II superconductors in rotating magnetic fields," *Phys. Rev. B*, vol. 30, no. 9, pp. 5041–5047, Nov. 1984.

[183] H. Ruiz and A. Badía-Majós, "Smooth double critical state theory for type-II superconductors," *Supercond. Sci. Technol.*, vol. 23, no. 10, p. 105007, Oct. 2010.

[184] D. Karmakar and K. V. Bhagwat, "Critical state behaviour under rotating magnetic field: Minimum flux-change technique," *Phys. C, Supercond.*, vol. 406, no. 3/4, pp. 210–222, Jul. 2004.

[185] V. Meerovich, M. Sinder, V. Sokolovsky, S. Goren, G. Jung, G. E. Shter, and G. S. Grader, "Penetration dynamics of a magnetic field pulse into high- T_c superconductors," *Supercond. Sci. Technol.*, vol. 9, no. 12, pp. 1042–1047, Dec. 1996.

[186] S. Takács and F. Gömöry, "Hysteresis and coupling losses of superconducting cables at additional change of the applied magnetic field," *Supercond. Sci. Technol.*, vol. 18, no. 3, pp. 340–345, Mar. 2005.

[187] K. Kajikawa, R. Yokoo, K. Tomachi, K. Enpuku, K. Funaki, H. Hayashi, and H. Fujishiro, "Numerical evaluation of pulsed field magnetization in a bulk superconductor using energy minimization technique," *IEEE Trans. Appl. Supercond.*, vol. 18, no. 2, pp. 1557–1560, Jun. 2008.

[188] H. Fujishiro and T. Naito, "Simulation of temperature and magnetic field distribution in superconducting bulk during pulsed field magnetization," *Supercond. Sci. Technol.*, vol. 23, no. 10, p. 105021, Oct. 2010.

[189] A. Kawagoe, F. Sumiyoshi, M. Nakanishi, T. Mito, and T. Kawashima, "A new winding method to reduce AC losses in stable LTS pulse coils," *IEEE Trans. Appl. Supercond.*, vol. 13, no. 2, pp. 2404–2407, Jun. 2003.

[190] S. Lee, Y. Chu, W. H. Chung, S. J. Lee, S. M. Choi, S. H. Park, H. Yonekawa, S. H. Baek, J. S. Kim, K. W. Cho, K. R. Park, B. S. Lim, Y. K. Oh, K. Kim, J. S. Bak, and G. S. Lee, "AC loss characteristics of the KSTAR CSMC estimated by pulse test," *IEEE Trans. Appl. Supercond.*, vol. 16, no. 2, pp. 771–774, Jun. 2006.

[191] Z. Hong, W. Yuan, M. Ainslie, Y. Yan, R. Pei, and T. Coombs, "AC losses of superconducting racetrack coil in various magnetic conditions," *IEEE Trans. Appl. Supercond.*, vol. 21, no. 3, pp. 2466–2469, Jun. 2011.

[192] L. Bottura, P. Bruzzone, J. B. Lister, C. Marinucci, and A. Portone, "Computations of AC loss in the ITER magnets during fast field transients," *IEEE Trans. Appl. Supercond.*, vol. 17, no. 2, pp. 2438–2441, Jun. 2007.

[193] J. L. Giordano, J. Luzuriaga, A. Badía-Majós, G. Nieva, and I. Ruiz-Tagle, "Magnetization collapse in polycrystalline YBCO under transport current cycles," *Supercond. Sci. Technol.*, vol. 19, no. 4, pp. 385–391, Apr. 2006.

[194] T. Ogasawara, K. Yasuköchi, S. Nose, and H. Sekizawa, "Effective resistance of current-carrying superconducting wire in oscillating magnetic fields 1: Single core composite conductor," *Cryogenics*, vol. 16, no. 1, pp. 33–38, Jan. 1976.

[195] M. P. Oomen, J. Rieger, M. Leghissa, B. ten Haken, and H. H. J. ten Kate, "Dynamic resistance in a slab-like superconductor with $Jc(B)$ dependence," *Supercond. Sci. Technol.*, vol. 12, no. 6, pp. 382–387, Jun. 1999.

[196] N. Schönborg and S. P. Hörnfeldt, "Losses in a high-temperature superconductor exposed to AC and DC transport currents and magnetic fields," *IEEE Trans. Appl. Supercond.*, vol. 11, no. 3, pp. 4086–4089, Sep. 2001.

[197] Y. Wang, Y. Zheng, H. Liu, S. Dai, H. Zhang, X. Guan, Y. Teng, L. Zhao, J. Xue, and L. Lin, "A novel approach for design of DC HTS cable," *IEEE Trans. Appl. Supercond.*, vol. 21, no. 3, pp. 1042–1045, Jun. 2011.

[198] L. M. Fisher, A. V. Kalinov, S. E. Savel'ev, I. F. Voloshin, V. A. Yampol'skii, M. A. R. LeBlanc, and S. Hirscher, "Collapse of the magnetic moment in a hard superconductor under the action of a transverse AC magnetic field," *Phys. C, Supercond.*, vol. 278, no. 3/4, pp. 169–179, May 1997.

[199] A. Badía and C. López, "Critical state theory for nonparallel flux line lattices in type-II superconductors," *Phys. Rev. Lett.*, vol. 87, no. 12, p. 127004, Sep. 2001.

[200] E. H. Brandt and G. P. Mikitik, "Why an AC magnetic field shifts the irreversibility line in type-II superconductors," *Phys. Rev. Lett.*, vol. 89, no. 2, p. 027002, Jul. 2002.

[201] P. Vanderbemden, Z. Hong, T. A. Coombs, S. Denis, M. Ausloos, J. Schwartz, I. B. Rutel, N. H. Babu, D. A. Cardwell, and A. M. Campbell, "Behavior of bulk high-temperature superconductors of finite thickness subjected to crossed magnetic fields: Experiment and model," *Phys. Rev. B*, vol. 75, no. 17, pp. 174515-1–174515-14, May 2007.

[202] G. P. Mikitik and E. H. Brandt, "Theory of the longitudinal vortex-shaking effect in superconducting strips," *Phys. Rev. B*, vol. 67, no. 10, pp. 104511-1–104511-8, Mar. 2003.

[203] E. E. Kriezis, T. D. Tsiboukis, S. M. Panas, and J. A. Tegopoulos, "Eddy currents: Theory and applications," *Proc. IEEE*, vol. 80, no. 10, pp. 1559–1589, Oct. 1992.

[204] J. C. Nedelec, "Computation of eddy currents on a surface in R^3 by finite element methods," *SIAM J. Numer. Anal.*, vol. 15, no. 3, pp. 580–594, Jun. 1978.

[205] J. C. Vérité, "Computation of eddy currents on the alternator output conductors by a finite element method," *Int. J. Elect. Power Energy Syst.*, vol. 1, no. 3, pp. 193–198, Oct. 1979.

[206] M. V. K. Chari, "Finite-element solution of the eddy-current problem in magnetic structures," *IEEE Trans. Power App. Syst.*, vol. PAS-93, no. 1, pp. 62–72, Jan. 1974.

[207] J. H. McWhirter, R. J. Duffin, P. J. Brehm, and J. J. Oravec, "Computational methods for solving static field and eddy current problems via Fredholm integral equations," *IEEE Trans. Magn.*, vol. MAG-15, no. 3, pp. 1075–1084, May 1979.

[208] A. Bossavit and J.-C. Vérité, "A mixed FEM-BIEM method to solve 3-D eddy-current problems," *IEEE Trans. Magn.*, vol. MAG-18, no. 2, pp. 431–435, Mar. 1982.

[209] J.-L. Coulomb, "Finite elements three dimensional magnetic field computation," *IEEE Trans. Magn.*, vol. MAG-17, no. 6, pp. 3241–3246, Nov. 1981.

[210] O. Bíró and K. Preis, "Finite element analysis of 3-D eddy currents," *IEEE Trans. Magn.*, vol. 26, no. 2, pp. 418–423, Mar. 1990.

[211] A. Bossavit, "On the numerical analysis of eddy-current problems," *Comput. Methods Appl. Mech. Eng.*, vol. 27, no. 3, pp. 303–318, Jul. 1981.

[212] A. Bossavit, "Parallel eddy-currents: Relevance of the boundary-operator approach," *Integr. Equations Oper. Theory*, vol. 5, no. 1, pp. 447–457, 1982.

[213] C. W. Trowbridge, "Three-dimensional field computation," *IEEE Trans. Magn.*, vol. MAG-18, no. 1, pp. 293–297, Jan. 1982.

[214] C. J. Carpenter, "A network approach to the numerical solution of eddy-current problems," *IEEE Trans. Magn.*, vol. MAG-11, no. 5, pp. 1517–1522, Sep. 1975.

[215] K. Yamazaki, "Modeling and analysis of canned motors for hermetic compressors using combination of 2D and 3D finite element method," in *Proc. IEMD*, 1999, pp. 377–379.

[216] C. S. Biddlecombe, E. A. Heighway, J. Simkin, and C. W. Trowbridge, "Methods for eddy current computation in three dimensions," *IEEE Trans. Magn.*, vol. MAG-18, no. 2, pp. 492–497, Mar. 1982.

[217] L. Kettunen and L. R. Turner, "A volume integral formulation for nonlinear magnetostatics and eddy currents using edge elements," *IEEE Trans. Magn.*, vol. 28, no. 2, pp. 1639–1642, Mar. 1992.

[218] R. J. Lari and L. R. Turner, "Survey of eddy current programs," *IEEE Trans. Magn.*, vol. MAG-19, no. 6, pp. 2474–2477, Nov. 1983.

[219] S. J. Salon and J. M. Schneider, "A hybrid finite element-boundary integral formulation of the eddy current problem," *IEEE Trans. Magn.*, vol. MAG-18, no. 2, pp. 461–466, Mar. 1982.

[220] T. Tarhasaari, A. Koski, K. Forsman, and L. Kettunen, "Hybrid formulations for eddy current problem with moving objects," *IEEE Trans. Magn.*, vol. 34, no. 5, pp. 2660–2663, Sep. 1998.

[221] C. M. Elliott and Y. Kashima, "A finite-element analysis of critical-state models for type-II superconductivity in 3D," *IMA J. Numer. Anal.*, vol. 27, no. 2, pp. 293–331, Apr. 2007.

[222] O. Bíró, "Edge element formulations of eddy current problems," *Comput. Methods Appl. Mech. Eng.*, vol. 169, no. 3/4, pp. 391–405, Feb. 1999.

[223] A. Bossavit, "Whitney forms: A class of finite elements for three-dimensional computations in electromagnetism," *Proc. Inst. Elect. Eng. A, Phys. Sci., Meas. Instrum., Manag. Educ. Rev.*, vol. 135, no. 8, pp. 493–500, Nov. 1988.

[224] A. Bossavit, "A rationale for 'edge-elements' in 3-D fields computations," *IEEE Trans. Magn.*, vol. 24, no. 1, pp. 74–79, Jan. 1988.
[225] J. P. Webb and B. Forghani, "A scalar-vector method for 3D eddy current problems using edge elements," *IEEE Trans. Magn.*, vol. 26, no. 5, pp. 2367–2369, Sep. 1990.
[226] A. Kameari, "Calculation of transient 3D eddy current using edge-elements," *IEEE Trans. Magn.*, vol. 26, no. 2, pp. 466–469, Mar. 1990.
[227] K. Preis, I. Bardi, O. Biro, C. Magele, G. Vrisk, and K. R. Richter, "Different finite element formulations of 3D magnetostatic fields," *IEEE Trans. Magn.*, vol. 28, no. 2, pp. 1056–1059, Mar. 1992.
[228] R. Brambilla, F. Grilli, and L. Martini, "Development of an edge-element model for AC loss computation of high-temperature superconductors," *Supercond. Sci. Technol.*, vol. 20, no. 1, pp. 16–24, Jan. 2007.
[229] *Electromagnetic and Thermal Finite Element Analysis Software Flux*. [Online]. Available: http://www.cedrat.com
[230] *Electromagnetic Design Software Opera 2D and Opera 3D*. [Online]. Available: http://www.cobham.com
[231] *Finite-Element Software Package Comsol Multiphysics*. [Online]. Available: http://www.comsol.com
[232] C. Geuzaine and J.-F. Remacle, "Gmsh: A 3-D finite element mesh generator with built-in pre- and post-processing facilities," *Int. J. Numer. Methods Eng.*, vol. 79, no. 11, pp. 1309–1331, Sep. 2009.
[233] J. de Launay, R. L. Dolecek, and R. T. Webber, "Magnetoresistance of copper," *J. Phys. Chem. Solids*, vol. 11, no. 1/2, pp. 37–42, Sep. 1959.
[234] B. Lengeler, W. Schilling, and H. Wenzl, "Deviations from Matthiessen's rule and longitudinal magnetoresistance in copper," *J. Low Temp. Phys.*, vol. 2, no. 2, pp. 237–254, Mar. 1970.
[235] T. Takagi, M. Hashimoto, S. Arita, S. Norimatsu, T. Sugiura, and K. Miya, "Experimental verification of 3D eddy current analysis code using T-method," *IEEE Trans. Magn.*, vol. 26, no. 2, pp. 474–477, Mar. 1990.
[236] Z. Wang, W. Huang, W. Jia, Q. Zhao, Y. Wang, and W. Yan, "3D multifields FEM computation of transverse flux induction heating for moving-strips," *IEEE Trans. Magn.*, vol. MAG-35, no. 3, pp. 1642–1645, May 1979.
[237] J. A. Ferreina, "Application of the poynting vector for power conditioning and conversion," *IEEE Trans. Educ.*, vol. 31, no. 4, pp. 257–264, Nov. 1988.
[238] M. Oomen, "AC loss in superconducting tapes and cables," Ph.D. dissertation, Univ. Twente, Enschede, The Netherlands, 2000.
[239] A. Kalimov, S. Vaznov, and T. Voronina, "Eddy current calculation using finite element method with boundary conditions of integral type," *IEEE Trans. Magn.*, vol. 33, no. 2, pp. 1326–1329, Mar. 1997.
[240] S. J. Salon, "The hybrid finite element-boundary element method in electromagnetics," *IEEE Trans. Magn.*, vol. MAG-21, no. 5, pp. 1829–1834, Sep. 1985.
[241] E. Darve, "The fast multipole method: Numerical implementation," *J. Comput. Phys.*, vol. 160, no. 1, pp. 195–240, May 2000.
[242] R. Albanese and G. Rubinacci, "Solution of three dimensional eddy current problems by integral and differential methods," *IEEE Trans. Magn.*, vol. 24, no. 1, pp. 98–101, Jan. 1988.
[243] P. N. Barnes, M. D. Sumption, and G. L. Rhoads, "Review of high power density superconducting generators: Present state and prospects for incorporating YBCO windings," *Cryogenics*, vol. 45, no. 10/11, pp. 670–686, Oct./Nov. 2005.
[244] P. Vase, R. Flükiger, M. Leghissa, and B. Glowacki, "Current status of high- T_c wire," *Supercond. Sci. Technol.*, vol. 13, no. 7, pp. R71–R84, Jul. 2000.
[245] S. Stavrev and B. Dutoit, "Frequency dependence of AC loss in Bi(2223)/Ag-sheathed tapes," *Phys. C, Supercond.*, vol. 310, no. 1–4, pp. 86–89, Dec. 1998.
[246] S. Stavrev, B. Dutoit, N. Nibbio, and L. Le Lay, "Eddy current self-field loss in Bi-2223 tapes with A.C. transport current," *Phys. C, Supercond.*, vol. 307, no. 1/2, pp. 105–116, Oct. 1998.
[247] J. Paasi, M. Laforest, D. Aized, S. Fleshler, G. Snitchler, and A. P. Malozemoff, "AC losses in multifilamentary Bi-2223/Ag superconducting tapes," *IEEE Trans. Magn.*, vol. 32, no. 4, pp. 2792–2795, Jul. 1996.
[248] N. Magnusson, "Semi-empirical model of the losses in HTS tapes carrying AC currents in AC magnetic fields applied parallel to the tape face," *Phys. C, Supercond.*, vol. 349, no. 3/4, pp. 225–234, Jan. 2001.
[249] M. Majoros, L. Ye, A. V. Velichko, T. A. Coombs, M. D. Sumption, and E. W. Colling, "Transport AC losses in YBCO coated conductors," *Supercond. Sci. Technol.*, vol. 20, no. 9, pp. S299–S304, Sep. 2007.
[250] R. C. Duckworth, M. J. Gouge, J. W. Lue, C. L. H. Thieme, and D. T. Verebelyi, "Substrate and stabilization effects on the transport AC losses in YBCO coated conductors," *IEEE Trans. Appl. Supercond.*, vol. 15, no. 2, pp. 1583–1586, Jun. 2005.
[251] S. Stavrev, "Modelling of high temperature superconductors for AC power applications," Ph.D. dissertation, École Polytechnique Fédérale de Lausanne, Lausanne, Switzerland, 2002.
[252] M. Sumption, E. Collings, and P. Barnes, "AC loss in striped (filamentary) YBCO coated conductors leading to designs for high frequencies and field-sweep amplitudes," *Supercond. Sci. Technol.*, vol. 18, no. 1, pp. 122–134, Jan. 2005.
[253] C. M. Friend, C. Beduz, B. Dutoit, R. Navarro, E. Cereda, and J. Alonso-Llorente, "A European project on the AC losses of Bi-2223 tapes for power applications," *IEEE Trans. Appl. Supercond.*, vol. 9, no. 2, pp. 1165–1168, Jun. 1999.
[254] S. Takács, "AC losses in superconducting cables and their expected values in magnetic systems," *Supercond. Sci. Technol.*, vol. 10, no. 10, pp. 733–748, Oct. 1997.
[255] I. Hlásnik, "Review on AC losses in superconductors," *IEEE Trans. Magn.*, vol. MAG-17, no. 5, pp. 2261–2269, Sep. 1981.
[256] F. Gömöry, J. Šouc, M. Vojenèiak, E. Seiler, B. Klinèok, J. M. Ceballos, E. Pardo, A. Sanchez, C. Navau, S. Farinon, and P. Fabbricatore, "Predicting AC loss in practical superconductors," *Supercond. Sci. Technol.*, vol. 19, no. 3, pp. S60–S66, Mar. 2006.
[257] N. Amemiya, F. Kimura, and T. Ito, "Total AC loss in twisted multifilamentary coated conductors carrying AC transport current in AC transverse magnetic field," *IEEE Trans. Appl. Supercond.*, vol. 17, no. 2, pp. 3183–3186, Jun. 2007.
[258] D. Zola, F. Gömöry, M. Polichetti, F. Stryèek, E. Seiler, I. Hušek, P. Kováè, and S. Pace, "A study of coupling loss on bi-columnar BSCCO/Ag tapes through AC susceptibility measurements," *Supercond. Sci. Technol.*, vol. 17, no. 3, pp. 501–511, Mar. 2004.
[259] A. M. Campbell, "An introduction to numerical methods in superconductors," *J. Supercond. Novel Magnet.*, vol. 24, no. 1/2, pp. 27–33, Jan. 2011.
[260] M. Costa, E. Martinez, C. Beduz, Y. Yang, F. Grilli, B. Dutoit, E. Vinot, and P. Tixador, "3D modeling of coupling between superconducting filaments via resistive matrix in AC magnetic field," *IEEE Trans. Appl. Supercond.*, vol. 13, no. 2, pp. 3634–3637, Jun. 2003.
[261] M. Costa Bouzo, F. Grilli, and Y. Yang, "Modelling of coupling between superconductors of finite length using an integral formulation," *Supercond. Sci. Technol.*, vol. 17, no. 10, pp. 1103–1112, Oct. 2004.
[262] F. Grilli, M. C. Bouzo, Y. Yang, C. Beduz, and B. Dutoit, "Finite element method analysis of the coupling effect between superconducting filaments of different aspect ratio," *Supercond. Sci. Technol.*, vol. 16, no. 10, pp. 1228–1234, Oct. 2003.
[263] G. P. Lousberg, M. Ausloos, C. Geuzaine, P. Dular, P. Vanderbemden, and B. Vanderheyden, "Simulation of the highly non linear properties of bulk superconductors: Finite element approach with a backward Euler method and a single time step," in *Proc. 4th Int. Conf. Adv. Comput. Methods Eng.*, 2008, pp. 1–5.
[264] G. P. Mikitik, "Critical states in thin planar type-II superconductors in a perpendicular or inclined magnetic field (Review)," *Low Temp. Phys.*, vol. 36, no. 1, pp. 13–38, Jan. 2010.
[265] M. N. Wilson, "NbTi superconductors with low AC loss: A review," *Cryogenics*, vol. 48, no. 7/8, pp. 381–395, Jul./Aug. 2008.
[266] D. Abraimov, A. Gurevich, A. Polyanskii, X. Y. Cai, A. Xu, S. Pamidi, D. Larbalestier, and C. L. H. Thieme, "Significant reduction of AC losses in YBCO patterned coated conductors with transposed filaments," *Supercond. Sci. Technol.*, vol. 21, no. 8, p. 082004, Aug. 2008.
[267] S. P. Ashworth and F. Grilli, "A strategy for the reduction of AC losses in YBCO coated conductors," *Supercond. Sci. Technol.*, vol. 19, no. 2, pp. 227–232, Feb. 2006.
[268] W. J. Carr, Jr. and C. E. Oberly, "Filamentary YBCO conductors for AC applications," *IEEE Trans. Appl. Supercond.*, vol. 9, no. 2, pp. 1475–1478, Jun. 1999.
[269] O. Tsukamoto, N. Sekine, M. Ciszek, and J. Ogawa, "A method to reduce magnetization losses in assembled conductors made of YBCO coated conductors," *IEEE Trans. Appl. Supercond.*, vol. 15, no. 2, pp. 2823–2826, Jun. 2005.
[270] M. Polak, J. Kvitkovic, P. Mozola, E. Usak, P. N. Barnes, and G. A. Levin, "Frequency dependence of hysteresis loss in YBCO tapes," *Supercond. Sci. Technol.*, vol. 20, no. 9, pp. S293–S298, Sep. 2007.
[271] K. Seo, K. Fukuhara, and M. Hasegawa, "Analyses for inter-strand coupling loss in multi-strand superconducting cable with distributed

contact resistance between strands," *Cryogenics*, vol. 412, pp. 131–137, Feb. 2001.
[272] W. Goldacker, A. Frank, A. Kudymow, R. Heller, A. Kling, S. Terzieva, and C. Schmidt, "Status of high transport current ROEBEL assembled coated conductor cables," *Supercond. Sci. Technol.*, vol. 22, no. 3, p. 034003, Mar. 2009.
[273] G. Pasztor, P. Bruzzone, A. Anghel, and B. Stepanov, "An alternative CICC design aimed at understanding critical performance issues in Nb_3Sn conductors for ITER," *IEEE Trans. Appl. Supercond.*, vol. 14, no. 2, pp. 1527–1530, Jun. 2004.
[274] S. Kasai and N. Amemiya, "Numerical analysis of magnetization loss in finite-length multifilamentary YBCO coated conductors," *IEEE Trans. Appl. Supercond.*, vol. 15, no. 2, pp. 2855–2858, Jun. 2005.
[275] J. Paasi and M. Lahtinen, "Computational comparison of AC losses in different kinds of HTS composite conductors," *IEEE Trans. Appl. Supercond.*, vol. 7, no. 2, pp. 322–325, Jun. 1997.
[276] Y. A. Genenko, A. Snezhko, and H. C. Freyhardt, "Overcritical states of a superconductor strip in a magnetic environment," *Phys. Rev. B*, vol. 62, no. 5, pp. 3453–3472, Aug. 2000.
[277] Y. A. Genenko and A. Snezhko, "Superconductor strip near a magnetic wall of finite thicknes," *J. Appl. Phys.*, vol. 92, no. 1, pp. 357–360, Jul. 2002.
[278] Y. A. Genenko, "Strong reduction of AC losses in a superconductor strip located between superconducting ground plates," *Phys. C, Supercond.*, vol. 401, no. 1–4, pp. 210–213, Jan. 2004.
[279] Y. Mawatari, "Magnetic field distributions around superconducting strips on ferromagnetic substrates," *Phys. Rev. B*, vol. 77, no. 10, p. 104505, Mar. 2008.
[280] M. Suenaga, M. Iwakuma, T. Sueyoshi, T. Izumi, M. Mimura, Y. Takahashi, and Y. Aoki, "Effects of a ferromagnetic substrate on hysteresis losses of a $YBa_2Cu_3O_7$ coated conductor in perpendicular AC applied magnetic fields," *Phys. C, Supercond.*, vol. 468, no. 15–20, pp. 1714–1717, Sep. 2008.
[281] D. N. Nguyen, S. P. Ashworth, and J. O. Willis, "Experimental and finite-element method studies of the effects of ferromagnetic substrate on the total AC loss in a rolling-assisted biaxially textured substrate $YBa_2Cu_3O_7$ tape exposed to a parallel AC magnetic field," *J. Appl. Phys.*, vol. 106, no. 9, pp. 093913-1–093913-7, Nov. 2009.
[282] D. N. Nguyen, S. P. Ashworth, J. O. Willis, F. Sirois, and F. Grilli, "A new finite-element method simulation model for computing AC loss in roll assisted biaxially textured substrate YBCO tapes," *Supercond. Sci. Technol.*, vol. 23, no. 2, p. 025001, Feb. 2010.
[283] D. Miyagi, Y. Yunoki, M. Umabuchi, N. Takahashi, and O. Tsukamoto, "Measurement of magnetic properties of Ni-alloy substrate of HTS coated conductor in LN_2," *Phys. C, Supercond.*, vol. 468, no. 15–20, pp. 1743–1746, Sep. 2008.
[284] D. N. Nguyen, J. Y. Coulter, J. O. Willis, S. P. Ashworth, H. P. Kraemer, W. Schmidt, B. Carter, and A. Otto, "AC loss and critical current characterization of a noninductive coil of two-in-hand RABiTS YBCO tape for fault current limiter applications," *Supercond. Sci. Technol.*, vol. 24, no. 3, p. 035017, Mar. 2011.
[285] M. Zhang, J. Kvitkovic, S. V. Pamidi, and T. A. Coombs, "Experimental and numerical study of a YBCO pancake coil with a magnetic substrate," *Supercond. Sci. Technol.*, vol. 25, no. 12, p. 125020, Dec. 2012.
[286] M. Zhang, J. Kvitkovic, J.-H. Kim, C.-H. Kim, S. V. Pamidi, and T. A. Coombs, "Alternating current loss of second-generation high-temperature superconducting coils with magnetic and non-magnetic substrate," *Appl. Phys. Lett.*, vol. 101, no. 10, pp. 102602-1–102602-4, Sep. 2012.
[287] D. Nguyen, S. Ashworth, and S. Fleshler, "Numerical calculation for AC losses in a three phase tri-axial cable of RABiTS YBCO tapes," unpublished.
[288] D. Miyagi, Y. Amadutsumi, N. Takahashi, and O. Tsukamoto, "FEM analysis of effect of magnetism of substrate on AC transport current loss of HTS conductor with ferromagnetic substrate," *IEEE Trans. Appl. Supercond.*, vol. 17, no. 2, pp. 3167–3170, Jun. 2007.
[289] D. Miyagi, M. Umabuchi, N. Takahashi, and O. Tsukamoto, "Analysis of effect of nonlinear magnetic property of magnetic substrate on AC transport current loss of HTS coated conductor using FEM," *IEEE Trans. Appl. Supercond.*, vol. 18, no. 2, pp. 1297–1300, Jun. 2008.
[290] F. Gömöry and F. Inanir, "AC losses in coil wound from round wire coated by a superconducting layer," *IEEE Trans. Appl. Supercond.*, vol. 22, no. 3, p. 4704704, Jun. 2012.
[291] Y. A. Genenko, H. Rauh, P. Krüger, and N. Narayanan, "Finite-element simulations of overcritical states of a magnetically shielded superconductor strip," *Supercond. Sci. Technol.*, vol. 22, no. 5, p. 055001, May 2009.
[292] Y. A. Genenko, H. Rauh, and P. Krüger, "Finite-element simulations of hysteretic AC losses in a bilayer superconductor/ferromagnet heterostructure subject to an oscillating transverse magnetic field," *Appl. Phys. Lett.*, vol. 98, no. 15, pp. 152508-1–152508-3, Apr. 2011.
[293] S. Farinon, P. Fabbricatore, and F. Gömöry, "Critical state and magnetization loss in multifilamentary superconducting wire solved through the commercial finite element code ANSYS," *Supercond. Sci. Technol.*, vol. 23, no. 11, p. 115004, Nov. 2010.
[294] S. Farinon, P. Fabbricatore, F. Grilli, and P. A. C. Krüger, "Applicability of the adaptive resistivity method to describe the critical state of complex superconducting systems," *J. Supercond. Novel Magn.*, vol. 25, no. 7, pp. 2343–2350, Oct. 2012.
[295] [Online]. Available: http://hypertextbook.com/facts/2007/KarenFan.shtml
[296] [Online]. Available: http://uk.lowtemp.org/1-Woodcraft.pdf
[297] M. J. Gouge, J. A. Demko, B. W. McConnell, and J. M. Pfotenhauer, Cryogenics assessment report, Oak Ridge Nat. Lab., Oak Ridge, TN, USA, Tech. Rep.. [Online]. Available: http://www.ornl.gov/sci/htsc/documents/pdf/CryoAssessRpt.pdf
[298] W. V. Hassenzahl, D. W. Hazelton, B. K. Johnson, P. Komarek, M. Noe, and C. T. Reis, "Electric power applications of superconductivity," *Proc. IEEE*, vol. 92, no. 10, pp. 1655–1674, Oct. 2004.
[299] Y. Zushi, I. Asaba, J. Ogawa, K. Yamagishi, and O. Tsukamoto, "AC losses in HTS bulk and their influence on trapped magnetic field," *Cryogenics*, vol. 45, no. 1, pp. 17–22, Jan. 2005.
[300] N. Amemiya, S. Kasai, K. Yoda, Z. Jiang, G. A. Levin, P. N. Barnes, and C. E. Oberly, "AC loss reduction of YBCO coated conductors by multifilamentary structure," *Supercond. Sci. Technol.*, vol. 17, no. 12, pp. 1464–1471, Dec. 2004.
[301] M. D. Sumption, P. N. Barnes, and E. W. Collings, "AC losses of coated conductors in perpendicular fields and concepts for twisting," *IEEE Trans. Appl. Supercond.*, vol. 15, no. 2, pp. 2815–2818, Jun. 2005.
[302] M. Marchevsky, E. Zhang, Y. Xie, V. Selvamanickam, and P. G. Ganesan, "AC losses and magnetic coupling in multifilamentary 2G HTS conductors and tape arrays," *IEEE Trans. Appl. Supercond.*, vol. 19, no. 3, pp. 3094–3097, Jun. 2009.
[303] M. D. Ainslie, Y. Jiang, W. Xian, Z. Hong, W. Yuan, R. Pei, T. J. Flack, and T. A. Coombs, "Numerical analysis and finite element modelling of an HTS synchronous motor," *Phys. C, Supercond.*, vol. 470, no. 20, pp. 1752–1755, Nov. 2010.
[304] H. Sugimoto, T. Tsuda, T. Morishita, Y. Hondou, T. Takeda, H. Togawa, T. Oota, K. Ohmatsu, and S. Yoshida, "Development of an axial flux type PM synchronous motor with the liquid nitrogen cooled HTS armature windings," *IEEE Trans. Appl. Supercond.*, vol. 17, no. 2, pp. 1637–1640, Jun. 2007.
[305] Y. Chen, W. Yuan, M. Zhang, and T. A. Coombs, "The experiment to evaluate the AC loss of 2G HTS windings in the application of rotating electric machines," *IEEE Trans. Appl. Supercond.*, vol. 22, no. 3, p. 4705204, Jun. 2012.
[306] W. Nick, J. Grundmann, and J. Frauenhofer, "Test results from siemens low-speed, high-torque HTS machine and description of further steps towards commercialization of HTS machines," *Phys. C, Supercond.*, vol. 482, pp. 105–110, Nov. 2012.
[307] M. Gouge, D. Lindsay, J. Demko, R. Duckworth, A. Ellis, P. Fisher, D. James, J. Lue, M. Roden, I. Sauers, J. Tolbert, C. Traeholt, and D. Willen, "Tests of tri-axial HTS cables," *IEEE Trans. Appl. Supercond.*, vol. 15, no. 2, pp. 1827–1830, Jun. 2005.
[308] H. Noji, "AC loss of a high- T_c superconducting power-cable conductor," *Supercond. Sci. Technol.*, vol. 10, no. 8, pp. 552–556, Aug. 1997.
[309] H. Noji, K. Haji, and T. Hamada, "AC loss analysis of 114 MVA high-T_c superconducting model cable," *Phys. C, Supercond.*, vol. 392–396, pp. 1134–1139, Oct. 2003.
[310] J. R. Clem and A. P. Malozemoff, "Theory of AC loss in power transmission cables with second generation high temperature superconductor wires," *Supercond. Sci. Technol.*, vol. 23, no. 3, p. 034014, Mar. 2010.
[311] A. Malozemoff, G. Snitchler, and Y. Mawatari, "Tape-width dependence of AC losses in HTS cables," *IEEE Trans. Appl. Supercond.*, vol. 19, no. 3, pp. 3115–3118, Jun. 2009.
[312] S. Fukui, R. Kojima, J. Ogawa, M. Yamaguchi, T. Sato, and O. Tsukamoto, "Numerical analysis of AC loss characteristics of cable conductor assembled by HTS tapes in polygonal arrangement," *IEEE Trans. Antennas Propag.*, vol. 16, no. 2, pp. 143–146, Jun. 2006.
[313] Q. Li, N. Amemiya, K. Takeuchi, T. Nakamura1, and N. Fujiwara, "AC loss characteristics of superconducting power transmission cables: Gap effect and J_c distribution effect," *Supercond. Sci. Technol.*, vol. 23, no. 11, p. 115003, Nov. 2010.

[314] M. Takayasu, L. Chiesa, L. Bromberg, and J. V. Minervini, "HTS twisted stacked-tape cable conductor," *Supercond. Sci. Technol.*, vol. 25, no. 1, p. 014011, Jan. 2012.
[315] M. Staines, N. Glasson, M. Pannu, K. P. Thakur, R. Badcock, N. Allpress, P. D'Souza, and E. Talantsev, "The development of a Roebel cable based 1 MVA HTS transformer," *Supercond. Sci. Technol.*, vol. 25, no. 1, p. 014002, Jan. 2012.
[316] S. I. Schlachter, W. Goldacker, F. Grilli, R. Heller, and A. Kudymow, "Coated conductor rutherford cables (CCRC) for high-current applications: Concept and properties," *IEEE Trans. Appl. Supercond.*, vol. 21, no. 3, pp. 3021–3024, Jun. 2011.
[317] M. Noe, K.-P. Juengst, F. Werfel, L. Cowey, A. Wolf, and S. Elschner, "Investigation of high-T_c bulk material for its use in resistive superconducting fault current limiters," *IEEE Trans. Appl. Supercond.*, vol. 11, no. 1, pp. 1960–1963, Mar. 2001.
[318] A. Kudymow, C. Schacherer, M. Noe, and W. Goldacker, "Experimental investigation of parallel connected YBCO coated conductors for resistive fault current limiters," *IEEE Trans. Appl. Supercond.*, vol. 19, no. 3, pp. 1806–1809, Jun. 2009.
[319] Z. Hong, Z. Jin, M. Ainslie, J. Sheng, W. Yuan, and T. A. Coombs, "Numerical analysis of the current and voltage sharing issues for resistive fault current limiter using YBCO coated conductors," *IEEE Trans. Appl. Supercond.*, vol. 21, no. 3, pp. 1198–1201, Jun. 2011.
[320] M. Noe and M. Steurer, "High-temperature superconductor fault current limiters: Concepts, applications, and development status," *Supercond. Sci. Technol.*, vol. 20, no. 3, pp. R15–R29, Mar. 2007.
[321] R. Dommerque, S. Krämer, A. Hobl, R. Böhm, M. Bludau, J. Bock, D. Klaus, H. Piereder, A. Wilson, T. Krüger, G. Pfeiffer, K. Pfeiffer, and S. Elschner, "First commercial medium voltage superconducting fault-current limiters: Production, test and installation," *Supercond. Sci. Technol.*, vol. 23, no. 3, p. 034020, Mar. 2010.
[322] H. Heydari, F. Faghihi, and R. B. Aligholizadeh, "A new approach for AC loss reduction in HTS transformer using auxiliary windings, case study: 25 kA HTS current injection transformer," *Supercond. Sci. Technol.*, vol. 21, no. 1, p. 015009, Jan. 2008.
[323] M. K. Al-Mosawi, C. Beduz, Y. Yang, M. Webb, and A. Power, "The effect of flux diverters on AC losses of a 10 kVA high temperature superconducting demonstrator transformer," *IEEE Trans. Appl. Supercond.*, vol. 11, no. 1, pp. 2800–2803, Mar. 2001.
[324] K. Funaki, M. Iwakuma, K. Kajikawa, M. Takeo, J. Suehiro, M. Hara, K. Yamafuji, M. Konno, Y. Kasagawa, K. Okubo, Y. Yasukawa, S. Nose, M. Ueyama, K. Hayashi, and K. Sato, "Development of a 500 kVA-class oxide-superconducting power transformer operated at liquid-nitrogen temperature," *Cryogenics*, vol. 38, no. 2, pp. 211–220, Feb. 1998.
[325] M. Iwakuma, K. Funaki, K. Kajikawa, H. Tanaka, T. Bohno, A. Tomioka, H. Yamada, S. Nose, M. Konno, Y. Yagi, H. Maruyama, T. Ogata, S. Yoshida, K. Ohashi, K. Tsutsumi, and K. Honda, "AC loss properties of a 1 MVA single-phase HTS power transformer," *IEEE Trans. Appl. Supercond.*, vol. 11, no. 1, pp. 1482–1485, Mar. 2001.
[326] P. Tixador, B. Bellin, M. Deleglise, J. Vallier, C. Bruzek, S. Pavard, and J. Saugrain, "Design of a 800 kJ HTS SMES," *IEEE Trans. Appl. Supercond.*, vol. 15, no. 2, pp. 1907–1910, Jun. 2005.
[327] K. Kim, A.-R. Kim, J.-G. Kim, M. Park, I.-K. Yu, M.-H. Sohn, B.-Y. Eom, K. Sim, S. Kim, H.-J. Kim, J.-H. Bae, and K.-C. Seong, "Analysis of operational loss characteristics of 10 kJ class toroid-type SMES," *IEEE Trans. Appl. Supercond.*, vol. 21, no. 3, pp. 1340–1343, Jun. 2011.
[328] J. Zhu, Q. Cheng, B. Yang, W. Yuan, T. Coombs, and M. Qiu, "Experimental research on dynamic voltage sag compensation using 2G HTS SMES," *IEEE Trans. Appl. Supercond.*, vol. 21, no. 3, pp. 2126–2130, Jun. 2011.
[329] J. Zhu, W. Yuan, T. Coombs, and Q. Ming, "Simulation and experiment of a YBCO SMES prototype in voltage sag compensation," *Phys. C, Supercond.*, vol. 471, no. 5/6, pp. 199–204, Mar. 2011.
[330] W. Yuan, W. Xian, M. Ainslie, Z. Hong, Y. Yan, R. Pei, Y. Jiang, and T. A. Coombs, "Design and test of a superconducting magnetic energy storage (SMES) coil," *IEEE Trans. Appl. Supercond.*, vol. 20, no. 3, pp. 1379–1382, Jun. 2010.
[331] M.-J. Park, S.-Y. Kwak, W.-S. Kim, S.-W. Lee, J.-K. Lee, J.-H. Han, K.-D. Choi, H.-K. Jung, K.-C. Seong, and S.-Y. Hahn, "AC loss and thermal stability of HTS model coils for a 600 kJ SMES," *IEEE Trans. Appl. Supercond.*, vol. 17, no. 2, pp. 2418–2421, Jun. 2007.
[332] J. Koláèek, P. Lipavsky, and E. H. Brandt, "Charge profile in vortices," *Phys. Rev. Lett.*, vol. 86, no. 2, pp. 312–315, Jan. 2001.
[333] J. Pearl, "Current distribution in superconducting films carrying quantized fluxoids," *Appl. Phys. Lett.*, vol. 5, no. 4, pp. 65–66, Aug. 1964.

Francesco Grilli received the M.S. degree in physics from the University of Genoa, Genoa, Italy, in 1998 and the Ph.D. degree from École Polytechnique Fédérale de Lausanne, Lausanne, Switzerland, in 2004.

From 2004 to 2007 and from 2007 to 2009, he was a Postdoctoral Researcher with Los Alamos National Laboratory, Los Alamos, NM, USA, and with École Polytechnique de Montréal, Montréal, QC, Canada, respectively. Since 2009, he has been working with Karlsruhe Institute of Technology, Karlsruhe, Germany, where he leads the group "AC Losses in High Temperature Superconductors." His main research interests include the 2-D and 3-D modeling of high-T_c superconductors and the dc and ac characterization of their properties.

Dr. Grilli received the 2008 Van Duzer Prize for the best contributed nonconference paper published in the IEEE TRANSACTIONS ON APPLIED SUPERCONDUCTIVITY and the 2011 Dr. Meyer-Struckmann Science Prize from the Brandenburg Technical University Cottbus for his work on numerical modeling of superconductors.

Enric Pardo (M'10) was born in Sabadell, Spain, in 1977. He received the M.S. degree in physics (with honors) and the Ph.D. degree from the Autonomous University of Barcelona, Barcelona, Spain, in 1999 and 2004, respectively. The Ph.D. studies were on modeling of demagnetizing effects in magnetic materials and ac loss in superconductors.

From 2004 to 2006, he made postdoctoral stays at several institutions: Institute of Electrical Engineering, Slovak Academy of Sciences, Bratislava, Slovakia; University of Cambridge, Cambridge, U.K.; and the Institute of Spacial Studies of Catalonia, Barcelona. Later, from 2006 to 2007, he worked as a Physics Teacher Assistant with the Autonomous University of Barcelona. He is currently a Senior Researcher with the Institute of Electrical Engineering, Slovak Academy of Sciences. His current research interests include superconductivity, particularly modeling of dc and ac electromagnetic properties of superconductors and inductive measurements. During his career, he also conducted research on modeling of demagnetizing effects in linear magnetic materials, flux cutting in YBCO, and Josephson junction arrays.

Dr. Pardo received a Marie Curie postdoctoral fellowship from the Institute of Electrical Engineering in Bratislava (2007–2009) and from the Vienna University of Technology, Vienna, Austria (2009–2010).

Antti Stenvall was born in Jyväskylä, Finland, in 1981. He received the M.S. and Ph.D. degrees in electrical engineering from the Tampere University of Technology, Tampere, Finland, in 2005 and 2008, respectively.

In 2004, he joined the Institute of Electromagnetics, Department of Electrical Engineering, Tampere University of Technology, as a Research Assistant, where he became a Researcher in 2005 and has been a Research Fellow since 2008. In 2011, he spent seven months with the Institute for Technical Physics, Karlsruhe Institute of Technology, Karlsruhe, Germany, as a Visiting Scientist. His current research interests include modeling of superconductor stability and ac losses in large-scale devices.

Dr. Stenvall received The European Society for Applied Superconductivity Prize for Young Researcher 2011 in the category "Large Scale."

Doan N. Nguyen received the B.S. degree in physics from Vietnam National University, Hanoi, Vietnam, in 2001 and the M.S. and Ph.D. degrees in physics from Florida State University, Tallahassee, FL, USA, in 2003 and 2007, respectively.

From 2007 to 2009, he was a Postdoctoral Associate with the Superconductivity Technology Center (STC), Los Alamos National Laboratory, Los Alamos, NM, USA. Since 2009, he has been a Research Staff Member with the STC. His research interests include applied superconductivity, ac loss, quench stability, and electromechanical characterization of superconductors and superconducting systems.

Weijia Yuan received the Bachelor of Engineering degree from Tsinghua University, Beijing, China, and the Ph.D. degree from the University of Cambridge, Cambridge, U.K.

He was a Research Associate with the Department of Engineering, University of Cambridge, and a Junior Research Fellow with Wolfson College, University of Cambridge, Cambridge, U.K. Since 2011, he has been a Lecturer with the Department of Electronic and Electrical Engineering, University of Bath, Bath, U.K. His main research interests include electrical power applications of high-temperature-superconductor devices.

Fedor Gömöry (M'02) received the Diploma in electrical engineering (Ing.) in solid-state physics from Slovak University of Technology, Bratislava, Slovakia, in 1976; the Ph.D. degree from Slovak Academy of Sciences, Bratislava, in 1985, with a thesis dedicated to the problem of transient loss determination in superconducting magnets; and the D.Sc. degree from Slovak University of Technology in 1998, for the results in development of experimental methods for high-temperature superconductors.

In 1976, he joined the Institute of Electrical Engineering (IEE), Slovak Academy of Sciences, as a Research Engineer with the Superconducting Magnet Group. In 1980, he spent one year with the Institute of High Energy Physics, Serpukhov, Russia, to participate in the development of apparatus for loss measurements in superconducting accelerator magnets. During his two-year sabbatical stay at Pirelli Cables, Milan, Italy, in the mid-1990s, he took part in the development of power-transmission cables from the first generation of high-temperature-superconductor (HTS) tapes. He is currently the Leader of the AC Applications Group, IEE. His research activity is aimed at the utilization of hard superconductors in electric power. His group participated in several European projects dedicated to the development of power applications from the second generation of HTS tapes. In 2009, Slovak University of Technology appointed him as an Associate Professor in the field of new materials based on his research dedicated to the interaction of electromagnetic fields with superconducting materials. His current research interests include the development of numerical simulation techniques for composite superconducting wires and optimization of wire architecture from the point of ac loss reduction.